



Western Washington University  
Western CEDAR

---

WWU Graduate School Collection

WWU Graduate and Undergraduate Scholarship

---

Summer 2002

## Paleomagnetism of the Jura-Cretaceous Kyuquot Group, Vancouver Island, British Columbia

Chad K. Hults

Western Washington University, chadkh@msn.com

Follow this and additional works at: <https://cedar.wwu.edu/wwuet>



Part of the [Geology Commons](#)

---

### Recommended Citation

Hults, Chad K., "Paleomagnetism of the Jura-Cretaceous Kyuquot Group, Vancouver Island, British Columbia" (2002). *WWU Graduate School Collection*. 742.

<https://cedar.wwu.edu/wwuet/742>

This Masters Thesis is brought to you for free and open access by the WWU Graduate and Undergraduate Scholarship at Western CEDAR. It has been accepted for inclusion in WWU Graduate School Collection by an authorized administrator of Western CEDAR. For more information, please contact [westerncedar@wwu.edu](mailto:westerncedar@wwu.edu).

**Paleomagnetism of the Jura-Cretaceous Kyuquot  
Group, Vancouver Island, British Columbia**

by

Chad K Hults

Accepted in Partial Completion

Of the Requirements for the Degree

Master of Science

---

Moheb A. Ghali, Dean of the Graduate School

**ADVISORY COMMITTEE**

---

Chair, Dr. Bernard A. Housen

---

Dr. Russ Burmester

---

Dr. Chris A. Szczek

MASTER'S THESIS

In presenting this thesis in partial fulfillment of the requirements for a master's degree at Western Washington University, I agree that the Library shall make its copies freely available for inspection. I further agree that copying of this thesis in whole or in part is allowable only for scholarly purposes. It is understood, however, that any copying or publication of this thesis for commercial purposes, or for financial gain, shall not be allowed without my written permission.

Signature [Handwritten Signature]

Date 07-02-2002

## MASTER'S THESIS

In presenting this thesis in partial fulfillment of the requirements for a master's degree at Western Washington University, I grant to Western Washington University the non-exclusive royalty-free right to archive, reproduce, distribute, and display the thesis in any and all forms, including electronic format via any digital library mechanisms maintained by WWU.


I represent and warrant this is my original work and does not infringe or violate any rights of others. I warrant that I have obtained written permissions from the owner of any third party copyrighted material included in these files.

\_\_\_\_\_ I acknowledge that I retain ownership rights to the copyright of this work, including but not limited to the right to use all or part of this work in future works, such as articles or books.

Library users are granted permission for individual, research and non-commercial reproduction of this work for educational purposes only. Any further digital posting of this document requires specific permission from the author.

Any copying or publication of this thesis for commercial purposes, or for financial gain, is not allowed without my written permission.

Name: Chad Hults (2002)

Signature: 

Date: 5/24/2018

**Paleomagnetism of the Jura-Cretaceous Kyuquot  
Group, Vancouver Island, British Columbia**

A Thesis  
Presented to  
The Faculty of  
Western Washington University

In Partial Fulfillment  
Of the Requirements for the Degree  
Master of Science

by  
Chad K Hults  
June 2002

## Abstract

The Kyuquot Group is a series of marine clastic deposits of Late Jurassic to Early Cretaceous age located on the NW portion of Vancouver Island. These sediments have been folded, but not metamorphosed, and so provide an attractive target for paleomagnetic study. Results from these rocks fill a significant (50 m.y.) time gap in our knowledge of the paleomagnetic paleolatitude record of Wrangellia. Paleomagnetic results from the underlying Bonanza Volcanics (Symons, 1984) show no significant relative latitudinal displacement of Wrangellia with respect to North America. This, along with geological correlations between other similar-aged clastic sediment units, has led several workers (Brandon et al., 1988, McClelland et al., 1992) to propose that the Kyuquot Group represents a clastic overlap tying Wrangellia to the North American margin. Younger sedimentary rocks from Vancouver Island (the Upper Cretaceous Nanaimo Group) have shallow inclinations, indicative of 2500 km of translation (Enkin et al., 2001).

A total of 324 samples from the Jurassic Kapoose Formation and the Cretaceous One Tree Formation were collected. Thermal cleaning of 111 specimens from the Berriasian to Lower Valanginian One Tree Formation revealed two remanence components; one a low-unblocking temperature overprint, the other a high-unblocking temperature component displayed in 77 specimens. The high  $T_{ub}$  components pass both an inclination only test and a combined great circle and line-fit fold test after correction for a suspected small block rotation. The fold test results in a 100% bedding corrected direction of Dec.  $214.4^\circ$ , Inc.  $85.6^\circ$ ,  $\pm 3.3^\circ$ , and  $k = 25.2$ . Results from the Lower Callovian to Upper Tithonian Kapoose Formation are more scattered. 132 specimens were measured, 66 specimens have a recognizable high  $T_{ub}$  component. The high  $T_{ub}$  component fails both an inclination only fold test and a combined great circle and line-fit fold test.

The Lower Cretaceous One Tree Formation mean inclination corresponds to a paleolatitude of  $81.3^\circ \pm 6.5^\circ$ , which is  $28^\circ$  (3100km) north of the expected paleolatitude, assuming North American paleogeography. This high paleolatitude, combined with the low latitude results for the Late Cretaceous, is inconsistent with paleolatitudes predicted by models for Wrangellia (WV-1 and WV-2, Debiche et al., 1987). The high paleolatitude is consistent with the postulated revised plate model of Engebretson et al. (1995).

## **Acknowledgments**

Bernie Housen is responsible for influencing me to return to Western Washington University and work on a master's degree. He is responsible for the inception of this project and assisted shaping the ideas presented throughout. Russ Burmester helped clarify this thesis by suggesting intriguing ways to discover answers to the many questions that arose during the process. Throughout my college career Chris Suczek has given me direction and has helped develop my academic skills and knowledge. I also acknowledge my three field assistants, Chris Houck, and my parents, Larry and Sharon Hults. They all endured long hard workdays in the remote field area under unfavorable weather conditions. This project would not have been feasible without the financial support from the Geological Society of America, the Bureau for Faculty Research and the Western Washington University Department of Geology.

## Table of Contents

Abstract	iv
Acknowledgements	v
List of Tables and Figures	vii
Introduction	1
Geology and Structure of the Kyuquot Group	3
Sampling and Laboratory Techniques	6
Rock Magnetism	7
Anisotropy of Magnetic Susceptibility	8
Paleomagnetism (General)	11
Paleomagnetism of the Upper Jurassic Kapoose Formation	12
Paleomagnetism of the Lower Cretaceous One Tree Formation	13
Insular Paleogeography Implications	18
Conclusion	21
References	77



## Tables

<b>Table 1.</b>	Paleomagnetic Directions From Wrangellia and Connected Terranes.	22
<b>Table 2.</b>	Paleomagnetic Results from the Lower Cretaceous One Tree Formation on Grassy Island and Clark Island.	24

## Figures

<b>Figure 1.</b>	Location Map.	25
<b>Figure 2.</b>	Major terranes of western Canada and southern Alaska.	26
<b>Figure 3.</b>	Tectonostratigraphic diagram for the San Juan Islands and adjacent areas.	27
<b>Figure 4.</b>	Paleomagnetic paleolatitudes from Wrangellia and connected terranes.	28
<b>Figure 5.</b>	Kyuquot Group stratigraphic column.	29
<b>Figure 6.</b>	Photograph of the basal conglomerate of the Kapoose Formation at McLean Cove.	30
<b>Figure 7.</b>	Photograph of the basal conglomerate at the contact between the Upper Triassic Parson Bay Formation and the Upper Jurassic Kapoose Formation, located on Kapoose Rocks.	31
<b>Figure 8.</b>	Photograph of a conglomerate at Jurassic Point.	32
<b>Figure 9.</b>	Photograph of a bouma sequence seen in the Upper Jurassic Kapoose Formation at Jurassic Point.	33
<b>Figure 10.</b>	Photograph of the basal conglomerate of the Cretaceous One Tree Formation where it contacts the Upper Jurassic Kapoose Formation of Grassy Island.	34
<b>Figure 11.</b>	Photograph of steeply dipping beds of the Lower Cretaceous One Tree Formation on Grassy Island.	35
<b>Figure 12.</b>	Photograph of small-scale faulting of Grassy Island.	36
<b>Figure 13.</b>	Schematic cross-section through the line A-A' on Figure 1.	37
<b>Figure 14.</b>	Equal area plots of poles to bedding and fold axes from Grassy Island and Clark Island One Tree Formation locations.	38

<b>Figure 15.</b> Equal area plots showing a fold axis plunge and rotation correction for a suspected small block rotation.	39
<b>Figure 16.</b> Typical thermomagnetic susceptibility heating and cooling curves.	40
<b>Figure 17.</b> Derivative of a typical thermomagnetic heating curve.	41
<b>Figure 18.</b> Plot of typical magnetic susceptibility patterns observed during thermal demagnetization.	42
<b>Figure 19.</b> Typical hysteresis curves seen in samples from the Cretaceous One Tree and Jurassic Kapoose Formations.	43
<b>Figure 20.</b> Bi-logarithmic Day et al. (1977) plots.	44
<b>Figure 21.</b> Lower hemisphere equal area plots of in situ AMS data.	45-48
<b>Figure 22.</b> Flinn diagrams of Kyuquot Group AMS.	49
<b>Figure 23.</b> Comparison between the in situ principal AMS axes and the fold axes.	50
<b>Figure 24.</b> Equal area plots of tilt corrected AMS data.	51-53
<b>Figure 25.</b> Sketch map showing the AMS mean maximum axes.	54
<b>Figure 26.</b> Plots of typical demagnetization behavior.	55-57
<b>Figure 27.</b> Upper Jurassic Kapoose Formation low $T_{ub}$ component fold test.	58
<b>Figure 28.</b> Upper Jurassic Kapoose Formation high $T_{ub}$ component inclination only test.	59
<b>Figure 29.</b> Upper Jurassic Kapoose Formation high $T_{ub}$ component fold test.	60
<b>Figure 30.</b> Plot of a reversed direction demagnetization path from Clark Island, Lower Cretaceous One Tree Formation site 4.	61
<b>Figure 31.</b> Plot of a reversed direction demagnetization path from Clark Island, Lower Cretaceous One Tree Formation site 2.	62
<b>Figure 32.</b> Lower Cretaceous One Tree Formation low $T_{ub}$ component fold test.	63
<b>Figure 33.</b> Lower Cretaceous One Tree Formation high $T_{ub}$ component inclination only test.	64
<b>Figure 34.</b> Lower Cretaceous One Tree Formation high $T_{ub}$ component fold test.	65
<b>Figure 35.</b> Lower Cretaceous One Tree Formation high $T_{ub}$ component fold test, after correction for small block rotation using fold axes.	66
<b>Figure 36.</b> Equal area plot of the in situ and tilt corrected high $T_{ub}$ component linefits and great circle fits from the Lower Cretaceous One Tree Formation.	67

- Figure 37.** Lower Cretaceous One Tree Formation high  $T_{ub}$  component fold test, after correction for small block rotation using AMS mean maximum axis data. 68
- Figure 38.** Equal area plot of the Lower Cretaceous One Tree Formation reversed directions compared to the mean directions. 69
- Figure 39.** Equal area plot of the magnetic direction expected at the field area compared to the low  $T_{ub}$  component means from both the Lower Cretaceous One Tree Formation and the Upper Jurassic Kapoose Formation. 70
- Figure 40.** Paleomagnetic paleolatitudes from Wrangellia and connected terranes and the mean direction from the Lower Cretaceous One Tree Formation. 71
- Figure 41.** Vancouver Island terrane tracks developed by Debiche et al. (1987, Fig. 19, p. 37), based on the plate models by Engebretson et al. (1985). 72
- Figure 42.** Paleolatitude models for Vancouver Island (Debiche et al., Fig. 19, p. 37). 73
- Figure 43.** Vancouver Island terrane tracks based on the postulated revised plate motions of Engebretson (1995, personal communication). 74
- Figure 44.** North America absolute motion from 200-160 Ma (Beck and Housen, 2000) 75
- Figure 45.** North America absolute motion from 160-130 Ma (Beck and Housen, 2000). 76

## Introduction

This report is based on the paleomagnetic investigation of the Jura-Cretaceous Kyuquot (kɪ-yü'-kut) Group located on the NW coast of Vancouver Island, British Columbia (Fig. 1). The Kyuquot Group is a shallow marine sedimentary unit that unconformably overlies either the Lower Jurassic Bonanza Group or the Upper Triassic Vancouver Group of the Wrangell Terrane (Fig. 1, Muller et al., 1981). Hence, paleomagnetic results from the Kyuquot group can be used to fill the Late Jurassic to Early Cretaceous gap in the paleolatitude transport history of Wrangellia.

The objectives of this study were to 1) determine reliable paleomagnetic poles from both the Jurassic and Cretaceous formations of the Kyuquot Group for comparison with Jurassic and Cretaceous paleopoles from the North American craton, and 2) use anisotropy of magnetic susceptibility (AMS) to estimate paleocurrent directions. Comparison of the paleomagnetic paleopoles helps to answer the following questions concerning the tectonic evolution of the North American Cordillera. (1) What was the latest Jurassic and earliest Cretaceous paleomagnetic paleolatitude of Wrangellia? (2) Has the paleomagnetic declination of the Kyuquot group changed due to a rotation about a vertical axis? (3) What plate motion model best fits the paleomagnetic paleolatitude record of Wrangellia? The AMS data are used to test for inclination shallowing due to compaction and provide a paleocurrent direction that can be used for provenance studies.

Wrangellia is a Permian-Jurassic sequence of island arc volcanic and sedimentary rocks and is currently located along the west coast of North America stretching from Oregon to Alaska (Jones et al., 1977) (Fig. 2). The Wrangell, Alexander, and Peninsular terranes make up the larger terrane called the Insular Superterrane. The Upper Jurassic to Lower Cretaceous Gravina volcanic and volcanoclastic sequence overlaps Alexander and Wrangell terranes, tying them together by the Late Jurassic time (Berg et al., 1972). Wrangellia was joined to the Peninsular terrane by Cretaceous time, based on stratigraphic and fossil assemblage correlations (Jones, 1963). Cowan (1994) summarized the connection between the Insular Superterrane and the Coast Plutonic Complex, which were adjacent to each other by Late Cretaceous time, based on Cretaceous sedimentary overlapping sequences, detritus

from eastern imbricate zones within Cretaceous overlapping sequences, and Cretaceous intrusive contacts.

The Cretaceous paleogeography of the Insular Superterrane is in dispute. Magmatic and provenance links to the Intermontane Superterrane and the North American continent suggest the Insular Superterrane was adjacent to the eastern Intermontane Superterrane (Fig. 2) by the Middle Jurassic (e.g., van der Heyden, 1992; McClelland et al., 1992; Monger and Journeay, 1994). These models constrain the Insular Superterrane near its present position relative to the North American continent during the late Mesozoic Era (ca. 150-90 Ma., see summary in Cowan, 1994). Geological correlations between other similar-aged clastic sediment units has led several workers (Brandon et al., 1988, McClelland et al., 1992) to propose that the Kyuquot Group represents a clastic overlap tying Wrangellia to the North American margin (Fig. 3).

Existing paleomagnetic data do not provide support for a mid-Cretaceous northern paleolatitude for the Insular Superterrane during the Cretaceous. The data from the Insular Superterrane and all connected terranes are listed in Table 1 and plotted in Figure 4. The data show that the Insular Superterrane was at low paleolatitudes during the Triassic, mid-paleolatitudes during the Jurassic, mid-paleolatitudes during the mid-Cretaceous (see summaries in Beck, 1989, and Irving and Wynne, 1990, Irving et al., 1996). Note the gap in paleomagnetic studies between 110 and 160 Ma. Moores (1998) proposed that the Insular belt was well offshore before it accreted in the mid-Cretaceous at mid-latitudes, based on the distribution of ophiolites.

Late Jurassic to Early Cretaceous paleomagnetic data from the Kyuquot Group can be used to test the models discussed above and fill in the gap in Wrangellia displacement history between 160 and 110 Ma (Fig. 4 and Table 1). A better understanding of the relative motion between outboard terranes and North America can be used to evaluate models developed for oceanic plate motion (e.g., Engebretson et al., 1985, 1995). The Kyuquot Group is good for paleomagnetic study because the sequence is well described, has well-defined age constraints, and has not been metamorphosed (Jeletzky, 1950, Muller et al., 1981).

## Geology and Structure of the Kyuquot Group

### Geology

The Kyuquot Group is located along the coastline and offshore islands near Kyuquot Sound (Fig. 1). It consists of predominantly outer shelf deposits composed of sandstone, limy siltstone and shale, and a basal conglomerate (Fig. 5). Everywhere, fossils are abundant and well preserved. The sedimentary sequences and fossils were described and dated and named by Jeletzky (1950). The name for the Kyuquot Group was assigned in Jeletzky (1950), and the two formations, the Upper Jurassic Kapoose Formation and the Lower Cretaceous One Tree Formation, were assigned in Muller et al. (1981) (Fig. 5). The fossil dates that were assigned by Jeletzky (1950) were given minor revision by Muller et al. (1981). The following summary is from these two sources.

The Callovian to Kimmeridgian Kapoose Formation is located along the mainland coastline and on the northeastern sides of both Grassy Island and the McQuarrie Islets (Fig. 1). It unconformably overlies the Early Jurassic Bonanza Group or the Late Triassic Vancouver Group at McLean Cove and Jurassic Point, and the Triassic Parson Bay Formation at Kapoose Rocks (Fig. 1). A basal conglomerate lies directly on each of the contacts. It contains cobble size clasts and is thickest at McLean Cove. To the SE, it thins and reduces to gravel size clasts at Jurassic Point (compare Figs. 6, 7, and 8). The majority of beds are dark, limy siltstones (Fig. 9), with exception of the outcrop at McLean Cove location that is a basal conglomerate overlain with sands showing beach facies.

The Berriasian to Lower Valanginian One Tree Formation crops out on Grassy Island, Clark Island, and the McQuarrie Islets. There is a disconformity between the Kapoose Formation and the One Tree Formation on Grassy Island. The contact is identified on the NW side of Grassy Island by a basal conglomerate containing Cretaceous fossils (Fig. 10, Jeletzky, 1950). Most beds are gray to tan fossiliferous siltstones and sandstones (e.g., Fig. 11). Similar stratigraphic sections crop out on both islands, so it is assumed that they are the same section. The beds are primarily bioturbated with some density flow structures.

The Kyuquot Group sediments are primarily outer shelf deposits deposited in a neritic environment between wave base and ~200m depth (Muller et al., 1981). The Kyuquot Group comprises the southern extent of the Jura-Cretaceous Hectate forearc basin that also includes sedimentary units on North Vancouver Island and the Queen Charlotte Islands (Haggart, 1993). It has been proposed that sediments of the Hectate basin came predominantly from the east and contain clasts from Wrangellia and apparently the Coast Plutonic Complex (see summary, Haggart, 1993 and Monger et al., 1994). To the west, the expected subduction complex is missing. Haggart (1993) proposed that the Jura-Cretaceous Yakutat Terrane, located in southeast Alaska, contains the missing subduction complex. Other workers have proposed that the Jura-Cretaceous Pacific Rim Complex may be the missing subduction complex (e.g., Muller et al., 1981).

## **Structure**

Structural measurement and analysis is useful for constraining the age of the acquisition of remanent magnetism. Fold tests are used to decipher the proper orientation of the rock units based on the dispersion of the magnetic remanence directions. Correction of paleomagnetic and AMS data for dispersion due to folding and small block rotations is important for orientating a primary magnetic remanence to its position of acquisition. Deciphering the timing of folding, faulting and small block rotations is imperative for constraining the age of the acquisition of remanent magnetism.

There is an abundance of large-scale (Fig. 1) and small-scale (Figs. 8 and 12) faults in the field area (Jeletzky 1950). Northwest trending faults are shown on the schematic geologic map in Figure 1. Jeletzky (1950) mapped the faults as dextral strike slip faults. Muller et al. (1981) stated that the Westcoast fault runs through Brecciated Point and has undergone dextral oblique slip (Fig. 1). Muller et al. (1981) found evidence for constraining the motion of the Westcoast fault between the Late Jurassic and Early Eocene. It is assumed here that the fault between Clark Island and Grassy Island is a strand of the Westcoast fault system because of its proximity and parallel trend (Fig. 1). Faulting of the Westcoast fault is thus constrained between the Early Cretaceous and Early Eocene. A schematic cross-section, running from A-A' on the map in Figure 1, was made from the information from the geologic

map provided in Jeletzky (1950), and is shown in Figure 13. It emphasizes the effects of faulting and folding in the field area.

Muller et al. (1981) stated, “Apart from local syndepositional folding...Mesozoic and Tertiary formations [in the Nootka Sound Map-area] are mainly block-faulted.” Counter to this general statement, broad NW-SE trending folds were observed in the field and can be discerned on Jeletzky’s (1950) Map. The folds are shown in the cross-section in Figure 13. There is also evidence that some of deformation was taken up by small-scale faulting (e.g., Figs. 8 and 12).

### **Correction to a Common Framework**

A detailed structural analysis is necessary to restore the sampling locations to a common framework. Structural orientation data were taken in the field with a magnetic compass and from the geologic map provided by Jeletzky (1950). The poles to bedding for four locations are plotted on lower hemisphere of equal area plots in Figure 14. The fold axes were determined as the pole to the best-fit great circle through the poles to bedding. The corresponding fold axes are also plotted with their associated confidence ellipses (derived using a bootstrap procedure modified from Tauxe’s (1998) `boot_di.exe` program). The results show the GPJ location has a fold axis plunging shallowly to the SE, the KPJ location has a fold axis plunging shallowly to the NW, the CIK location has a fold axis plunging steeply to the S, and the GIK location has a fold axis plunging moderately to the SE.

If folding was before faulting then the fold axes should be a common linear feature that can be used to match individual blocks for a reconstruction. The discordant fold axes from the GIK and CIK locations suggest that folding occurred before faulting. Faulting is thus assumed to have offset and rotated the GIK location  $57^\circ$  counterclockwise relative to the CIK location.

An example of a small block rotation correction, using the fold axis as a common linear feature, is shown in Figure 15. The fold axes determined for the CIK location and the GIK location (Figs. 14, 15a) are first corrected for fold plunge (Fig. 15b, step 1). The fold



axes are then corrected for declination by arbitrarily fixing Clark Island and rotating the fold axis azimuth from Grassy Island  $57^\circ$  clockwise (cw) to match the Clark Island fold axis (Fig. 15b, step2).

### **Sampling and Laboratory Techniques**

Samples were collected on islands and outcrops along the rugged NW coast of Vancouver Island south of Kyuquot Sound and north of Esperanza Inlet (Fig. 1). Vegetation above winter wave height is substantial, so a 12-foot inflatable boat was necessary to access the islands and coastline. The inflatable boat and supplies were driven to a boat launch at Fair Harbor (~20km east of Rugged Point), which is the nearest access to Kyuquot sound. Base camp was located on the northeast side of Rugged Point (Fig. 1).

Every outcrop of the Kyuquot Group was sampled with exception of the McQuarrie Islets, because the water was always too rough to land on these rocky islets (Fig. 1). A copious selection of outcrops (Fig. 1) and steeply dipping beds (Fig. 11) made it possible to sample nearly the entire exposed section of the Kyuquot Group. An average of 8 oriented cores per site were collected from multiple beds spanning approximately 10m of sequence. Approximately 20m separated sites at each location. 133 cores were collected from 16 sites in the One Tree Formation over an available ~320 m thick sequence. 191 cores were collected from 25 sites in the Kapoose Formation over an estimated thickness of 400-800m. Extensive faulting and numerous isolated outcrops (Figs. 1, 8) make it difficult to estimate the total thickness of the Kapoose Formation. Cores were collected using a portable gasoline powered drill and oriented with a magnetic compass, and with a sun compass when the sun was available. Site latitudes and longitudes were taken with a recreation grade GPS unit.

In the laboratory, the 2.4cm diameter cores were cut to 2.2cm in length and measured first with a KLY-3 Kappabridge Spinning Sample Magnetic Susceptibility Anisotropy Meter. The specimens were then moved to a magnetically shielded room where the natural remanent magnetization (NRM) was measured on a 3-axis 2-G SQUID magnetometer. Specimens were thermally demagnetized in an ASC TD-48 magnetically shielded oven. The magnetic susceptibility of specimens was measured between each demagnetization step with a

Bartington susceptibility meter. Curie temperatures of selected samples were acquired using the KLY-3 Kappabridge within an Argon gas atmosphere to retard oxidation. Hysteresis curves were acquired at the University of Minnesota's Institute for Rock Magnetism.

### **Rock Magnetism**

To determine what magnetic minerals likely carry the remanence or influence susceptibility anisotropy, Curie temperatures and hysteresis parameters were determined on representative samples. An example of a typical thermomagnetic curve is shown in Figure 16. The second derivative of the thermomagnetic temperature heating curve shows a peak between 570 and 580° C, indicating that magnetite is the main carrier of NRM (Fig. 17, Tauxe, 1998). The increase in the total magnetic susceptibility on the cooling curves indicates the growth of new minerals during heating. The magnetic susceptibility measured between each thermal demagnetization step also showed an increase in susceptibility above ~350°C during thermal demagnetization (Fig. 18).

Hysteresis curves for 53 representative samples were acquired at the University of Minnesota's Institute for Rock Magnetism. Typical hysteresis curves for both the Kapoose and One Tree formations are shown in Figure 19. Parameters of the hysteresis curves are shown on Day et al. (1977) plots in Figure 20. The data are concentrated in the pseudo-single-domain field (PSD) with some in the multidomain field (MD). Also shown are the trends for North American remagnetized limestones from Jackson (1990) and single domain (SD) & multidomain (MD) magnetite mixtures from Parry (1982). Comparison of the Kyuquot Group data to the trends from Jackson (1990) and Parry (1982) suggests that the mineral grains are a mixture of SD and MD sized magnetite grains with no influence of superparamagnetic grains.

## **Anisotropy of Magnetic Susceptibility**

### **Introduction**

The anisotropy of magnetic susceptibility (AMS) of sedimentary rocks can be used to estimate the paleocurrent direction (Hamilton and Rees, 1970, Ellwood, 1980, also see review in Tarling and Hrouda, 1993). Current flow during the time of deposition aligns the magnetic minerals similar to alignment of sediment particles commonly seen in river deposits. For moderate velocity flows, the long axes of particles lie along the direction of current flow. Sediments deposited in moderate velocity flows have an AMS lineation (axis of maximum susceptibility) parallel to the direction of current flow with an axis of minimum susceptibility nearly perpendicular to bedding (see review in Tarling and Hrouda, 1993). Under higher velocity flow conditions, the long axis of elongate particles will be aligned perpendicular to the current flow, due to rolling. In this case, the axis of maximum susceptibility will be oriented perpendicular to the direction of current flow and the axis of minimum susceptibility will dip up current (see review in Tarling and Hrouda, 1993).

### **Methods and Results**

Susceptibility of 84 One Tree Formation specimens and 162 Kapoose Formation specimens was measured on a KLY-3 Kappabridge Spinning Sample Magnetic Susceptibility Anisotropy Meter. The data were reduced with the program SUSAR supplied with the instrument, then plotted along with means and their bootstrap confidence ellipses using Tauxe's (1998) plotams.exe program. The resulting in situ AMS data are plotted on the lower hemisphere of equal area plots (EA) in Figure 21. Flinn (1962) diagrams of the AMS data are shown in Figure 22. The Flinn (1962) diagrams show that the One Tree Formation and the Kapoose Formation have triaxial anisotropy that is slightly oblate. The Flinn (1962) diagrams also show that One Tree Formation has a slightly higher anisotropy compared to the Kapoose Formation.

## Analysis

Before paleocurrent estimations can be made, a tectonically influenced AMS fabric caused by folding must be ruled out. If the AMS fabric is dominated by a cleavage-bedding intersection lineation, then the maximum axes should lie along that lineation intersection. No cleavage is visible in the rocks sampled, so to evaluate whether an incipient cleavage controls orientation of the maximum susceptibility axes, maximum directions were first compared with fold axes. This comparison assumes that the cleavage would be axial planar.

If the folding event controls the AMS fabric, then the maximum AMS axis will lie along the direction of the fold axis. Figure 23 shows the AMS data compared to the fold axes calculated above for the four most structurally intact locations, Grassy Island (GIK), Clark Island (CIK), Gross Point (GPJ), and Kapoose Point (KPJ). The 95% confidence ellipses for the mean maximum AMS axes and the fold axes overlap from three of the four locations (CIK, GPJ, and KPJ, Fig. 23). The mean maximum AMS axes from these three locations are close enough to the fold axes to warrant suspicion that the AMS data include a mixture of tectonic origin (bedding cleavage intersection) lineation in some specimens and sedimentary origin in others. Yet, a tectonic influence cannot be ruled out. A purely tectonic fabric cannot explain the bimodal distribution of maximum susceptibility axes from the GIJ location (Fig. 21) or the dissimilar fold axis and mean maximum AMS lineation seen in the GIK location (Fig. 23).

If the AMS fabrics is dominated by current flow then the patterns should be consistent with the following: 1) calmly settled sediments should have a minimum susceptibility axis perpendicular to bedding (vertical); 2) moderate current flow should align the maximum susceptibility axis along the direction of current flow, 3) high current flow should align the maximum axes perpendicular to current direction and streak the minimum axes in the direction of current flow.

The in situ data from the One Tree Formation were corrected first for fold plunge (Fig. 15b, step 1), and then corrected to paleohorizontal. The Kapoose Formation data were

corrected to paleohorizontal without correction for fold plunge. The tilt corrected AMS data are shown in Figure 24.

Since it is possible that the AMS fabric contains a primary depositional fabric, then the AMS data plotted in Figure 24 can be analyzed for the above patterns. The AMS data from the One Tree Formation on Clark Island has a near horizontal maximum axis lineation trending NE-SW, consistent with paleocurrents directed NE or SW. The data from the One Tree Formation section of Grassy Island has a horizontal maximum axis trending NW-SE, consistent with paleocurrents directed NW or SE. Both sites have 95% confidence ellipses that are indistinguishable from vertical, which is consistent with the bedding plane.

The data from the Kapoose Formation are more complex. The AMS data from the Jurassic point location shows a mean maximum axis trending NW-SE with a mean minimum axis that is indistinguishable from vertical, which is consistent with a paleocurrent directed either NW or SE. The Kapoose Point and Kapoose Creek locations also show the dominant NW-SE maximum axis lineation but the minimum axes are streaked from vertical to the SW. These data possibly suggest a high flow regime with a paleocurrent directed to the SW. The data from the Grassy Island Kapoose Formation location show two clusters of maximum axes, one with a SSW trend and slight plunge, and the other with a horizontal NW-SE trend. The NW-SE maximum axis lineation is consistent with all Kapoose Formation locations and the minimum axes plot near vertical, so the pattern may represent a dominant paleocurrent directed either NW or SE. The SW cluster is anomalous and cannot be explained. The remaining data from Gross Point, McLean Cove, and Kapoose Rocks show a NW-SE maximum axis lineation, but have too few data to make definitive paleocurrent direction estimates. The mean maximum axis lineations are plotted on the location map in Figure 25.

## **Discussion**

The AMS data from every location shows a dominant NW-SE directed maximum axis lineation with exception of the CIK location. A SE directed paleocurrent direction is consistent with observations made in the field area of the basal conglomerate thinning to the SE with a corresponding clast size reduction (compare Figs. 6, 7, and 8). A SE directed

paleocurrent is also consistent with clasts within the Kyuquot group being similar to the lithology of the adjacent Bonanza or Vancouver Group, as suggested by Haggart (1993) and Monger et al. (1994).

Abundant faulting was seen throughout the field area, which may be associated with a small block rotation that rotated the CIK location maximum AMS axis lineation relative to all other locations. The paleocurrent directions for the One Tree Formation on Clark Island are rotated 53° cw from the One Tree Formation on Grassy Island. This rotation is similar to the disparity between the fold axes trends calculated for the two islands (57°, Figs. 14 and 15). The consistency of AMS maximum axes and the similarities of rotation estimates between the Clark Island and Grassy Island One Tree Formation locations validates the assumption that parallel folds developed before block rotation.

### **Paleomagnetism (General)**

#### **Methods**

The NRM of each specimen was measured on a 3-axis 2-G SQUID magnetometer. Specimens were demagnetized in an ASC TD-48 magnetically shielded oven. The magnetic susceptibility of specimens was measured between each demagnetization step with a Bartington susceptibility meter. The remanent magnetization was analyzed using principle component analysis (PCA) (Kirschvink, 1980) of visually identified linear and planar segments of thermal demagnetization paths.

Linear segments were fit with free lines using PCA. Best-fit free lines were accepted if their maximum angular deviation (MAD) was less than 10. It was also required that the last linear demagnetization segment either had an angle to the origin  $< 6^\circ$  or was indistinguishable from an anchored line fit. If the highest temperature demagnetization segment had a line fit MAD  $> 10$ , and appeared planar (showed streaking along a great circle path on an equal area plot), then the segment was fit with a best-fit plane. Only great circle fits with a MAD  $< 15$  were accepted. Magnetic stability tests used to constrain the age of magnetization of the line and great circle fits are the McFadden and Reid (1982) inclination only fold test, the McFadden and McElhinny (1988) combined great circle and line fit fold

test, and a reversal test. Line fits and great circle fits were all given equal weight for the stability tests.

## **Results**

Typical examples of thermal demagnetization paths are shown in Figure 26. Thermal demagnetization paths generally show two components, a low unblocking temperature (low  $T_{ub}$ ) component, and a high unblocking temperature (high  $T_{ub}$ ) component. The specimens that have only one linear component generally have a direction that is indistinguishable from the mean the low  $T_{ub}$  component discussed below. The typical unblocking temperature spectra for low  $T_{ub}$  components is from 80-200°C, and for the high  $T_{ub}$  components is from 250-450°C (e.g., Fig. 26).

### **Paleomagnetism of the Upper Jurassic Kapoose Formation**

#### **Kapoose Formation PCA Results**

Remanent magnetic directions from the Upper Jurassic Kapoose Formation are scattered. Of the 132 specimens measured, 74 specimens have an acceptable low  $T_{ub}$  component, and 66 specimens have a recognizable high  $T_{ub}$  component. Specimens were not used if they did not meet the criteria listed in “Paleomagnetic Methods.”

#### **Kapoose Formation Stability Tests**

The 74 acceptable low  $T_{ub}$  line fits fail the McFadden and McElhinny (1988) fold test with a maximum  $k$  at 20% and the minimum at 100% (10.8, and 3.4 respectively, Fig. 27). The 0% unfolding mean direction is,  $D = 32.6^\circ$ ,  $I = 72.7^\circ$ ,  $\alpha_{95} = 5.5^\circ$ .

The acceptable high  $T_{ub}$  components fail both a McFadden and Reid (1982) inclination only test and a McFadden and McElhinny (1988) combined great circle and line fit fold test. The inclination only fold test has a maximum  $k$  value at  $0^\circ$  (9.4, Fig. 28). The

combined great circle and line fit fold test has a maximum  $k$  value of 5.5 at 40% tilt correction (Fig. 29).

## **Paleomagnetism of the Lower Cretaceous One Tree Formation**

### **One Tree Formation PCA Results**

Thermal cleaning of 111 specimens from the Lower Cretaceous One Tree Formation revealed two components of remanence; one is a low  $T_{ub}$  component displayed in 91 specimens, the other is a high  $T_{ub}$  component displayed in 77 specimens (e.g., Fig. 26). Specimens were not used if they did not meet the criteria listed in “Paleomagnetic Methods.” Thirteen specimens were also rejected because they showed a demagnetization path with a line fittable low  $T_{ub}$  path but the path appeared to be section of a dominantly curvilinear path, because and influence from the high  $T_{ub}$  component could not be ruled out. Duplicate samples from 6 beds were also excluded.

Five specimens from four sites on Clark Island, from four different stratigraphic levels, show demagnetization paths with reversed directions that pass the criteria listed in “Paleomagnetic Methods.” Both sites 3 and 5 have a specimen with a multi-component demagnetization path that shows the high  $T_{ub}$  section of the path heading to the reversed direction. Site 4 contains two specimens with demagnetization paths going to the reversed direction. All four specimens above provide a path that can be fit with a best-fit great circle (e.g., Fig. 30). Site 2 has a specimen showing a reversed polarity demagnetization path that is line fittable (Fig. 31).

### **One Tree Formation Stability Tests**

The 91 acceptable low  $T_{ub}$  components fail the McFadden and McElhinny (1988) fold test with the maximum  $k$  value of 13 at 0% tilt correction and the minimum  $k$  value of 5 at 100% tilt correction (Fig. 32). The 0% unfolded mean direction is  $D = 29.0^\circ$ ,  $I = 74.9^\circ$ ,  $\alpha_{95} = 4.3^\circ$ .



The high  $T_{ub}$  component data (45 line fits) pass a McFadden and Reid (1982) inclination only test (Fig. 33). The inclination only fold test results in a large change of  $k$  from 6.2 at 0% tilt correction to the maximum 59.3 at 100% tilt correction. The 100% tilt corrected orientation inclination estimate is  $82.1^\circ$ ,  $\alpha_{95} = 3.3^\circ$ .

The McFadden and McElhinny (1988) combined great circle and line fit fold test results are shown in Table 2. Before correcting data for fold plunge and the suspected small block rotation, the combined great circle and line fit fold test results in a maximum  $k$  value of 26 at 70-80% tilt correction (Fig. 34). A common assumption for a mid-tilt correction peak in  $k$  is that it indicates a synfolding remagnetization. However, it could also result from combining data from blocks that have been rotated relative to one another. There is a major fault between Grassy and Clark Islands (Fig. 1, see map in Jeletzky, 1950). Small block rotations are commonly associated with faults, and since the line fit data pass an inclination only fold test at 100% unfolding, the mid-tilt correction peak might be due to a small block rotation that was subsequent to the folding event.

Correction of the paleomagnetic data for the suspected small block rotation requires that all blocks had a directional feature with a common orientation before rotation. One choice is to use the  $57^\circ$  disparity between the fold axis trends observed between Grassy and Clark Island (Fig. 14). The high  $T_{ub}$  component data are first corrected for fold plunge (Fig. 15b, step 1), then the Grassy Island data are rotated  $57^\circ$  clockwise (cw) to match the Clark Island fold axis (Fig. 15b step 2). After correction for fold plunge and the small block rotation, the high  $T_{ub}$  component data pass a McFadden and McElhinny (1988) combined great circle and line fit fold test (45 line fits, 32 great circle fits, Figs. 35, 36, and Table 2). The minimum  $k$  value is 8.5 at 0% tilt correction with the maximum  $k$  of 25.4 achieved at 90% tilt correction. The difference between the 90% tilt corrected  $k$  value and the 100%  $k$  value (25.2) is insignificant. The 100% tilt corrected mean direction is  $D=214.4^\circ$ ,  $I=85.6^\circ$ ,  $\alpha_{95}=3.3^\circ$ .

An alternative correction for the small block rotation is to use the  $53^\circ$  difference in the maximum susceptibility directions seen in Figure 23. The result of the McFadden and

McElhinny (1988) combined great circle and line fit fold test is shown in Figure 37. The minimum  $k$  value of 6.9 is at 0% tilt correction and a maximum  $k$  value of 25.1 is at 90% tilt correction. The difference between the 90% tilt corrected  $k$  value and the 100%  $k$  value (24.8) is insignificant. The 100% tilt corrected mean direction is  $D=186.8^\circ$ ,  $I=86.2^\circ$ ,  $\alpha_{95}=3.3^\circ$ .

Antipodal reversed directions are used to support the consistency of a remanent component and that the component was acquired over a suitable amount of time to average out secular variation. As seen in Figure 38, the 95% confidence circle of the fold corrected mean of the five reversed directions, flipped to the antipode, does not include the fold corrected mean for all the acceptable high  $T_{ub}$  components from Clark Island, nor the overall mean. The mean reversed directions fail the reversal test. Yet, more reversed directions are necessary for a significant reversal test, especially with line fittable paths to define sector constraints.

If the high  $T_{ub}$  component magnetization is not just pre-folding but detrital, then it may have been shallowed by compaction. Thirty-three specimens from Grassy Island and Clark Island, showing a line fittable high  $T_{ub}$  component, were used for a test for inclination error. The correlations between  $\tan I$  vs.  $k_{min}/k_{max}$  for all specimens, and for 13 specimens with  $k_{min} < 15^\circ$  from vertical, were found to be not significant at the 95% confidence level ( $R < t_{a/2}/(t_{a/2}^2 + N - 2)^{1/2}$ ). Three factors may contribute to the low correlation; 1) a small susceptibility anisotropy ( $k_{max}$  exceeding  $k_{min}$  by only 2.5%), 2) few samples with  $k_{min}$  axis  $< 15^\circ$  from vertical, and 3) inclination shallowing is insignificant in samples with a high mean inclination (Tauxe, 1998). Hence, the inclination shallowing estimate using the Hodych et al. (1999) method is not an appropriate correction. A detrital remanent magnetization with a steep inclination of  $85.6^\circ$  is unlikely to have been affected by inclination shallowing.

## Discussion

The low  $T_{ub}$  mean directions from both the Lower Cretaceous One Tree Formation ( $D = 29.0^\circ$ ,  $I = 74.9^\circ$ ,  $\alpha_{95} = 4.3^\circ$ ) and the Upper Jurassic Kapoose Formation ( $D = 34.2^\circ$ ,  $I = 74.1^\circ$ ,  $\alpha_{95} = 5.9^\circ$ ) are similar to the IGRF model expected present-day field, and closer to the

1945 expected field (Fig. 39). The two low  $T_{ub}$  component mean directions are indistinguishable (both confidence circles envelop both mean directions), so the remagnetization must have occurred after the folding and small block rotation events. The low  $T_{ub}$  components seen in the Kapoose and One Tree Formations show a direction that is probably a present day viscous remagnetization.

The high  $T_{ub}$  component seen in the Kapoose Formation specimens passes neither a McFadden and Reid (1982) inclination only test nor a McFadden and McElhinny (1988) combined great circle and line fit fold test. Failure of these tests indicates that the high  $T_{ub}$  component is not primary. The data are too scattered to estimate the proper orientation when the rocks acquired the remanent magnetization. The remanent magnetization may be a low temperature chemical remagnetization.

The One Tree Formation high  $T_{ub}$  components more clearly predate small block rotation and at least some folding, but whether they are primary and were acquired when the rocks were horizontal is less clear. The high  $T_{ub}$  components pass a McFadden and Reid (1982) inclination only test and, after correction for a small block rotation, a McFadden and McElhinny (1988) combined great circle and line fit fold test. Also, Five specimens carry a reversed direction. These results suggest that the high  $T_{ub}$  component is pre-folding and is possibly a primary detrital remanent magnetization (Figs. 33, 35, and Table 2). The inclination, after correcting for fold plunge and fold azimuth, is  $85.6^\circ \pm 3.3^\circ$ , which corresponds to a paleolatitude of  $81.3^\circ \pm 6.5^\circ$ . All three corrections result in a similar steep inclination (82-86°). The fold plunge and fold azimuth correction is preferred because it more accurately represents the paleomagnetic field than the inclination only result or the AMS maximum axis correction. The inclination only result does not take into account declination and has an inherent error at steep inclinations (i.e., 82°). The maximum AMS axis correction result has a 100% fold correction  $k$  value (24.8) is less than the fold plunge and fold azimuth corrected  $k$  value (25.2).

Assuming the magnetization is primary and was acquired while the beds were horizontal, the declination of the fold corrected Lower Cretaceous One Tree Formation high

$T_{ub}$  component deviates significantly from the declination expected assuming North America paleogeography during the time of deposition. Clark Island was chosen for the fixed block in the small block rotation correction (Fig. 15). The resulting declination is  $214^\circ \pm 43^\circ$ . If Grassy Island is held fixed, the resulting declination is  $157^\circ \pm 43^\circ$ . As a result, the declination lies between  $114^\circ$  and  $257^\circ$ . Error estimates for the declination are large because of the steep inclination and because of the suspected small block rotation between Clark and Grassy Islands. Even with this large error, there has been substantial clockwise ( $\sim 260^\circ$  cw  $\pm 43^\circ$ ) or counterclockwise ( $100^\circ$  ccw  $\pm 43^\circ$ ) rotation relative to the expected declination of  $316^\circ$  for the 140 Ma North American reference pole extrapolated from the paleomagnetic Euler pole path of Beck and Housen (2000).

If the high  $T_{ub}$  component represents a secondary magnetization then the most probable time for its acquisition would be during the Cretaceous Normal Superchron. The high percentage (96%) of samples retains a normal high  $T_{ub}$  component. Six reversed chrons span the depositional time represented by the Kyuquot Group (Gradstein et al., 1994). Only 5 specimens have a path that is fittable with a great circle or line fit (e.g., Figs. 30 and 31). The mean of these 5 reversed directions does not pass a reversal test (Fig. 38). Normal and reversed chrons are evenly distributed throughout the Berriasian and the Lower Valanginian, so there should be an equal probability of a specimen having a reversed direction as a normal direction. The low number of reversed directions is an argument for the remagnetization hypothesis for the high  $T_{ub}$  component seen in the One Tree Formation.

The fold tests establish that the high  $T_{ub}$  component was acquired before folding, so the beds had to have been coplanar during the time of the remagnetization. However, this does not mean that they were horizontal. Remagnetization of the One Tree Formation had to occur while the beds were in an orientation other than horizontal because the oversteepened inclination of  $85.6^\circ \pm 3.3^\circ$  does not resemble any paleolatitude from rocks of a younger age (Table 1). As a result, the following events would have had to occur: 1) Early Cretaceous deposition of the One Tree Formation, 2) tilting or large wavelength folding before the mid-Cretaceous, 3) acquisition of the high  $T_{ub}$  component during the Cretaceous Normal

Superchron 4) shorter wavelength folding, 5) faulting and small block rotation to their current configuration.

Remagnetization during the Cretaceous Normal Superchron does not explain why 5 specimens at four different sites carry reversed directions, unless they are some of the only specimens still holding the primary magnetization. The possibility exists that the high  $T_{ub}$  component from the Lower Cretaceous One Tree Formation is a primary detrital remanent magnetization.

### **Insular Paleogeography Implications**

This study was aimed at determining reliable paleomagnetic paleopoles for both the Upper Jurassic Kapoose Formation and the Lower Cretaceous One Tree Formation. The Kapoose Formation does not carry a stable paleomagnetic direction. The One Tree Formation has a high  $T_{ub}$  component that passes a fold test and has 5 specimens with reversed directions. If the One Tree Formation direction is primary (see discussion above) then the mean tilt corrected direction can be used to fill in the missing data for the paleomagnetic paleolatitude transport of Wrangellia and the Insular Superterrane.

The resulting paleolatitude from the tilt corrected mean direction from the One Tree Formation ( $81.3^\circ \pm 6.5^\circ$ ) is  $28^\circ$  north (3100 km) of the expected paleolatitude calculated for the 140 Ma North American reference pole ( $\lambda$   $70.3^\circ$ N,  $\phi$   $162.9^\circ$  E) extrapolated from the paleomagnetic Euler pole path of Beck and Housen (2000, Fig. 40). The  $81.3^\circ$  paleolatitude is also  $43^\circ$ , approximately 4700 km, north of the paleolatitude reported by Enkin et al. (2001) from the Upper Cretaceous Nanaimo Group ( $38.3^\circ \pm 3^\circ$ ) (Table 1, Fig. 40). Combined with other paleomagnetic studies from the Insular Superterrane (Fig. 40, Table 1), the paleolatitude path for the Insular Superterrane; starts at low latitudes during the Triassic; shifts to mid-latitudes during the Jurassic; shifts to near the north pole during the Early Cretaceous; then shifts back down to mid-latitudes during the Late Cretaceous; and finally northward to its position relative to North America by the Eocene.

The terrane motions of Vancouver Island developed by Debiche et al. (1987, Figs. 41 and 42), based on the plate motions of Engebretson et al. (1985), are not consistent with the rate of southward motion necessary to shift Wrangellia from  $81.3^{\circ} \pm 6.5^{\circ}$  N 140 Ma (this study) to  $38.3^{\circ} \pm 3^{\circ}$  N 78 Ma (Enkin et al., 2001). A minimum southward plate motion of 74 km/m.y. is required to move Wrangellia from  $81^{\circ}$ N to  $39^{\circ}$ N between 139 and 78 Ma. The Farallon plate motions predicted by Engebretson et al. (1985) cannot account for this high rate of southward displacement during the Cretaceous.

Rapid southward motion during the Early Cretaceous is consistent with the postulated revised Kula plate motions from Engebretson et al. (1995, Fig. 43). Prior models of Kula plate history (Engebretson et al., 1985) suggest that it was formed at 85 Ma. The postulated revised model by Engebretson et al. (1995) suggests that the Kula plate has been in existence since ca. 180 Ma. This revised model has the Kula plate rotating around an Euler pole located in the south Pacific between 180 Ma and 100 Ma. During this time, “the Kula plate had a SE directed absolute velocity of  $\sim 175$  km/m.y. along the west coast of North America” (Engebretson et al., 1995). The southward plate motion during the interval 180-120 Ma is consistent with Jurassic and Early Cretaceous sinistral strike slip structures observed along the Western boundary of North America (Avé Lallemant and Oldow, 1988; Monger et al., 1994; and Oldow et al., 1984) and the pattern of west coast paleomagnetic displacements recognized by Beck (1989).

Figure 43 shows the tracks that terranes would have traveled if they were riding on the Kula plate 180 to 100 Ma ((Engebretson et al., 1995). If the Wrangell terrane docked onto North America near its relative position to North America, then it would have traveled along the upper path. The lower track is for terranes that accreted onto North America down by Baja 90-100 Ma. The current mid-Cretaceous paleomagnetic data supports the lower terrane track (Fig. 40). The Lower Cretaceous One Tree Formation was deposited over a span that includes 140 Ma, which is the most northern point, relative to North America, on the curve shown in Figure 43. If North America was rotated clockwise relative to its present position, then it would place the lower terrane track far enough north to match the  $81^{\circ}$ N paleolatitude measured in the Lower Cretaceous One Tree Formation. The Absolute North

American motion developed by Beck and Housen (2000) shows that North America was rotated significantly clockwise relative to its present orientation 160 Ma (Fig. 44). North America then moved to its highest paleolatitude 140 Ma (Fig. 45 and 40). By combining the terrane tracks by Engebretson et al. (1995) with the North American orientation 140 Ma predicted by Beck and Housen (2000), an 81°N paleolatitude for the Wrangell terrane is consistent with the current paleomagnetic paleolatitude data from the Insular Superterrane (Fig. 40).

Terranes traveling on the Kula plate from the Late Jurassic to Early Cretaceous would be rotated clockwise (Engebretson et al., 1995, Fig. 43). The declination of the Lower Cretaceous One Tree Formation deviates 260° cw (100° ccw) and the Jurassic Bonanza Group deviates 285° cw (75° ccw) (Irving and Yole, 1987), relative to the extrapolated reference poles from the North American paleomagnetic Euler pole path of Beck and Housen (2000). Rotating Wrangellia about an Euler pole in the southeast paleopacific from 180 to 100 Ma, then adding more clockwise rotations due to small block rotations during dextral transpression along the west coast of North America after 100 Ma could explain the large clockwise deviations in declination. Alternatively, if Wrangellia were semi-accreted to North America by the Late Jurassic (e.g., van der Heyden, 1992; McClelland et al., 1992; Monger and Journeay, 1994), then blocks could have been rotated counterclockwise due to shear against North America caused by southeast directed motion of the Kula plate (Engebretson et al., 1995, Fig. 43). Small block rotations under a sinistral transpressional regime between 180 and 100 Ma could have created the smaller counterclockwise rotations. This combination could explain why the declination deviations from the three Triassic to Early Jurassic Vancouver Island units show an opposite deviation relative to the Middle Jurassic to Early Cretaceous results (VI Intrusions, 38°cw; West Coast Crystalline Complex, 43°cw; Karmutsen Formation, 41°cw, Table 1, Symons, 1984; Irving and Yole, 1987; Irving and Wynne, 1990).

Few paleocurrent studies consider vertical axis rotations when estimating possible source areas (i.e., Mustard et al., 1994). Given the paleomagnetic declination deviations discussed above, the SE directed paleocurrent direction, estimated from the AMS maximum

axes and field observations, should be rotated  $100^{\circ} \pm 43^{\circ}$  ccw. The resulting paleogeography places the sedimentary source area to the southwest of the basin, with the paleocurrent directed to the NE. If the Wrangell terrane did travel along the path postulated by Engebretson et al. (1995, Fig. 43), then possible sedimentary sources are autochthonous sediment from Wrangellia or allochthonous sediment from the Eurasian Plate.

### **Conclusion**

Paleomagnetic results from the Insular Superterrane for the Middle Jurassic to Early Cretaceous were nonexistent (Fig. 4 and Table 1). Revised plate motions for the Pacific basin by Engebretson et al. (1995) suggest a possible northern paleolatitude for terranes traveling on the Kula plate during this time. The paleomagnetic results presented here from the Lower Cretaceous One Tree Formation place Vancouver Island  $28^{\circ}$  (3100km) north of its present location relative to North America. This large amount of northern displacement of west coast terranes during the Late Jurassic or Early Cretaceous is unprecedented. Studies from similarly aged rocks of the Insular Superterrane are warranted.



Table 1. Paleomagnetic Directions From Wrangellia and Connected Terranes

Age Ma	Age Error	D°	I°	$\alpha_{95}$	$\lambda_p$	$\lambda+$	$\lambda-$	Rock-Unit	Terrane	Reference
46	11				49.0			Tolstoi	PN	Stone and Packer (1979)*
50	7	302	84	4.5	78.1	8.9	8.5	Talkeetna Mt. Vol	AX	Panuska et al. (1990)
51	1	350	69	7.0	52.5	11.0	9.2	Flores Vol.	WR*	Irving and Brandon (1990)
59	6	314	63	18.8	44.7	29.6	18.6	Arkose Rdg	AX	Stamatatos et al. (1989)
59	6	248	70	8.2	53.4	13.3	10.8	Chickaloon Fm	AX	Stamatatos et al. (1989)
61	5	143	85	5.4	80.3	9.7	10.2	Cantwell Vol	PN	Hillhouse and Gromme (1982)
70	5	226	51	9.1	31.9	9.4	7.6	McColl Rdg Fm	WR	Panuska (1985)
70	5				19.0			Chingnik/Hoodoo	PN	Stone and Packer (1979)*
76	4	30	43	3.9	24.6	3.1	2.9	Nanaimo Group	WR*	Ward et al. (1997)
78	5	2	58	6.7	38.3	7.9	6.6	Nanaimo Group	WR	Enkin et al. (2001)
79	5				16.0			Chingnik/Hoodoo	PN	Stone and Packer (1979)*
79	2	140	69	6.0	52.5	9.3	8.0	McColl Rdg Fm	WR	Stamatatos et al. (2001)
86	7	285	53	10.8	33.4	11.8	9.1	Powell Cr. Vol.	CB	Wynne et al. (1995)
95	3	323	57	5.3	37.2	5.9	5.2	Silverquick Cong.	CB	Wynne et al. (1995)
95	2	16	49	4.6	30.3	4.3	3.9	Mount Stuart Pluton	CPC	Ague and Brandon (1996)
98	8	30	57	4.9	37.3	5.5	4.8	Spuzzum & Porteau Plutons	CPC	Irving et al. (1985)
104	8	13	53	7.2	33.6	7.6	6.4	Stephens Island Pluton	CPC	Symons (1977)
111	6	21	61	7.1	42.1	9.1	7.6	Captains Cove Pluton	CPC	Symons (1977)
160	14				31.0			Naknek/Chinitna	PN	Stone and Packer (1979)
178	10	8	50	10.2	30.9	10.4	8.2	VI Intrusions	WR*	Symons (1984)
180	10	13	47	5.0	27.9	4.4	3.9	W. Coast Xtlm Cmpx	WR*	Symons (1984)
196	9	276	42	6.0	24.2	4.8	4.3	Bonanza Group	WR*	Irving and Yole (1987)
225	17	74	20	5.9	10.4	3.3	3.2	Nikolai Greenstone	WR	Hillhouse (1977)
229	6	3	33	6.0	18.0	4.1	3.7	Karmutsen Fm	WR*	Irving and Wynne (1990)**
290	34	226	11	14.9	5.5	8.1	7.5	Station Cr. Fm	WR	Panuska and Stone (1981)

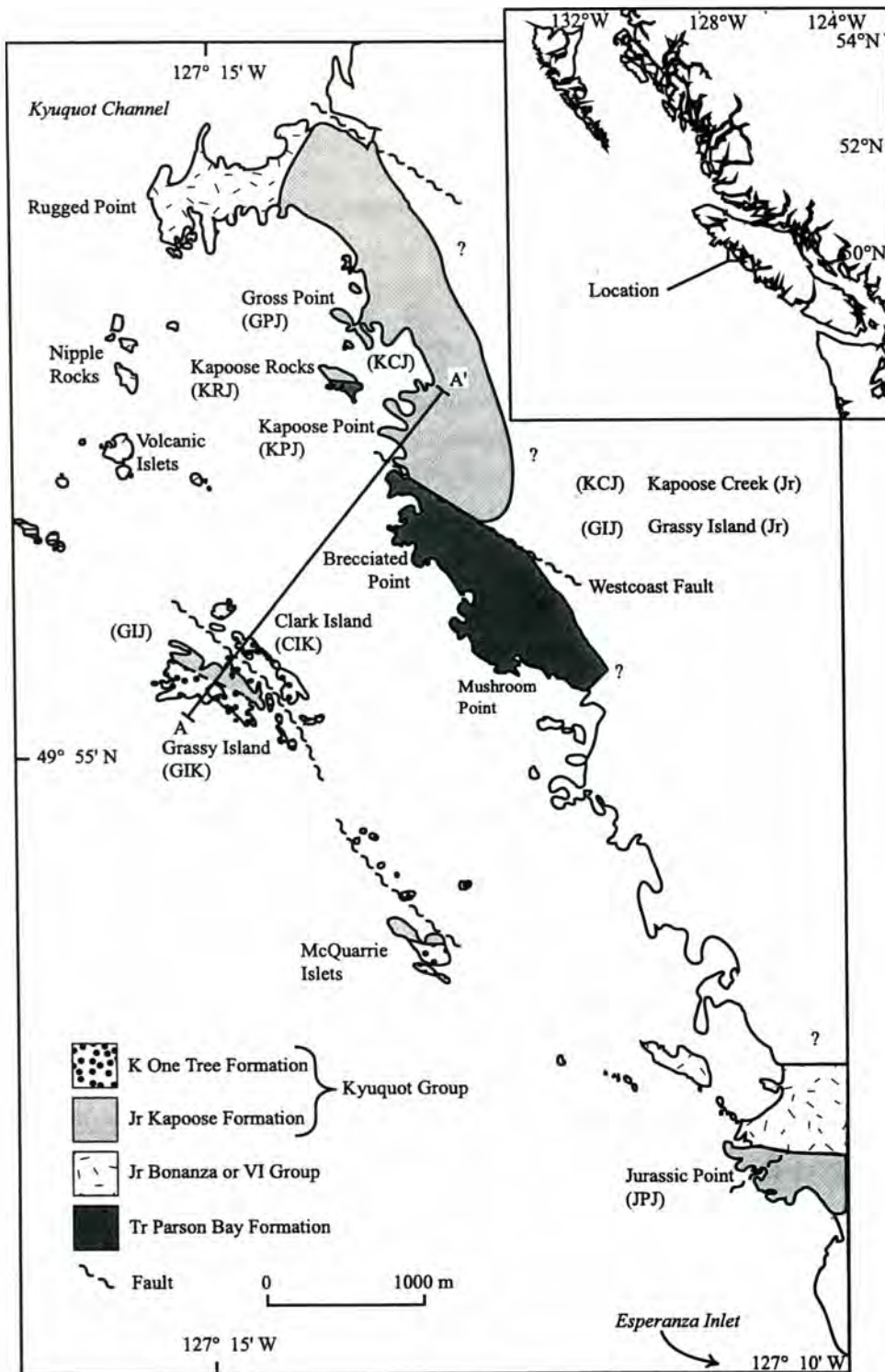
*Notes for table 1:* Columns 1-8 are calculated using data from the original reference or the Global Paleomagnetic Database (McElhinny and Lock, 1990a,b; see also Lock and McElhinny, 1991, and McElhinny and Lock, 1993, 1996).  $D/I$  are the declination and inclination of the mean direction of remanent magnetization;  $\alpha_{95}$  is the radius of the 95% circle of confidence;  $\lambda_p$  is the paleolatitude calculated by the inclination with the associated error limits ( $\lambda+$ ,  $\lambda-$ ). Terrane symbols are as follows: PN Peninsular Terrane; AX Alexander Terrane; WR Wrangell Terrane; WR\* Wrangell Terrane located on Vancouver Island; CB Coast Belt; CPC Coast Plutonic Complex. \*Direction is from Table 1 Panuska and Stone (1985); \*\*Direction is the combined result of Yole & Irving (1980) and Schwarz et al. (1980).

Table 2. Paleomagnetic Results from the Lower Cretaceous One Tree Formation on Grassy Island and Clark Island.

Direction	Un-Rotated Data						Rotation Corrected Data*							
	N	D°	I°	k	$\alpha_{95}$	R	$\lambda_p$	D°	I°	k	$\alpha_{95}$	R	$\lambda_p$	
<b>Grassy Island</b>														
L	0%	17	19	14.2	33.1	6.3	16.5	7.2	89.5	17.5	31.8	6.4	16.5	9.0
	100%		150.8	86	27.4	6.9	16.4	82.0	176.8	85.4	28	6.9	16.4	80.9
L & P	0%	36	18.3	17.5	31.8	4.3	35.2	9.0	91.8	20.2	30.1	4.4	35.2	10.4
	100%		187.1	83.9	23.9	5.0	34.9	77.9	206.8	83.1	24.8	4.9	35.0	76.4
<b>Clark Island</b>														
L	0%	26	26.2	32.2	19.5	6.6	24.7	17.5	88.7	65.6	19.5	6.6	24.7	47.8
	100%		263.4	85.0	27.5	5.5	25.1	80.1	247.9	85.0	27.5	5.5	25.1	80.1
L & P	0%	36	28.1	34.3	18.0	5.8	34.3	18.8	94.4	64.5	18.0	5.8	34.3	46.4
	100%		246.5	85.5	26.5	4.7	34.9	81.1	234.5	85.4	26.6	4.7	34.9	80.9
<b>Reversed</b>														
L & P	0%	5	29.2	30.8	10.0	31.3	4.8	16.6	87.3	62.7	10.0	31.3	4.8	44.1
	100%		49.2	79.3	31.3	17.2	4.9	69.3	28.5	75.9	37.8	15.7	4.9	63.3
<b>Combined Results</b>														
All L	0%	45	23.2	25.2	7.1	8.6	38.8	13.2	90.1	45.6	4.9	10.7	36.1	27.0
	100%		229.4	86.4	8.0	8.0	39.5	82.8	220.2	85.1	8.1	8.0	39.6	80.3
All P	0%	32	29.1	34.9	18.6	6.1	31.2	19.2	101.4	34.2	14.2	7.0	30.9	18.8
	100%		186.5	79.7	24.3	5.3	31.4	70.0	207.7	80.7	22.2	5.6	31.3	71.9
All L & P	0%	77	24.2	27.2	17.5	4.0	73.6	14.4	92.5	43.5	8.5	5.8	70.0	25.4
	100%		207.5	86.3	24.7	3.3	74.6	82.6	214.4	85.6	25.2	3.3	74.6	81.3

Notes for Table 2: L, lines; P, great circle planes; N, number of samples; D°, declination; I°, inclination; k Fisher's precision parameter;  $\alpha_{95}$ , 95% confidence circle; R, Fisher's resultant vector length;  $\lambda_p$ , paleolatitude.

\*Rotation corrected data are first rotated to correct for fold plunge (Grassy Island data rotated 46° cw about a horizontal axis trending 210°, Clark Island data rotated 55° cw about a horizontal axis trending 267°), then the Grassy Island fold axis is rotated about a vertical axis (57° cw) to match the trend of the Clark Island fold axis (Fig. 15)



**Figure 1.** Sketch map showing the extent of the Kyuquot Group and regional geology (modified map from Jeletzky, 1950). Sampling locations are identified with the three-letter acronym used to name the samples. Westcoast fault location is from Muller et. al (1981).

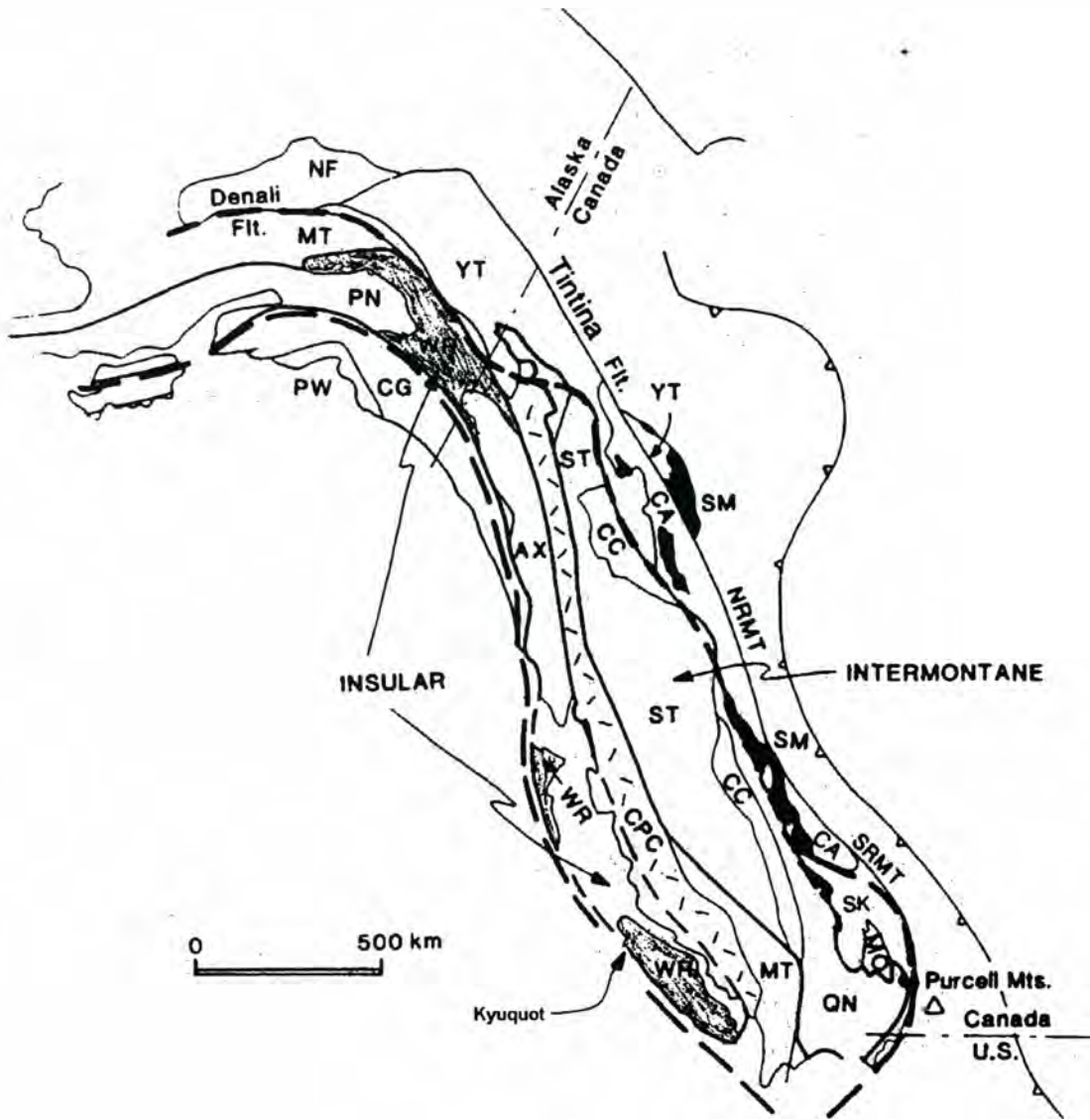


**Figure 2.** Major terranes of western Canada and southern Alaska. Wide dashed lines show margin of Baja BC. Terrane abbreviations: Alexander (AX), Cassiar (CA), Cache Creek (CC), Chugach (CG), Miniterranes (MT), Monashee (MO), Nixon Fork (NF), Penninsular (PN), Quesnellia (QN), Selkirk (SK), Slide Mountain (SM), Stikine (ST), Wrangellia (WR), Yukon-Tanana (YT), SM in black, Coast Plutonic Complex, CPC (Modified figure and text from Umhoefer, 1987).



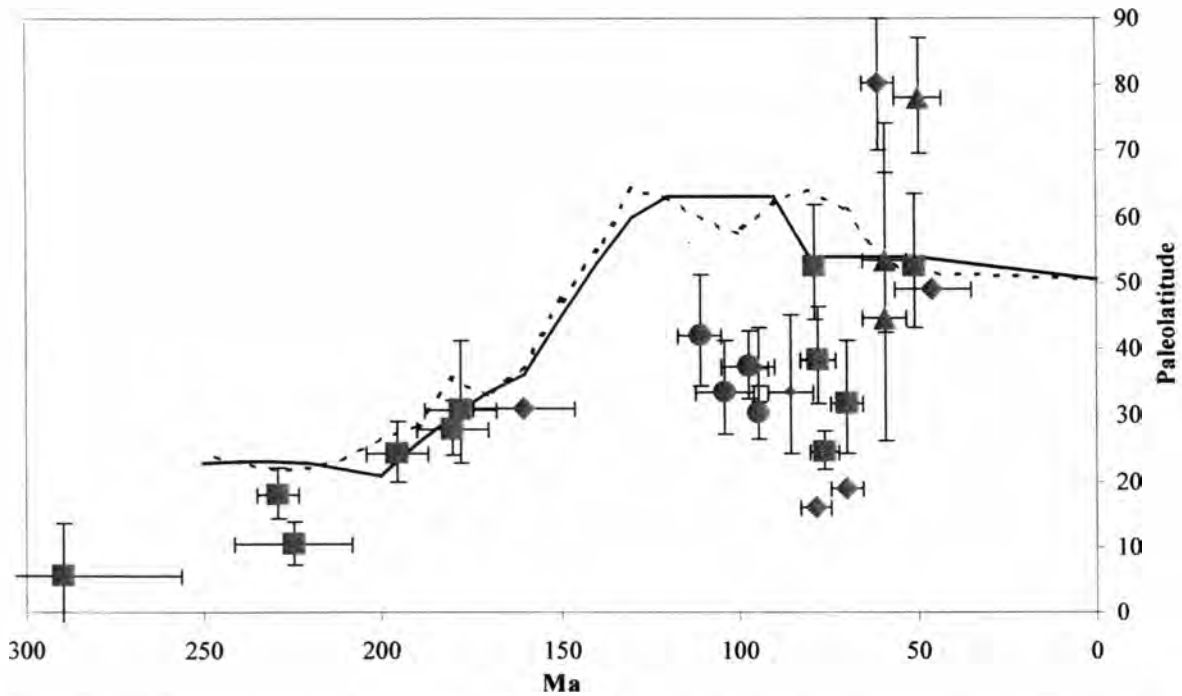


**Figure 4.** Paleomagnetic paleolatitudes from Wrangellia and connected terranes plotted using the data shown in Table 1. Also shown are the expected paleolatitude North American paleolatitude paths from Beck and Housen (2000, blue solid) and Van der Voo and Torsvik (2001, red dashed). ■ - Wrangell Terrane (WR); ▲ - Alexander Terrane (AX); ◆ - Peninsular Terrane (PN); ● - Coast Plutonic Complex (CPC); • - Coast Belt (CB).





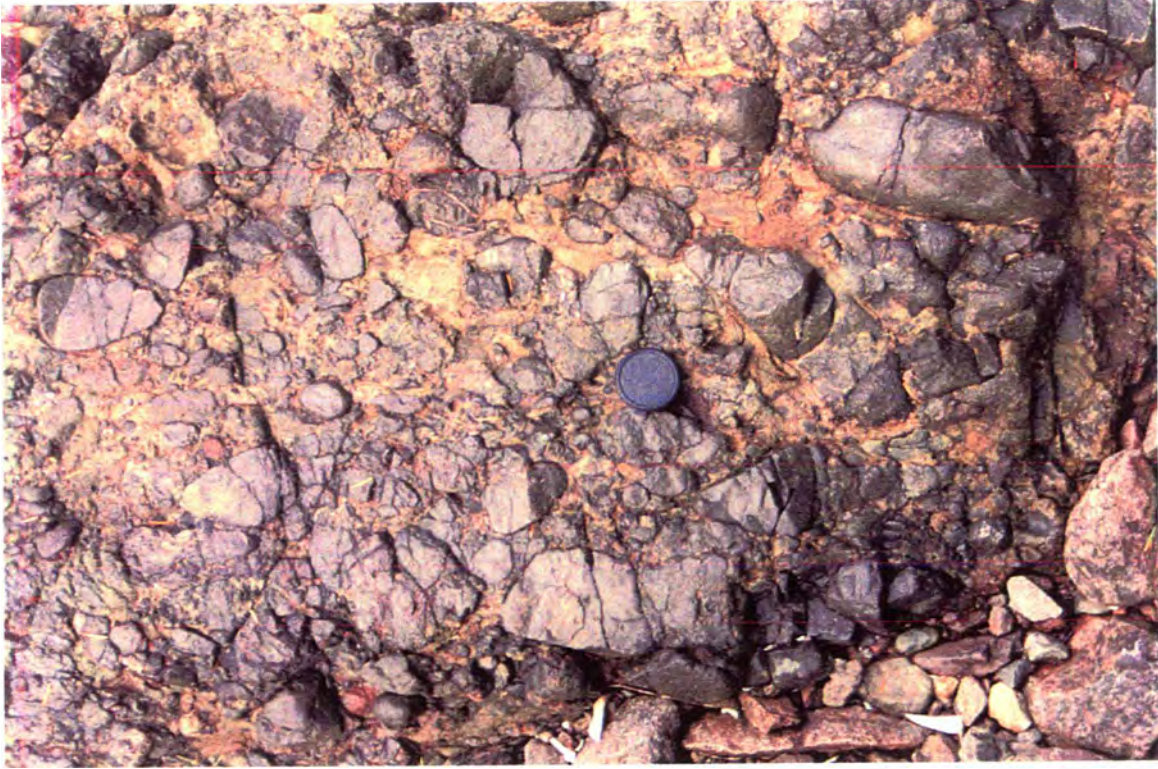


**Figure 6.** Photograph of the basal conglomerate of the Kaposse Formation located at McLean Cove (see Fig., 1). The conglomerates are over 20 meters thick at this location. The lens cap is 52mm in diameter.



**Figure 7.** Photograph of the basal conglomerate at the contact between the Upper Triassic Parson Bay Formation and the Upper Jurassic Kapoose Formation, located on Kapoose Rocks. Hammer handle is 35cm long.



**Figure 8.** Photograph of a conglomerate at Jurassic Point. The bed is approximately 1/2 meter thick and has been offset by numerous faults (shown as black lines).

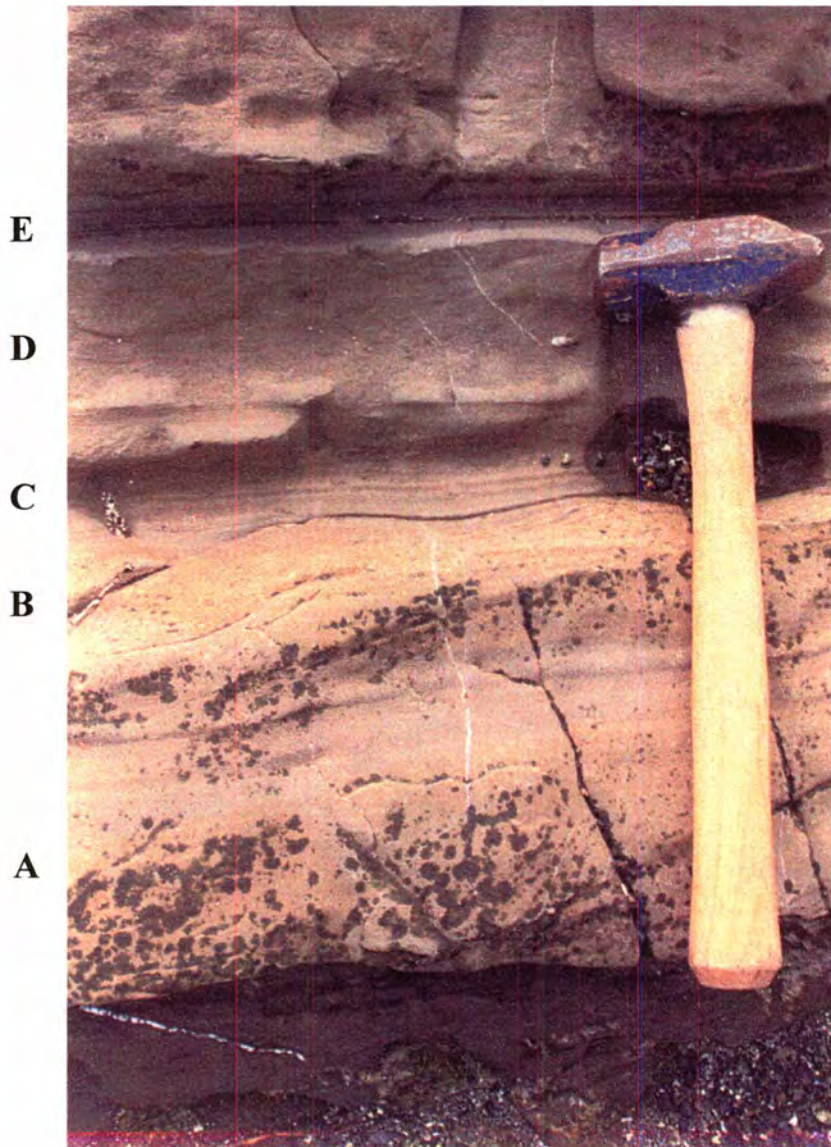


**Figure 9.** Photograph of a complete Bouma sequence seen in the Upper Jurassic Kapoose Formation at Jurassic Point.



**Figure 10.** Photograph of the basal fossiliferous conglomerate of the Lower Cretaceous One Tree Formation where it contacts the Upper Jurassic Kapoose Formation on Grassy Island. Note belemnoid fossils.



**Figure 11.** Photograph of steeply dipping beds of the Lower Cretaceous One Tree Formation on Grassy Island. Note the gentle syncline that curves the beds off to the right into the background. The individual beds in the foreground are approximately  $\frac{1}{2}$  meter thick. Photograph was taken from the western most part of the island facing east toward the “grassy” part of the island.



**Figure 12.** Photograph of small-scale faulting near the northwest end of Grassy Island. Photo was taken facing along strike to the east.

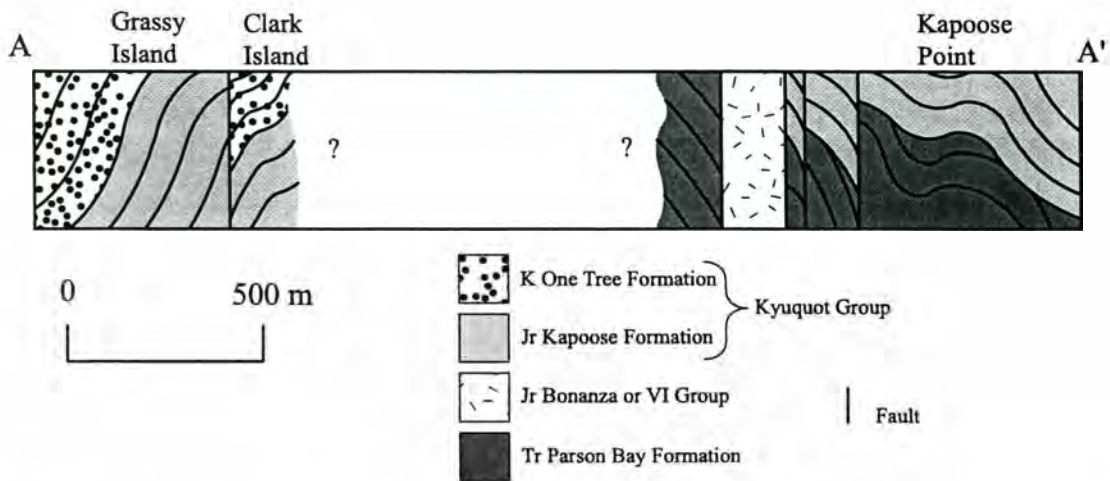


**Figure 13.** Schematic cross-section through the line A - A' on Figure 1. The cross-section is derived from the map provided in Jeletzky (1950). It is assumed by Muller et al. (1981) that the faults are vertical. It is assumed here that all the faults shown in this cross section are strands of the Westcoast Fault System (see text).



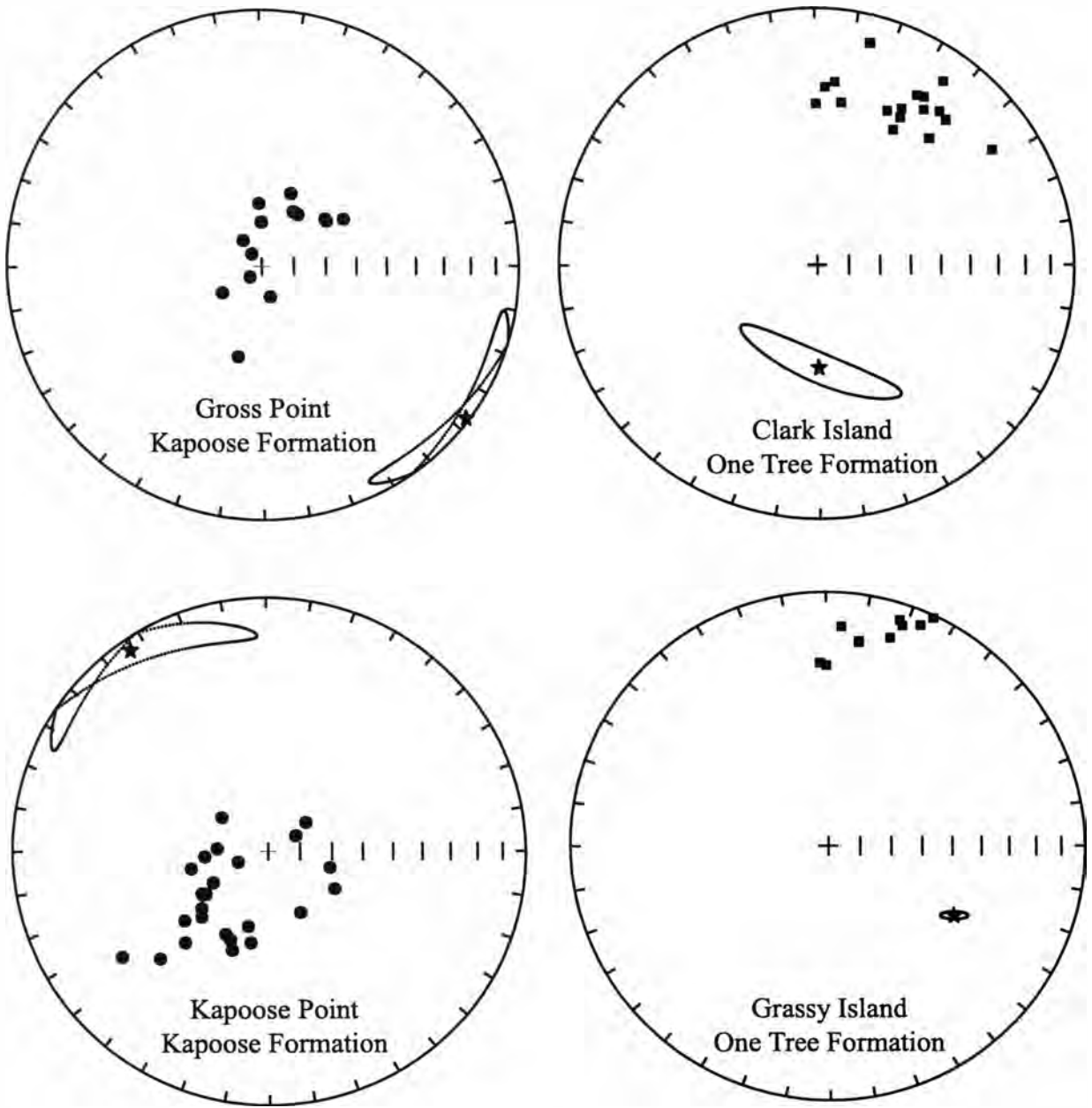


**Figure 14.** Lower hemisphere equal area plots of poles to the bedding orientations collected from the field and from the map provided by Jeletzky (1950), shown with the best fit fold axis (star) with the corresponding 95% simple bootstrap ellipses using a method adopted from the Tauxe (1998) `boot_di.exe` program.

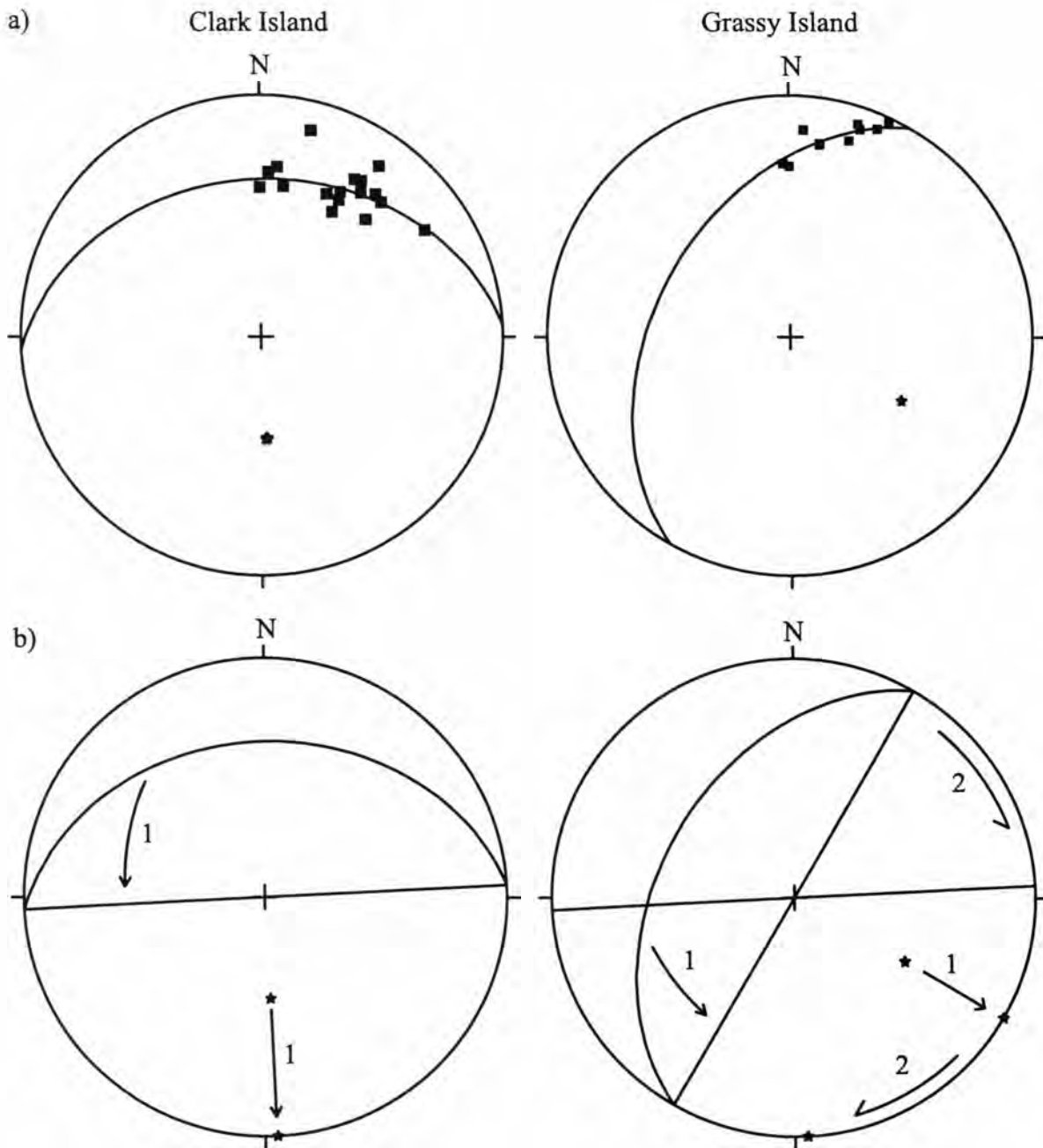


**Figure 15.** Lower hemisphere equal area plots showing the fold axis plunge and rotation corrections used to correct the Cretaceous One Tree Formation on Grassy Island and Clark Island for a suspected small block rotation. a) Poles to bedding measured in the field are shown with a girdle fit through the poles (from Fig. 14). The stars are the poles to the girdles, which are assumed to be the same fold axis before the block rotation. b) In step 1, the fold plunge is removed. The fold axis of Grassy Island is rotated  $46^\circ$  cw about an axis trending  $210^\circ$  and the Clark Island fold axis is rotated  $55^\circ$  cw about an axis trending  $267^\circ$ . In step 2, the Grassy Island fold axis is rotated about a vertical axis  $57^\circ$  cw to match the Clark Island fold azimuth.

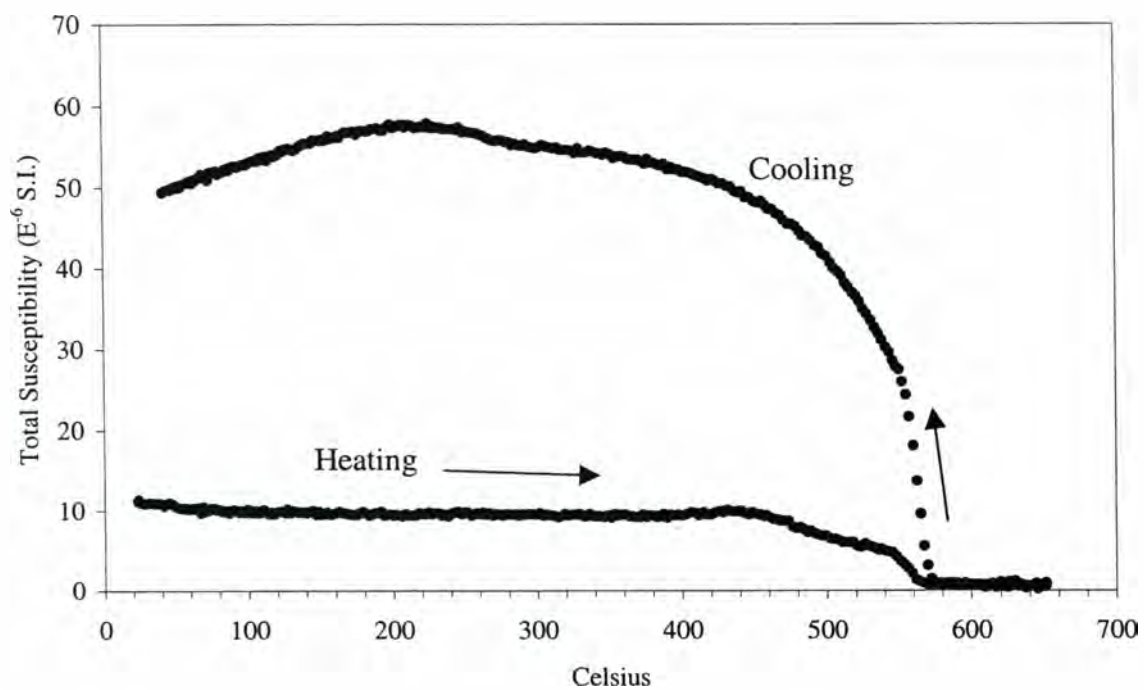


**Figure 16.** Typical thermomagnetic susceptibility heating and cooling curves. An increase in susceptibility after heating occurred in all the specimens measured in these experiments.

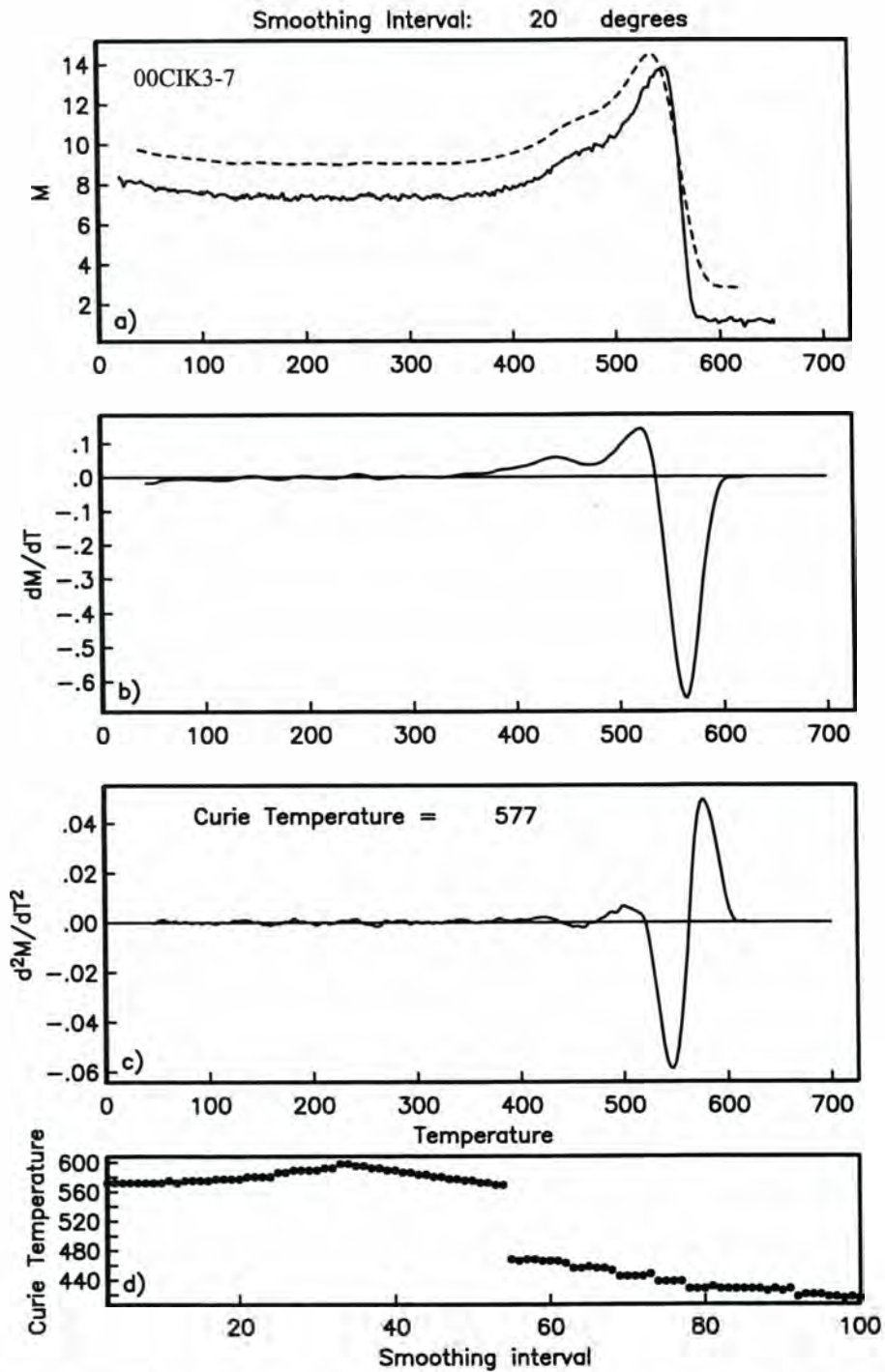


**Figure 17.** Derivative of a typical thermomagnetic heating curve for a specimen from the Lower Cretaceous One Tree Formation. The second derivative shows a peak at 577° C, indicates magnetite is the primary magnetic mineral (using Tauxe's (1998) curie.exe program).

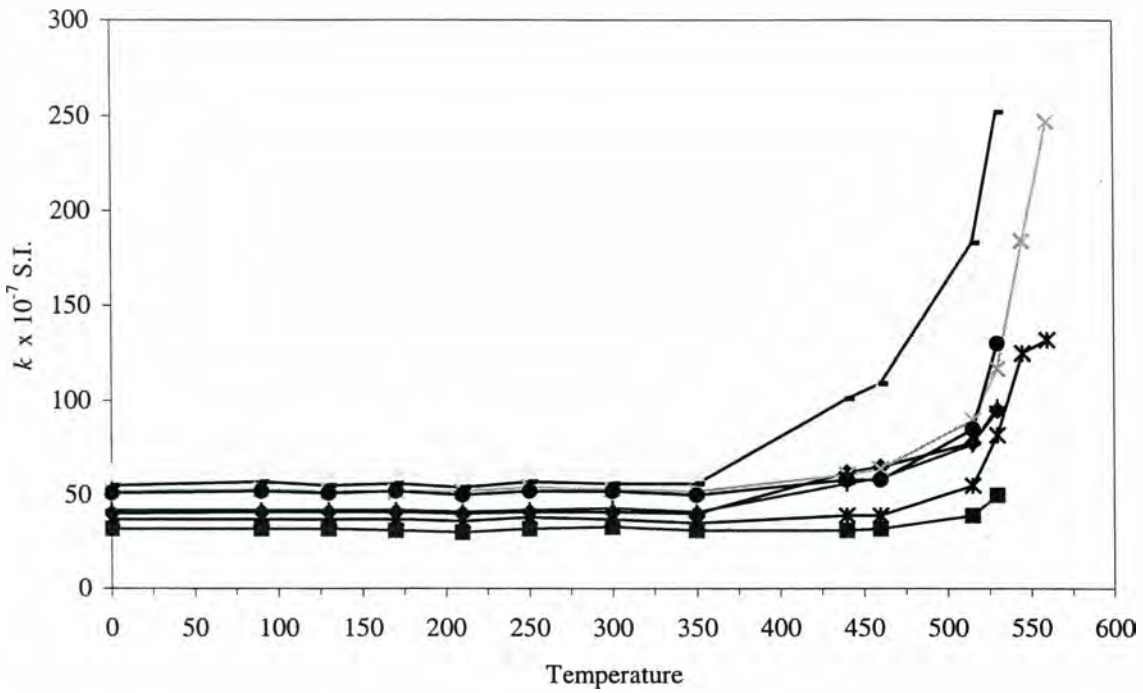


**Figure 18.** Plot of typical magnetic susceptibility patterns observed during thermal demagnetization. Magnetic susceptibility was measured after each thermal demagnetization step. Note the increasing magnetic susceptibility above 400-450°C.

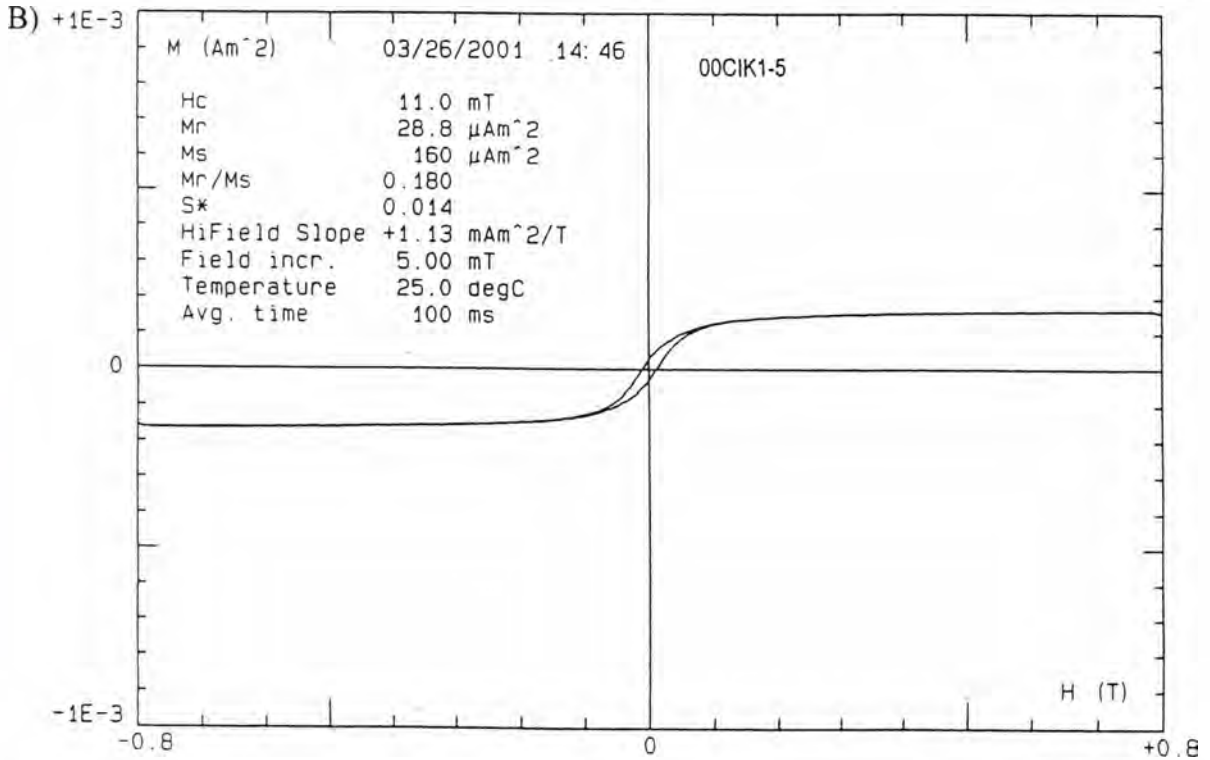
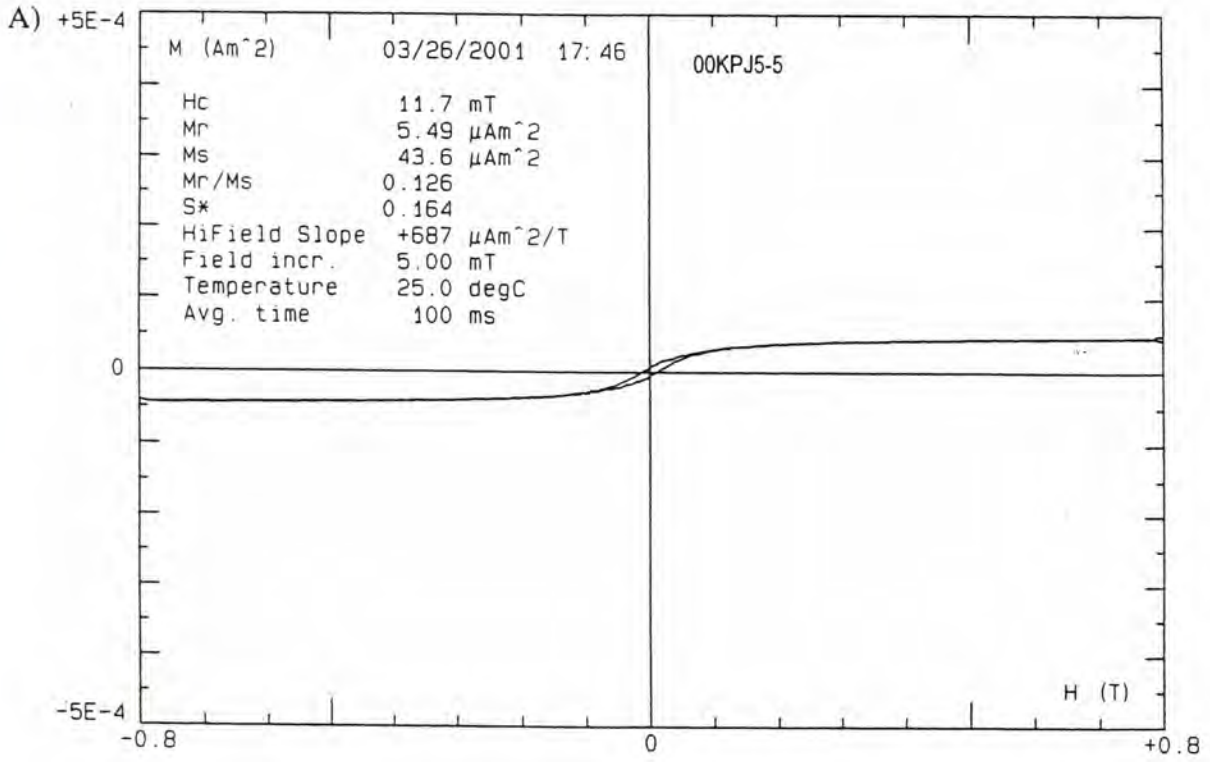


**Figure 19.** Typical hysteresis curves for A) the Kapoose Formation, and B) the One Tree Formation.

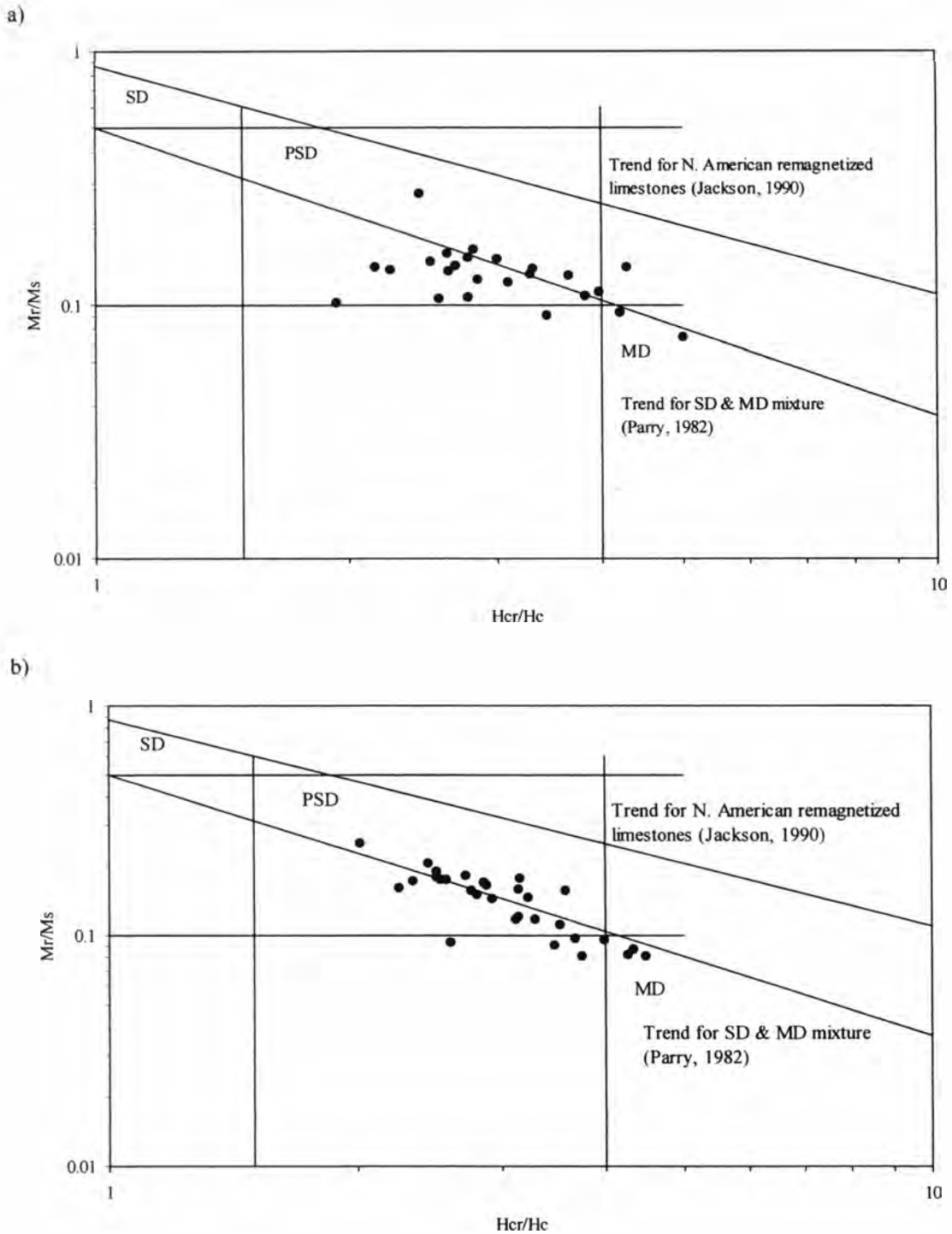


**Figure 20.** Bi-logarithmic Day et al. (1977) plots for a) samples from the Upper Jurassic Kapoose Formation and b) specimens from the Lower Cretaceous One Tree Formation. Both trends fall along the mixing trend for single domain (SD) and multidomain (MD) magnetites, and not the trend from superparamagnetic-influenced limestones. The majority of samples lie in the pseudo-single domain magnetite field (PSD).





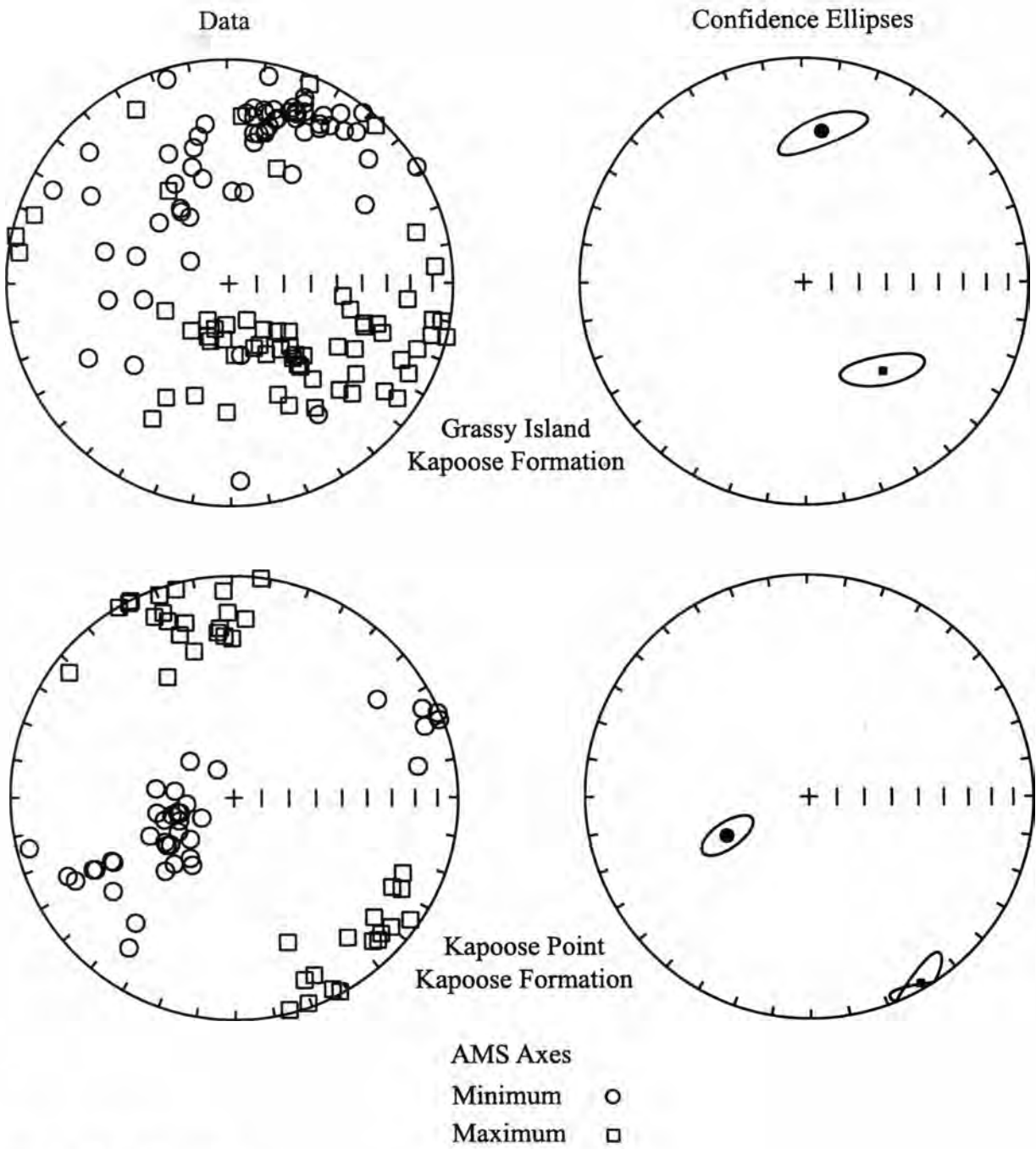
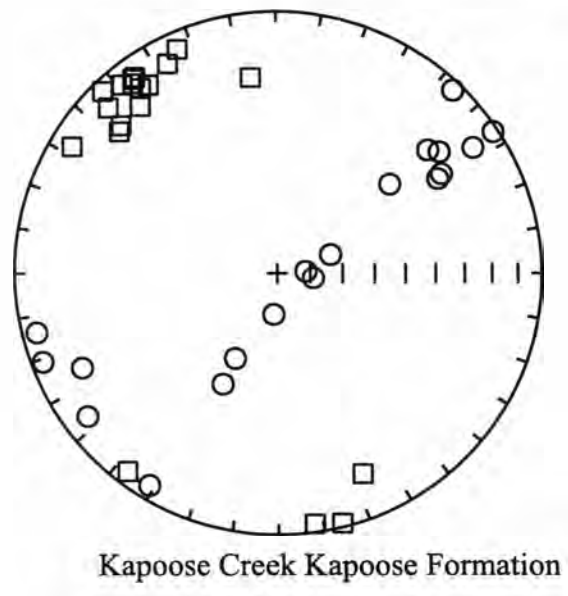
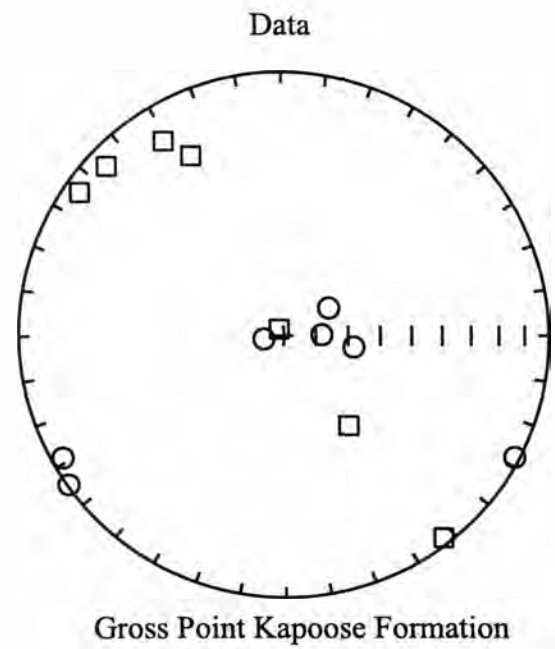
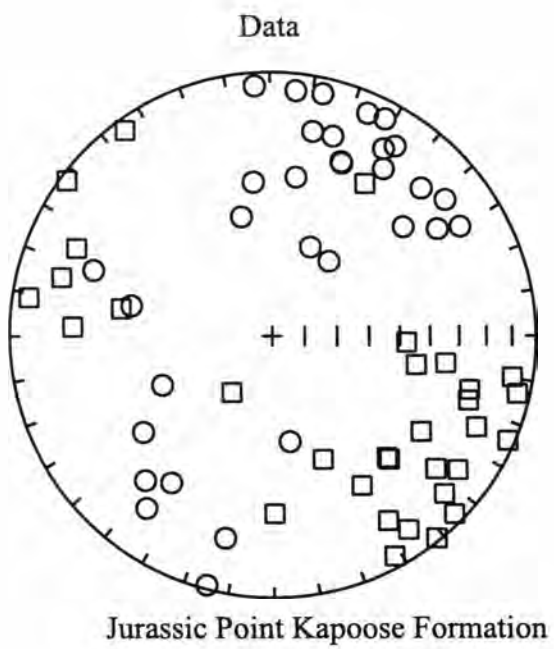


Figure 21 (Cont'd).



AMS Axes  
 Minimum ○  
 Maximum □

**Figure 21 (Cont'd).**

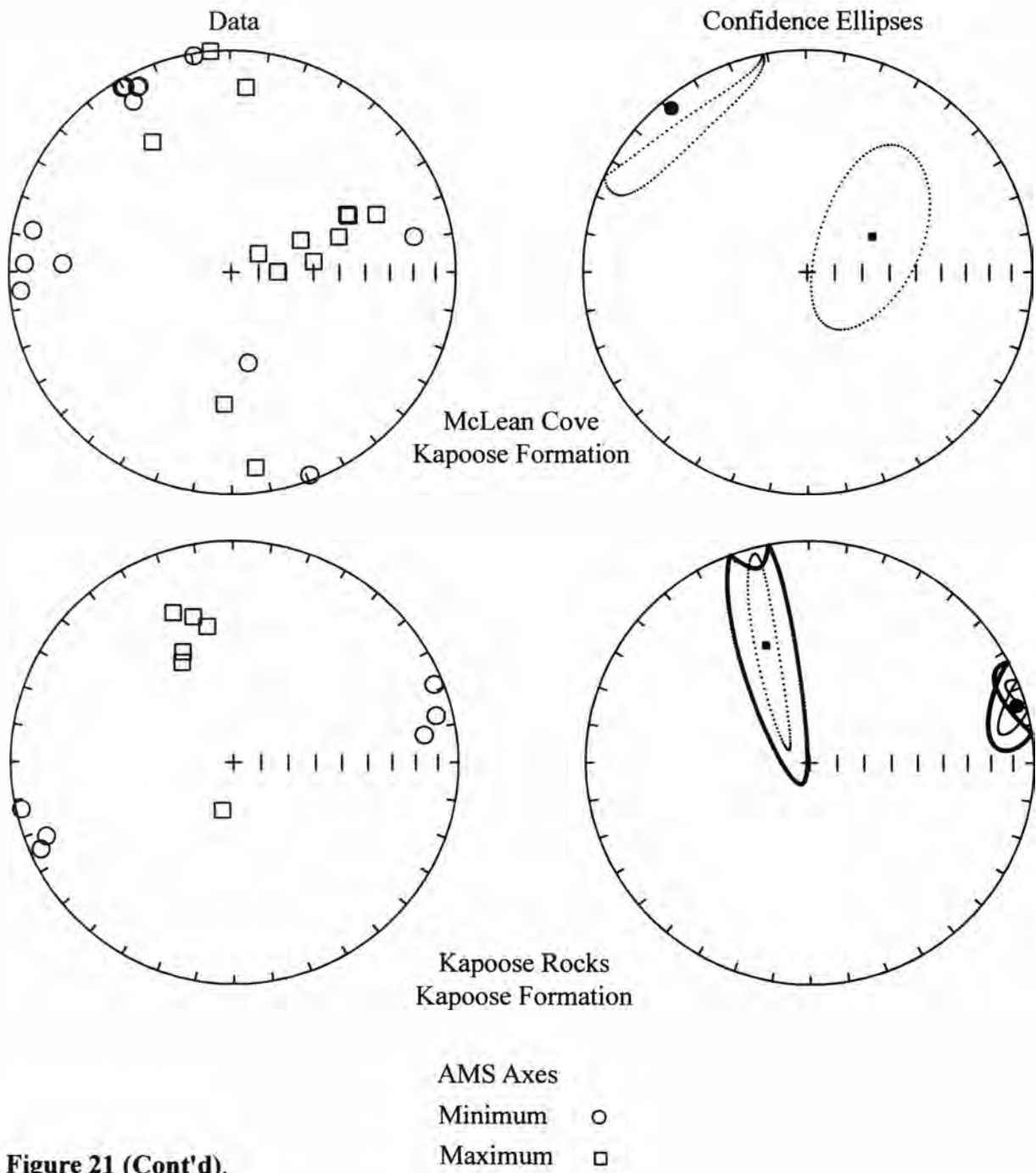
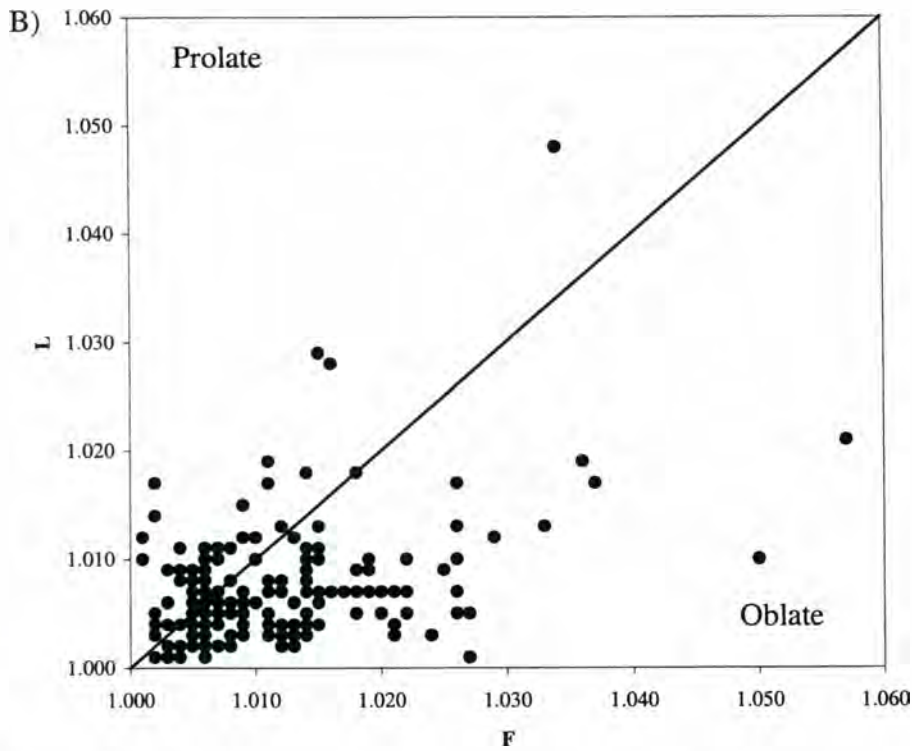
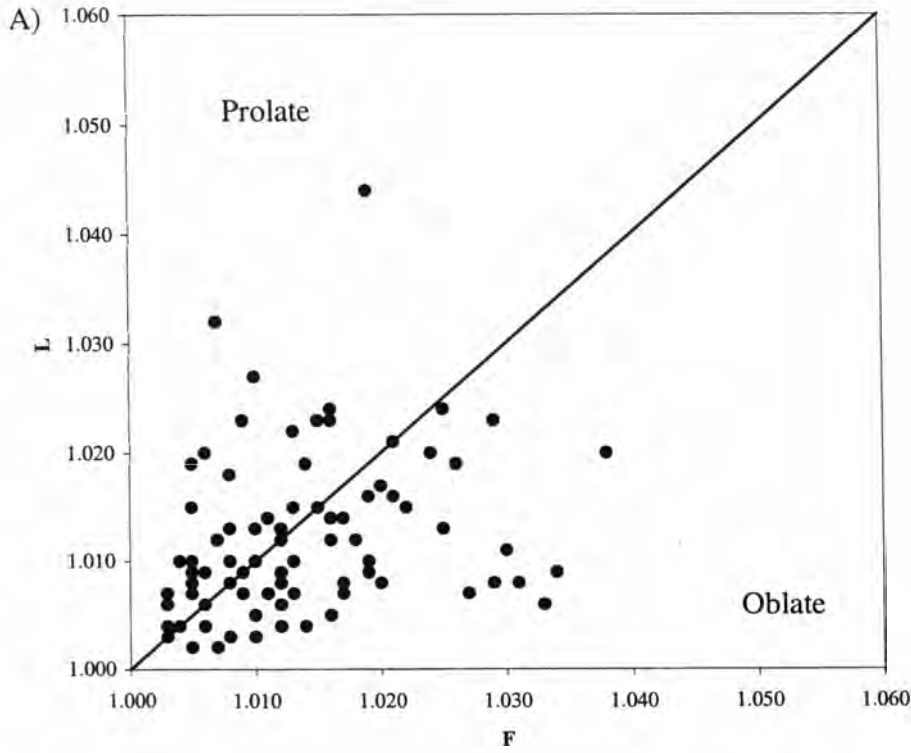
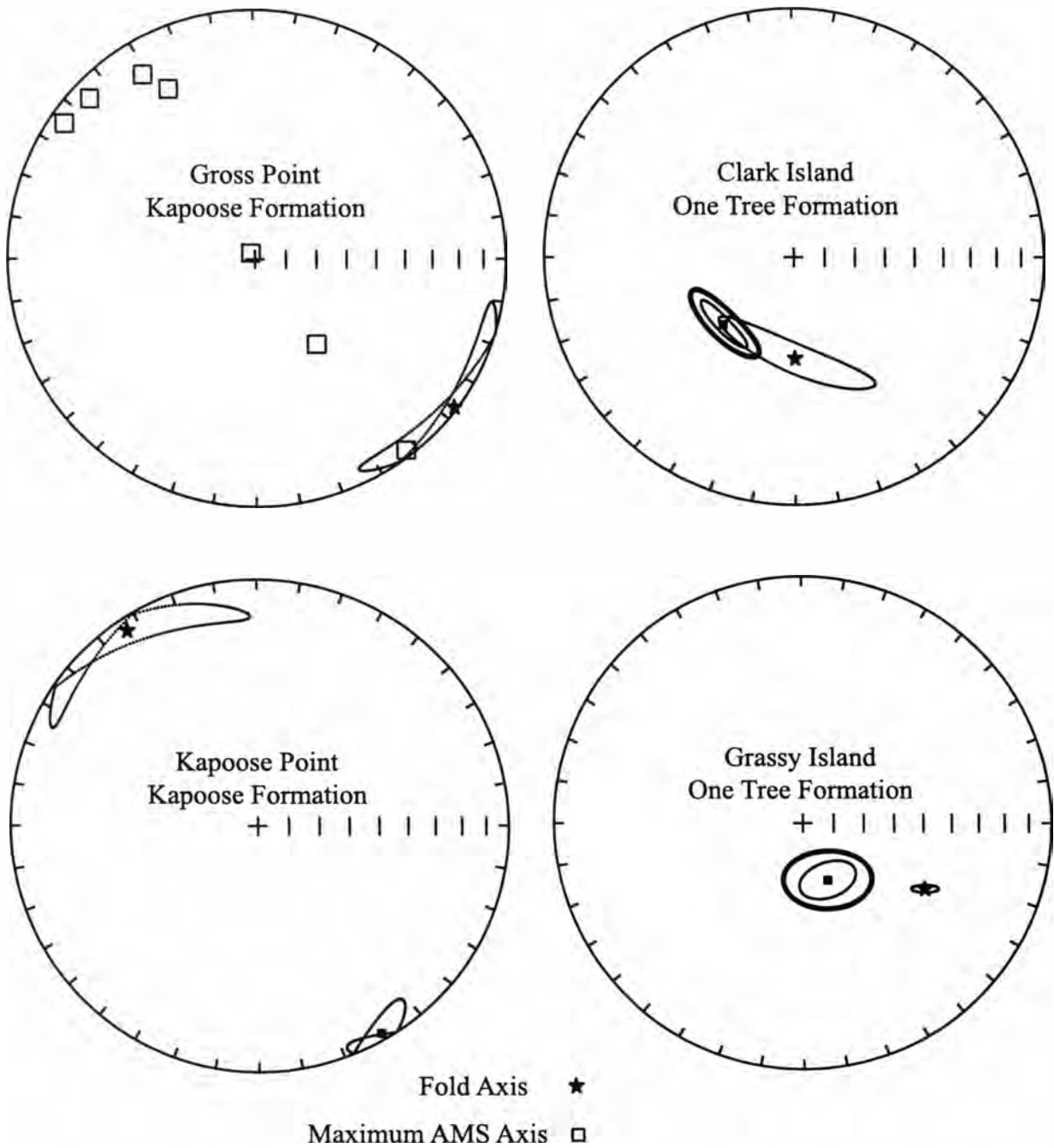


Figure 21 (Cont'd).



**Figure 22.** Flinn (1963) diagrams of the anisotropy of magnetic susceptibility measured for the A) One Tree Formation, and B) Kapoose Formation.



**Figure 23.** Comparison between the in situ principal AMS axes from Figure 21 and the fold axes from Figure 14. Lower hemisphere equal area plots of in situ AMS data from the localities shown in Figure 1. 95% confidence ellipses are shown for data with significant clustering; smaller ellipses are simple bootstrap and larger ellipses are parametric bootstrap. Plotted using the Tauxe (1998) plotams.exe program.

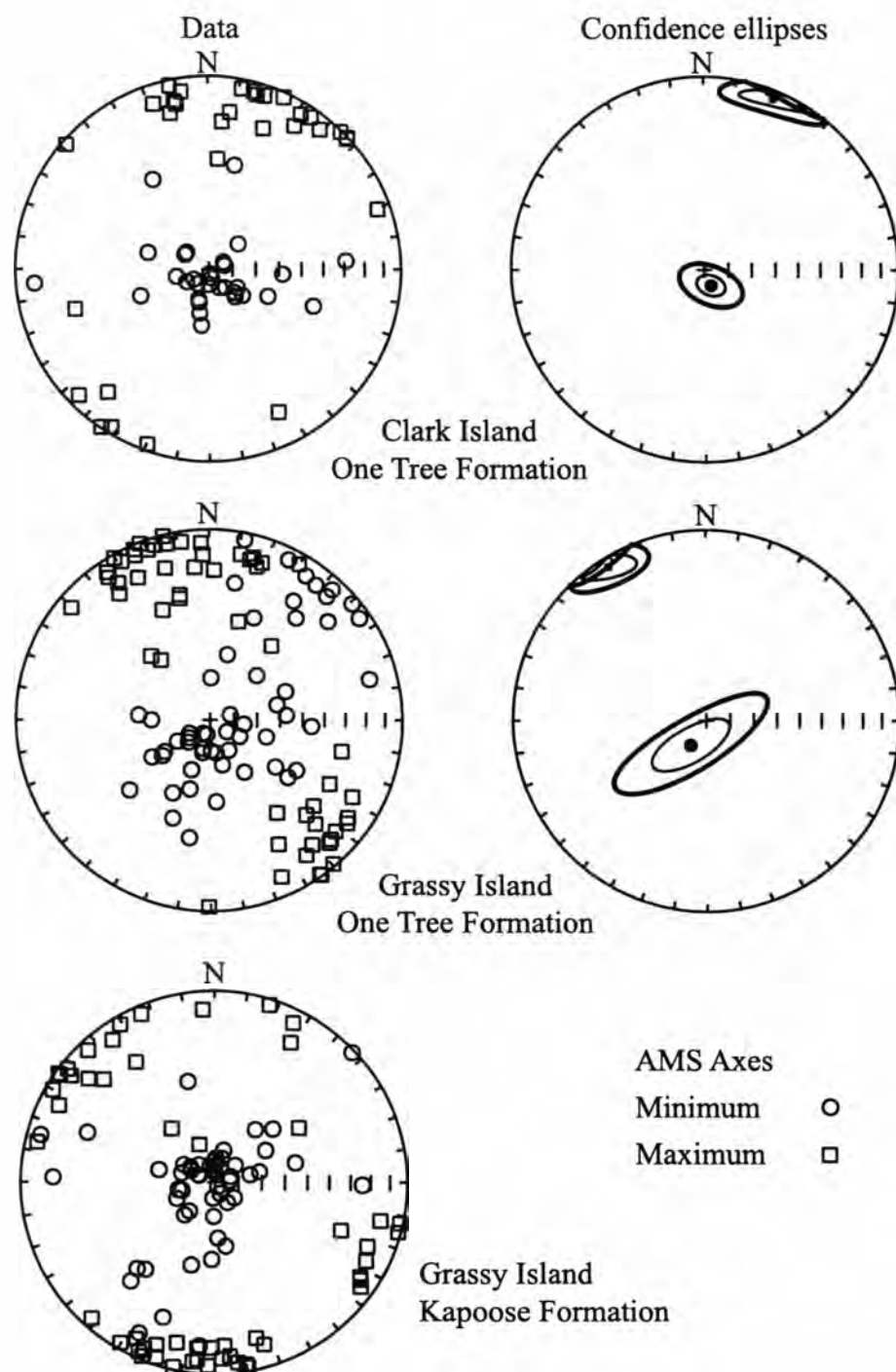


**Figure 24.** Lower hemisphere equal area plots of AMS data from the locations shown in Figure 1. The data from the One Tree Formation are corrected to paleohorizontal after correction for fold plunge (Fig. 15b, step 2). The AMS data from the Kapoose Formation are corrected to paleohorizontal using bedding orientation without correction for fold plunge. 95% confidence ellipses are shown for data with significant clustering; smaller ellipses are simple bootstrap and larger ellipses are parametric bootstrap. Plotted using the Tauxe (1998) `plotams.exe` program.

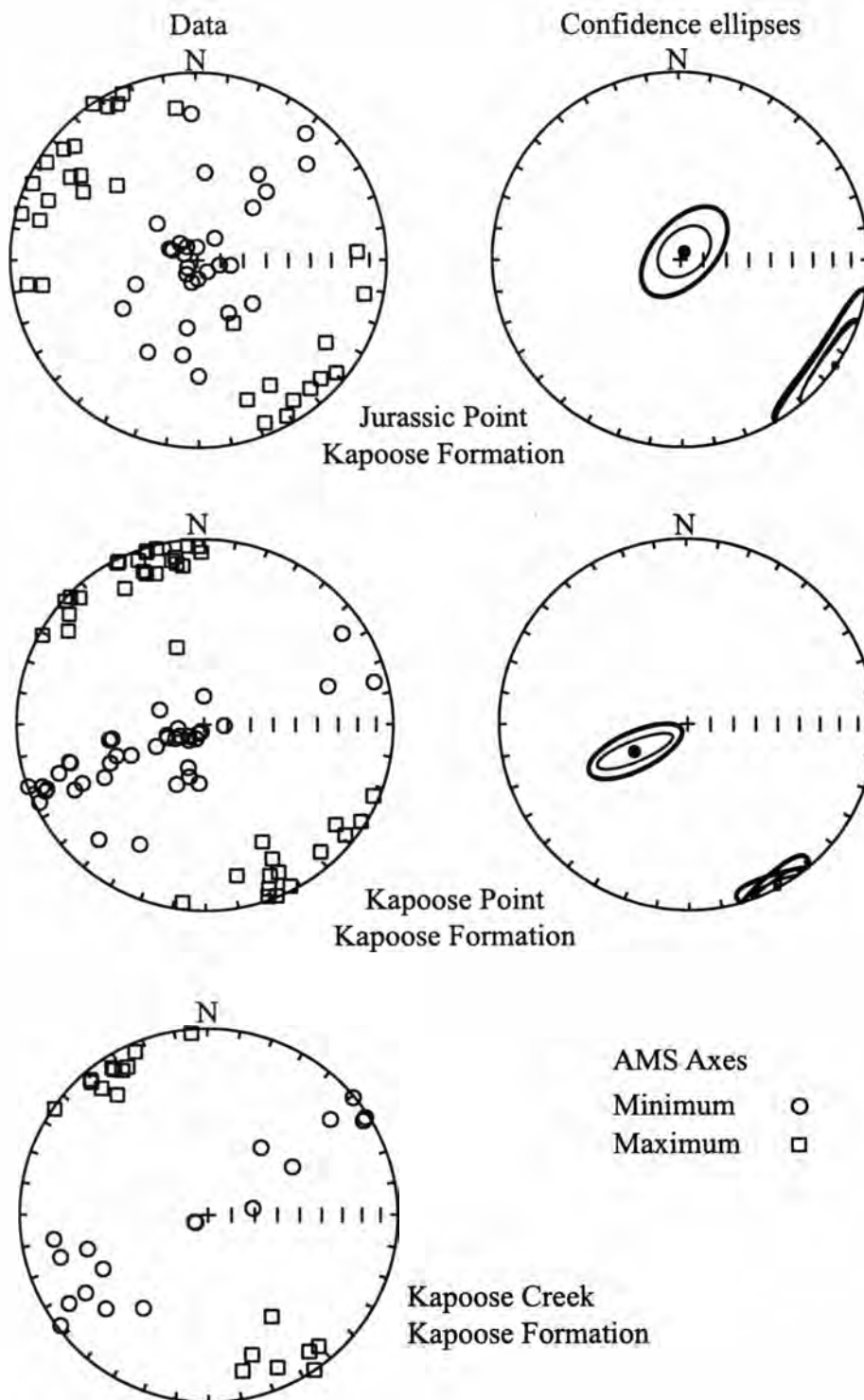


Figure 24 (Cont'd).

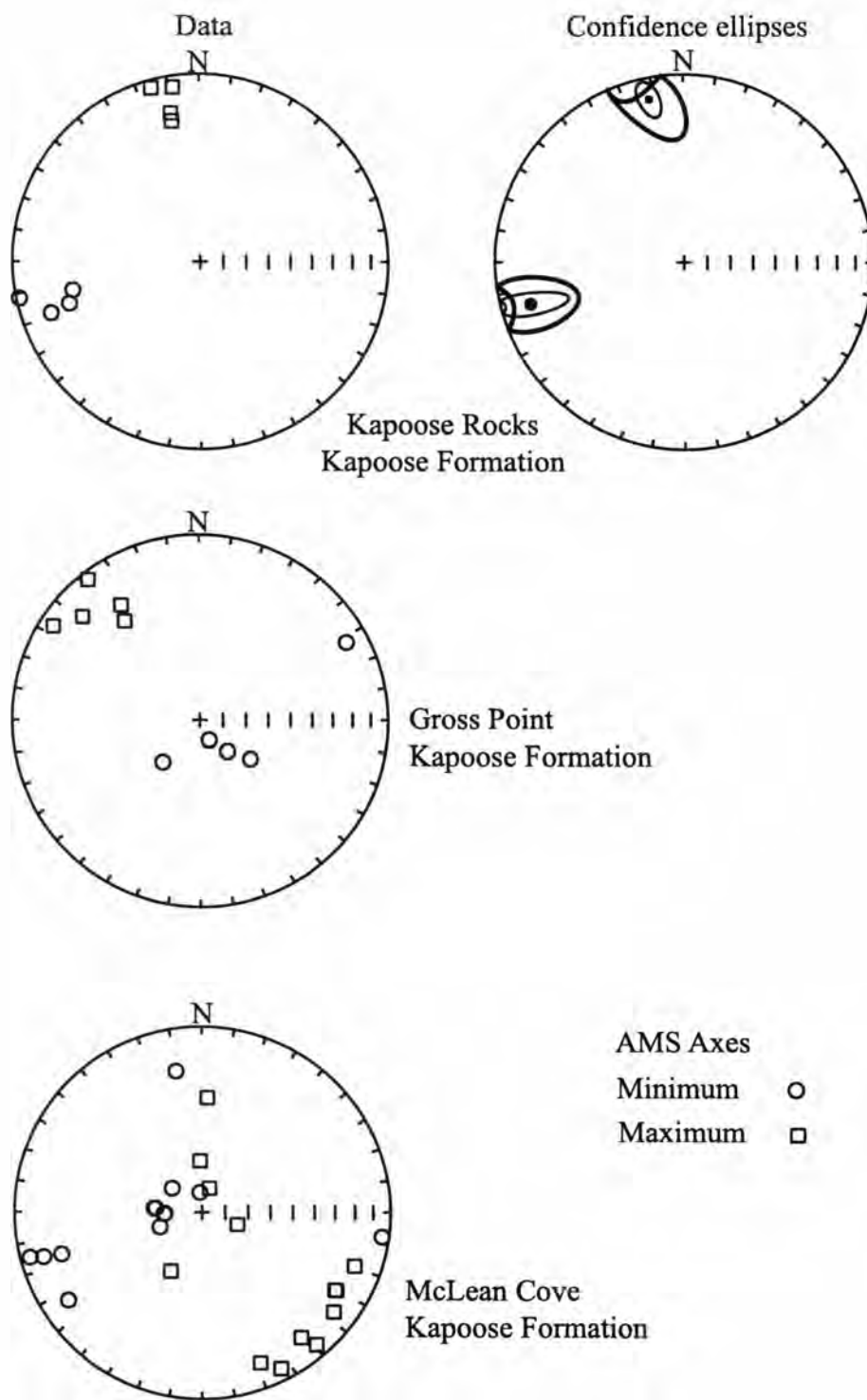
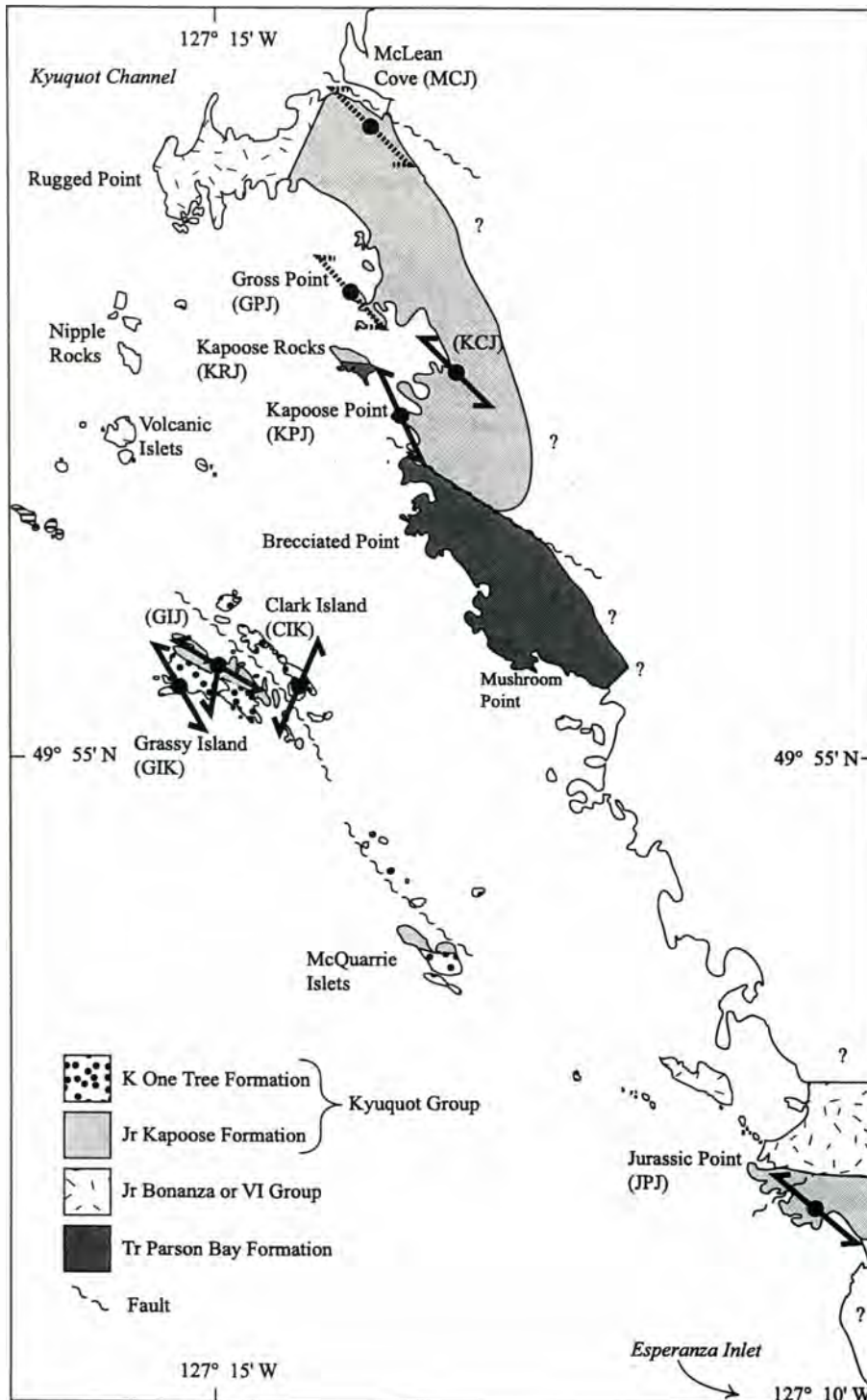
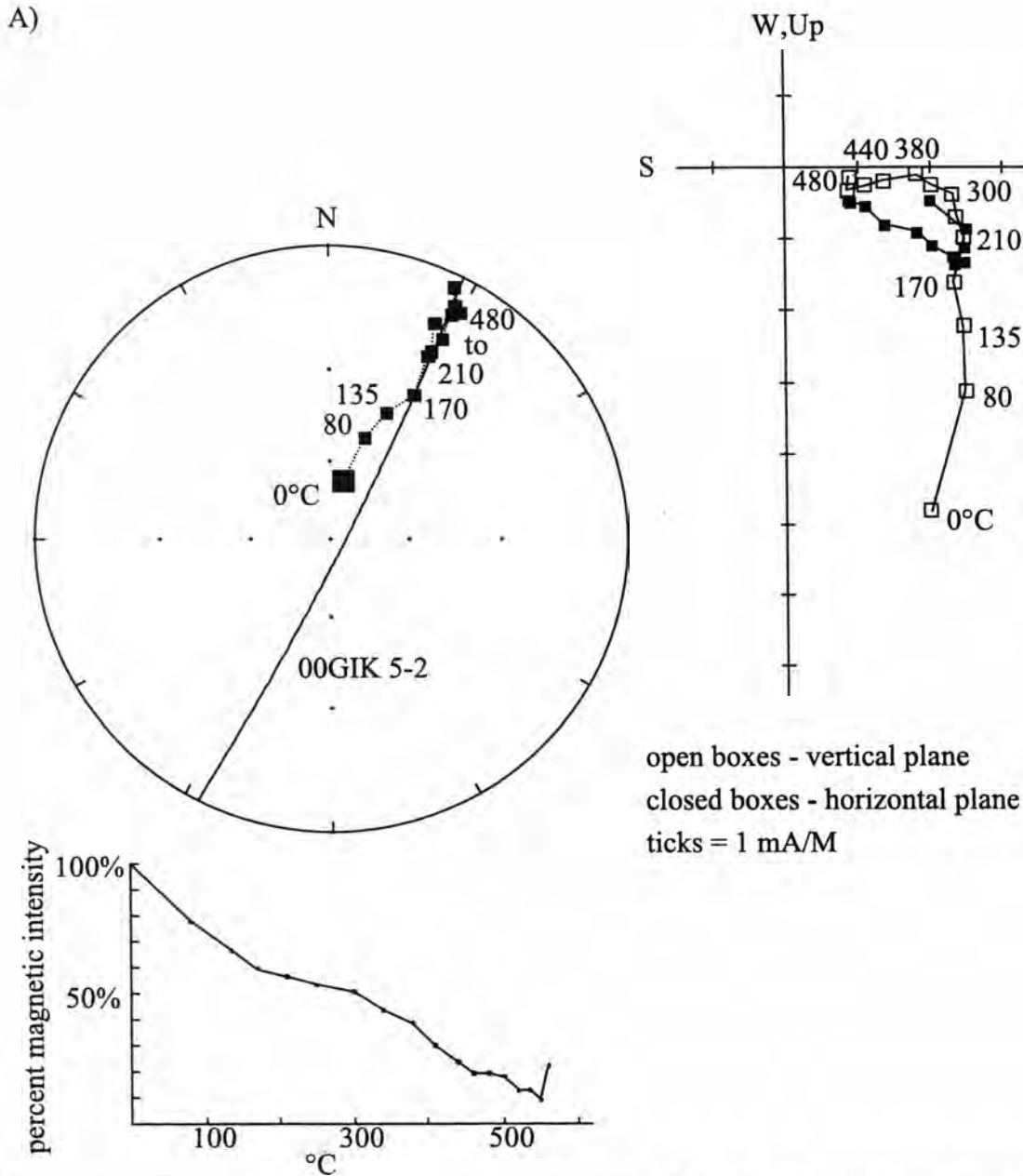


Figure 24 (Cont'd).





**Figure 25.** Location map from Figure 1 showing the AMS mean maximum axes (arrows) from Figure 24. Dashed arrows are for locations with insufficient data. The GIJ location is the only location showing a bimodal maximum axis distribution.



**Figure 26.** Typical multi component demagnetization behavior for specimens from both the One Tree Formation (A &B) and the Kapoose Formation (C). Demagnetization paths are shown on lower hemisphere equal area plots and Zijderveld plots along with the percent magnetic intensity vs. temperature plots. A) Typical demagnetization path that shows a streak along the equal area plot is defined by two components; a low unblocking temperature ( $T_{ub}$ ) component and a high  $T_{ub}$  component. A great circle fit is shown through steps 170-480°C. B) Typical demagnetization path showing the influence of multiple components with a line fittable path of the high  $T_{ub}$  component from 380-500°C and a low  $T_{ub}$  component from 80-210°C. C) Typical demagnetization path from the Kapoose Formation that has a line fittable high  $T_{ub}$  component from 230-480°C and a low  $T_{ub}$  component from 80-230°C.

B)

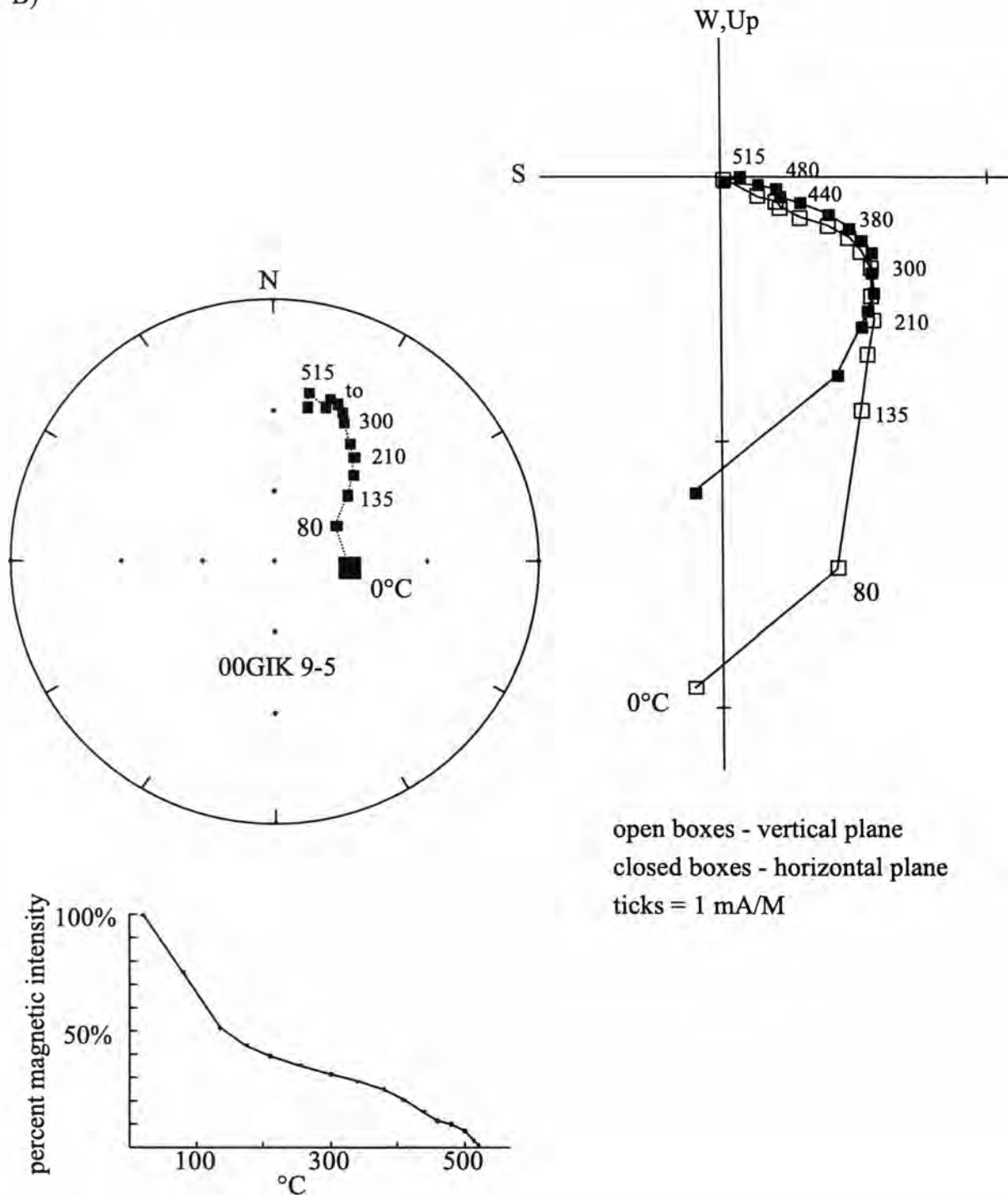


Figure 26 (Cont'd).

C)

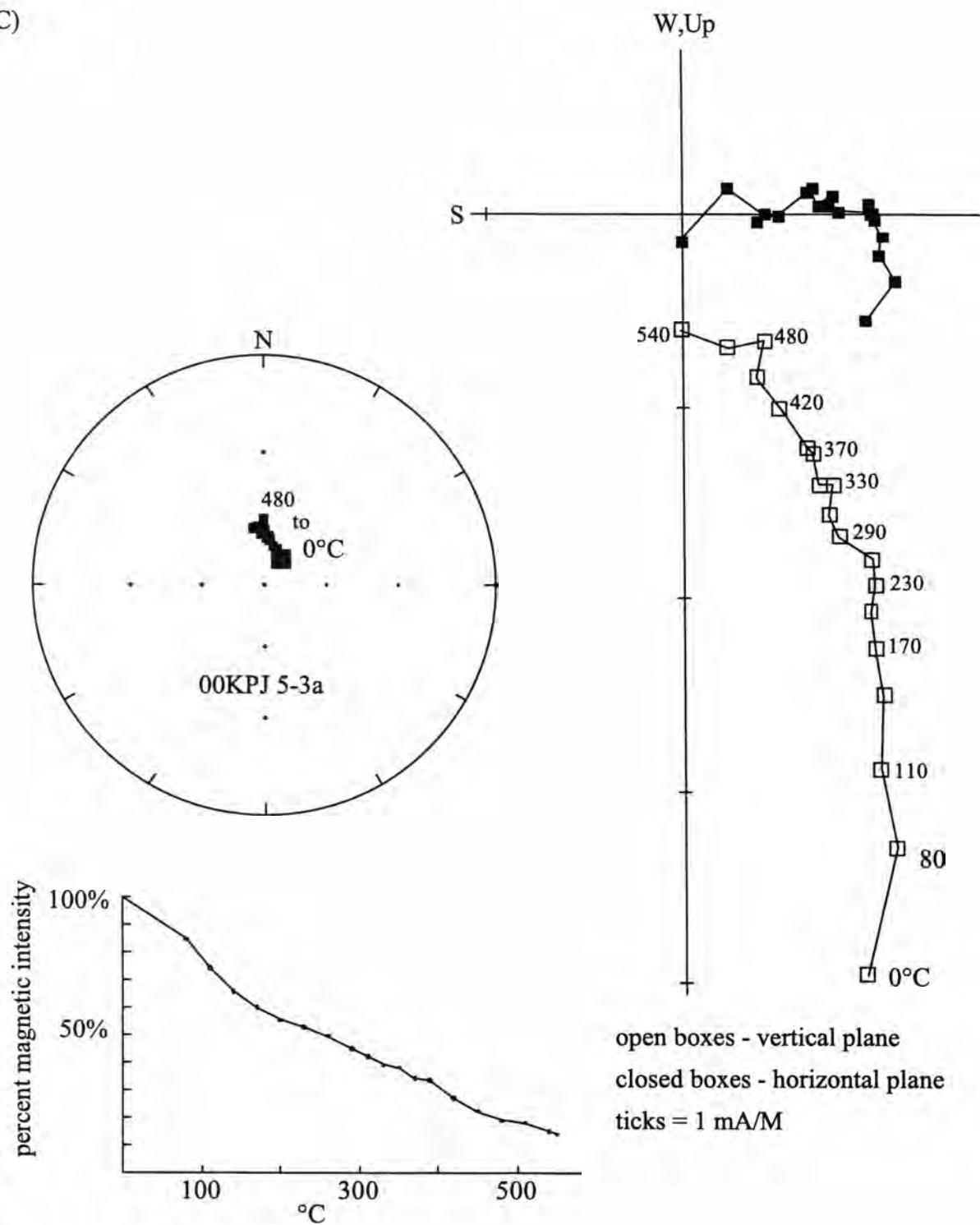
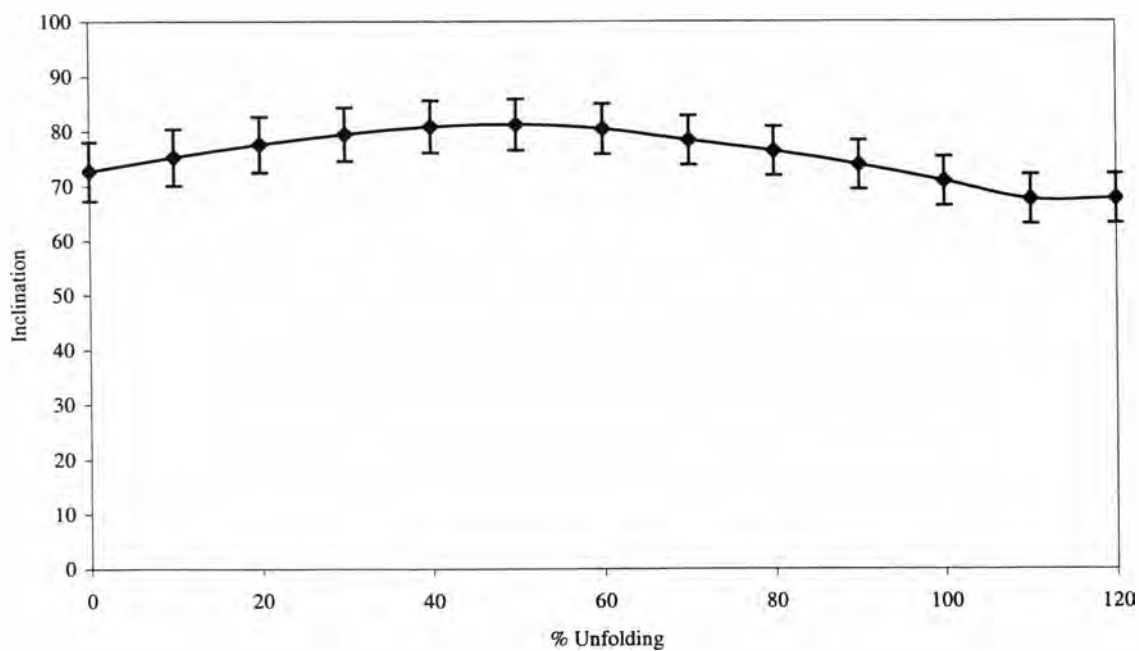
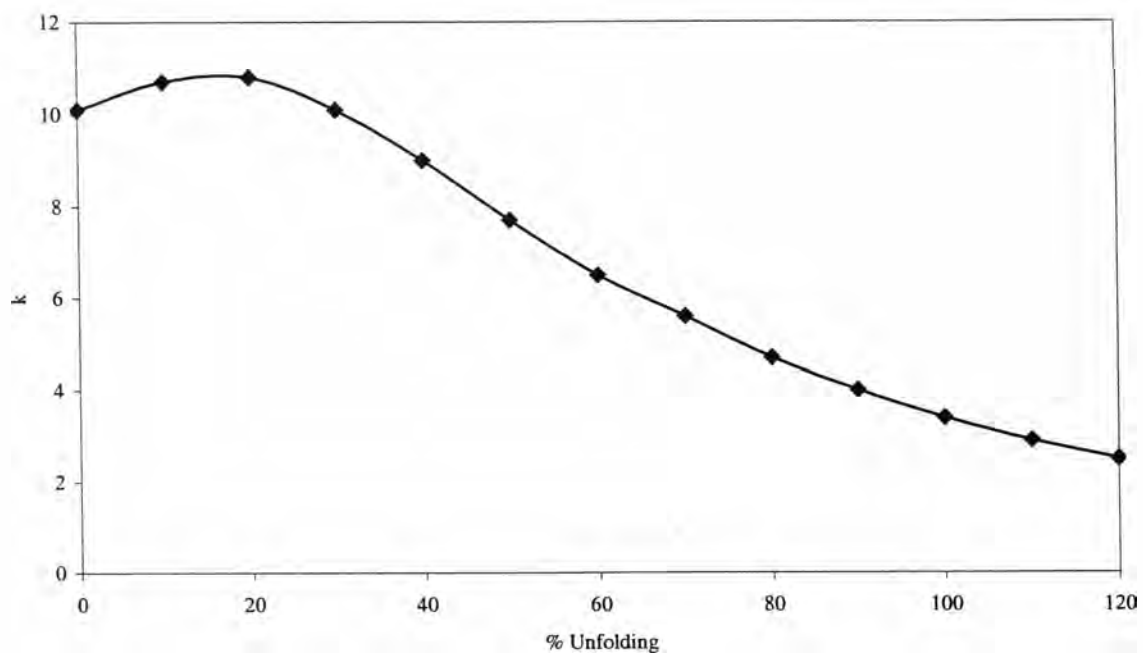
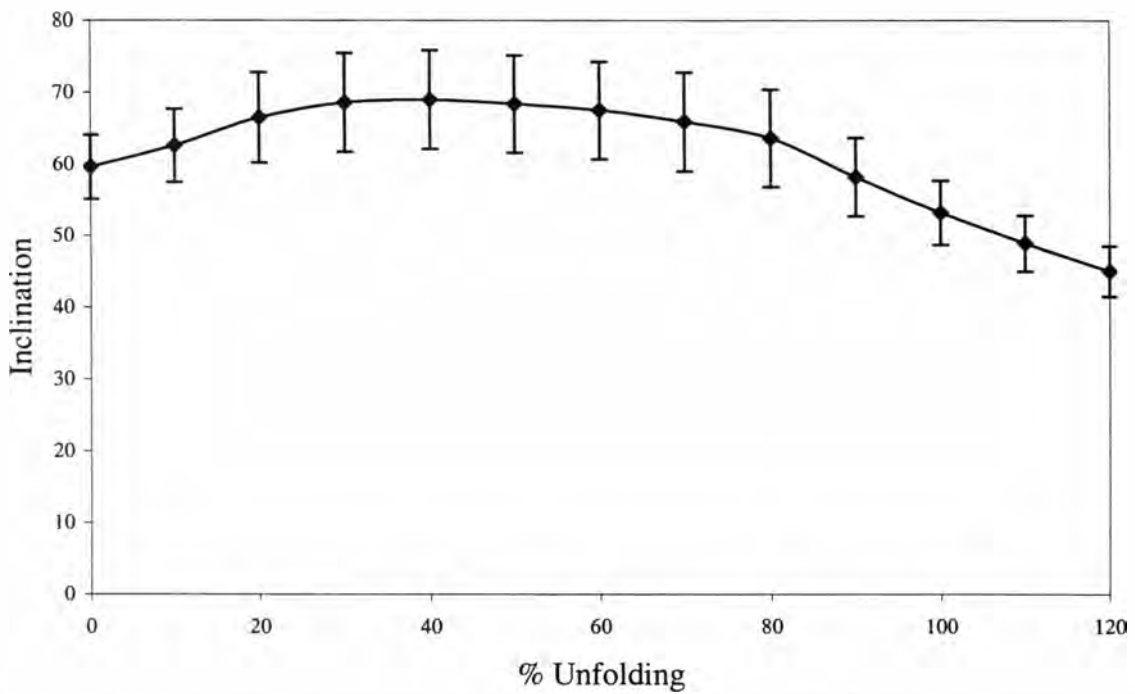
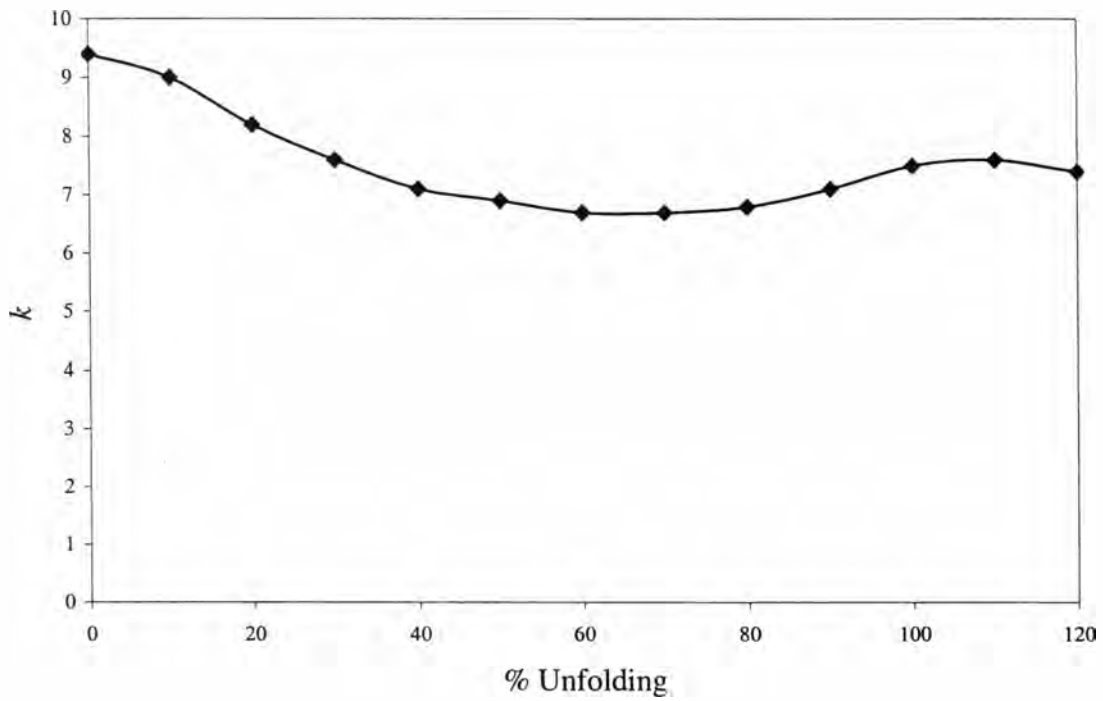


Figure 26 (Cont'd.)



**Figure 27.** McFadden and McElhinny (1988) line-fit fold test for the low  $T_{ub}$  component line fits from the Upper Jurassic Kapoose Formation.



**Figure 28.** McFadden and Reid (1982) inclination only fold test for the high  $T_{ub}$  component line fits from the Upper Jurassic Kapoose Formation.

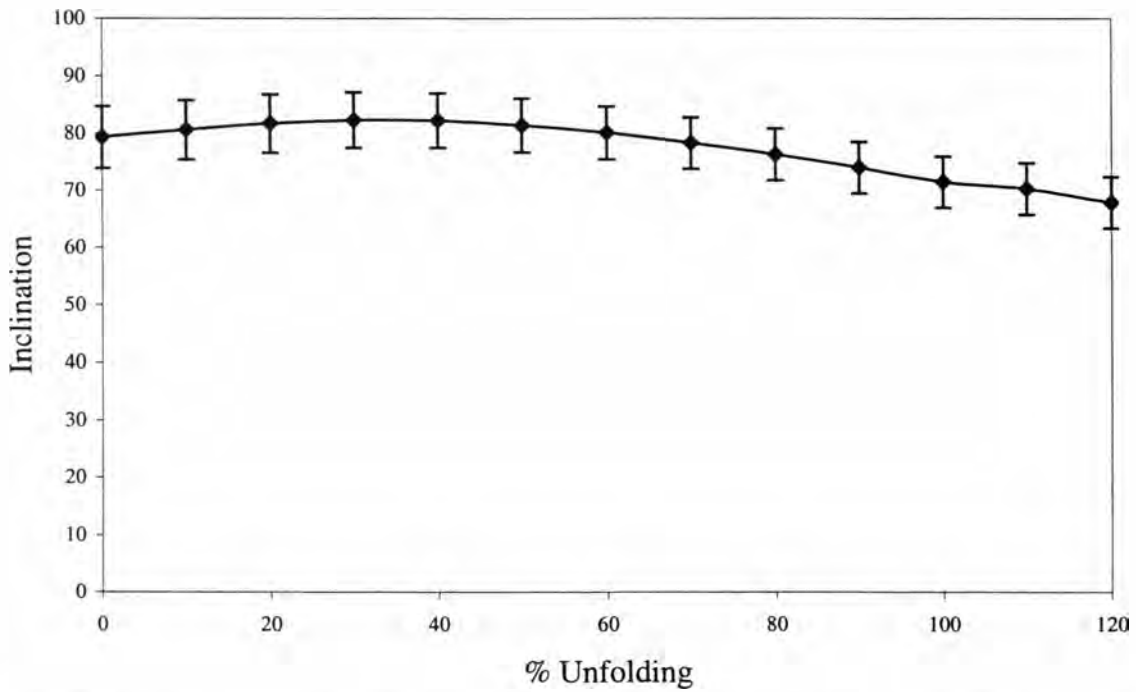
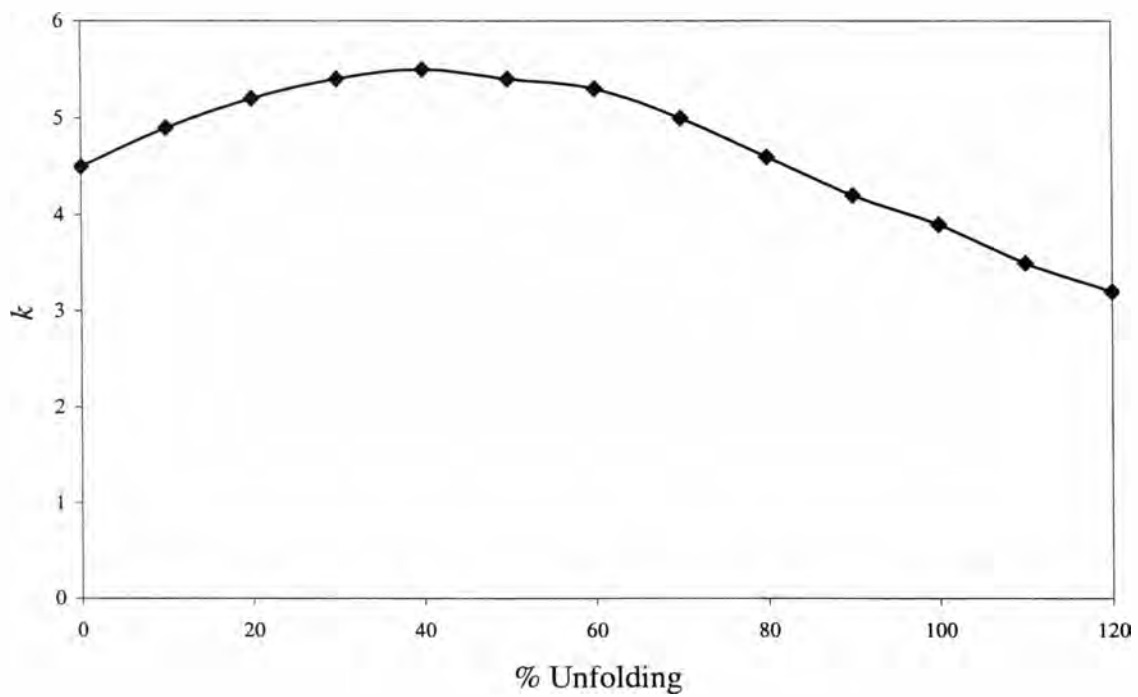


**Figure 29.** McFadden and McElhinny (1988) combined great circle and line-fit fold test for the high  $T_{ub}$  components from the Upper Jurassic Kapoose Formation.

00CIK4-3  
0-500 C

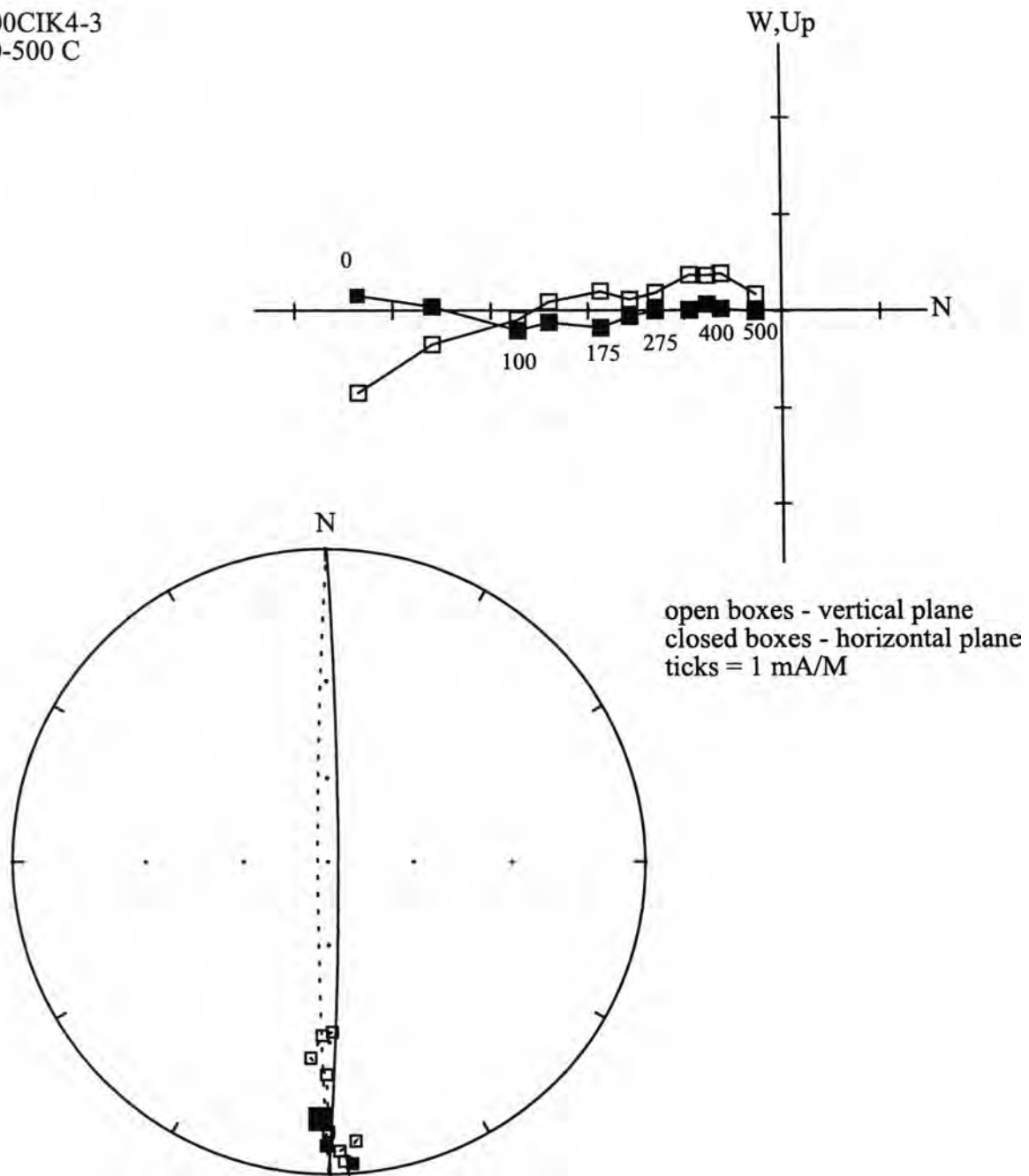


**Figure 30.** Zijderveld and equal area plots of a specimen demagnetization path from Clark Island site 4, corrected for tilt. The demagnetization path shows a reversed direction with a great circle fittable path heading to a reversed direction. The demagnetization path on the equal area plot starts at the large square. Closed squares and solid great circle are projected on the lower hemisphere, open squares and dashed great circle are projected on the upper hemisphere.



00CIK2-13  
0-535 C

open boxes - vertical plane  
closed boxes - horizontal plane  
ticks = 1 mA/M

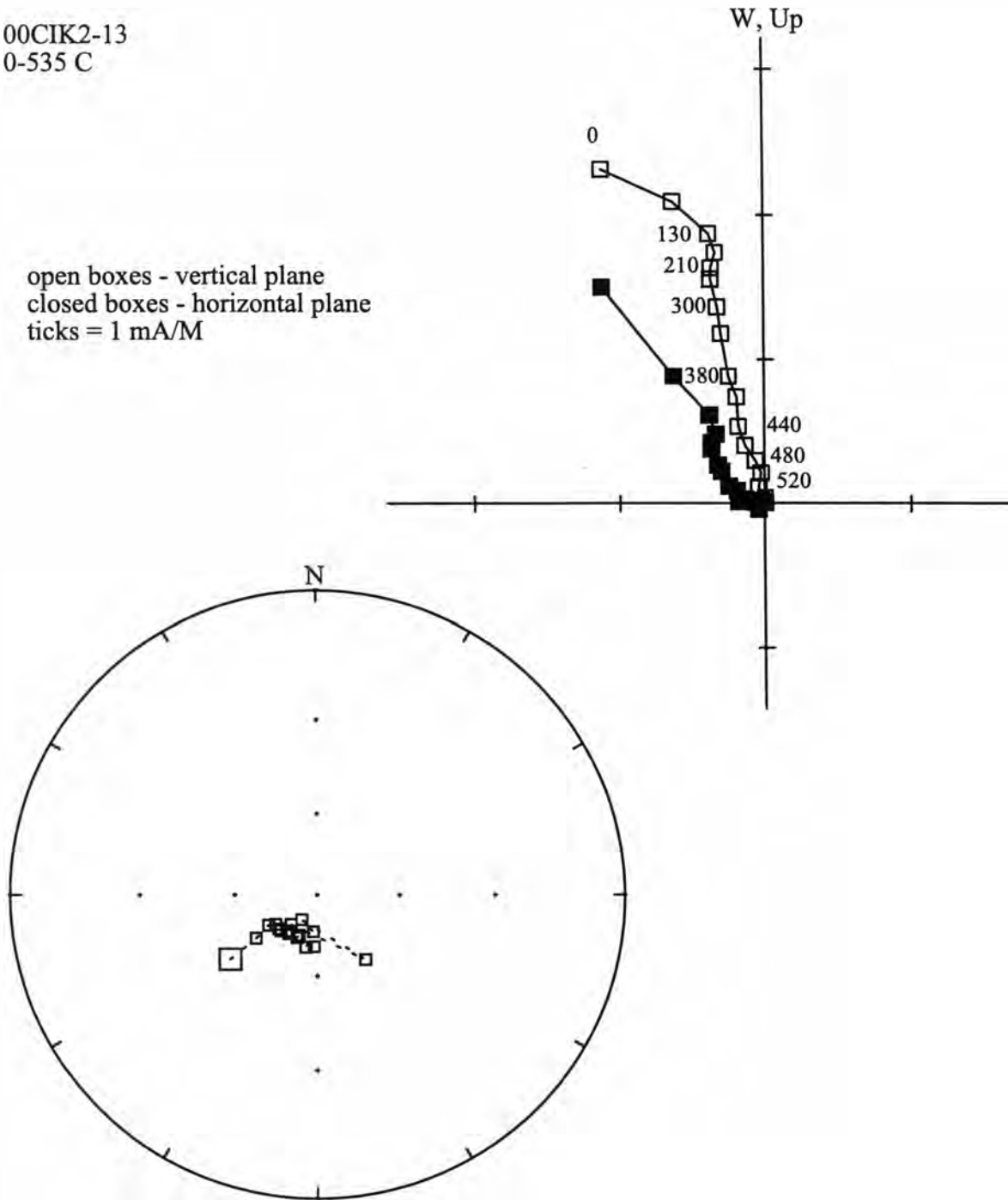


**Figure 31.** Zijderveld and equal area plots of a specimen demagnetization path from Clark Island site 2, corrected for bedding. The demagnetization path shows a linefitable reversed direction going to the origin. The demagnetization path on the equal area plot starts at the large square. Open squares are projected on the upper hemisphere.

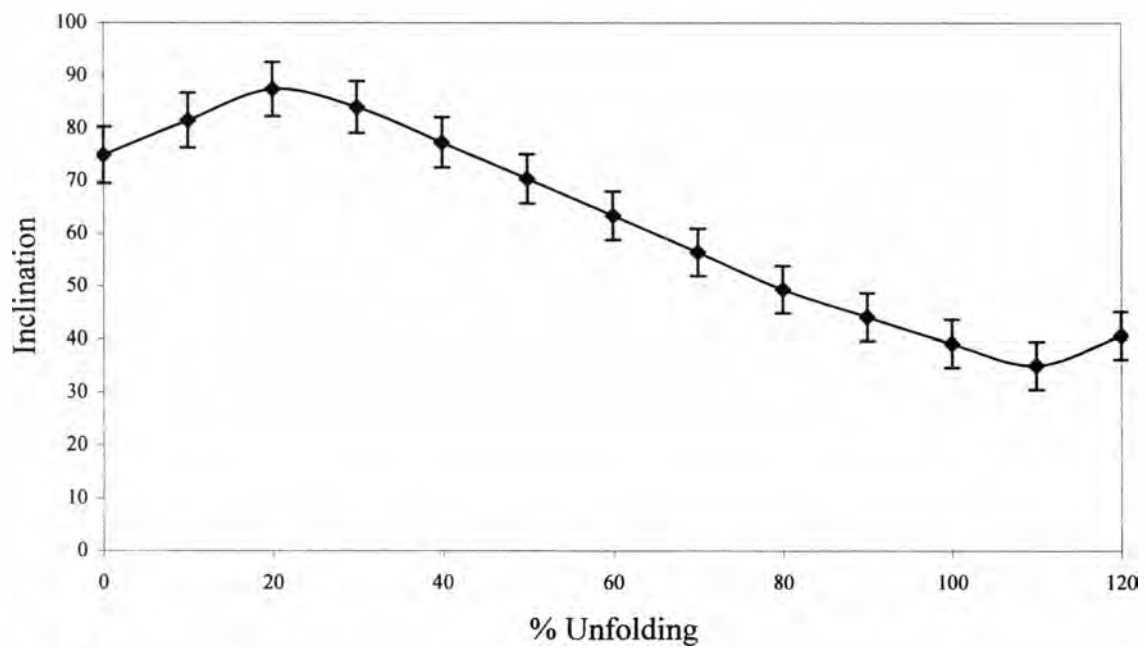
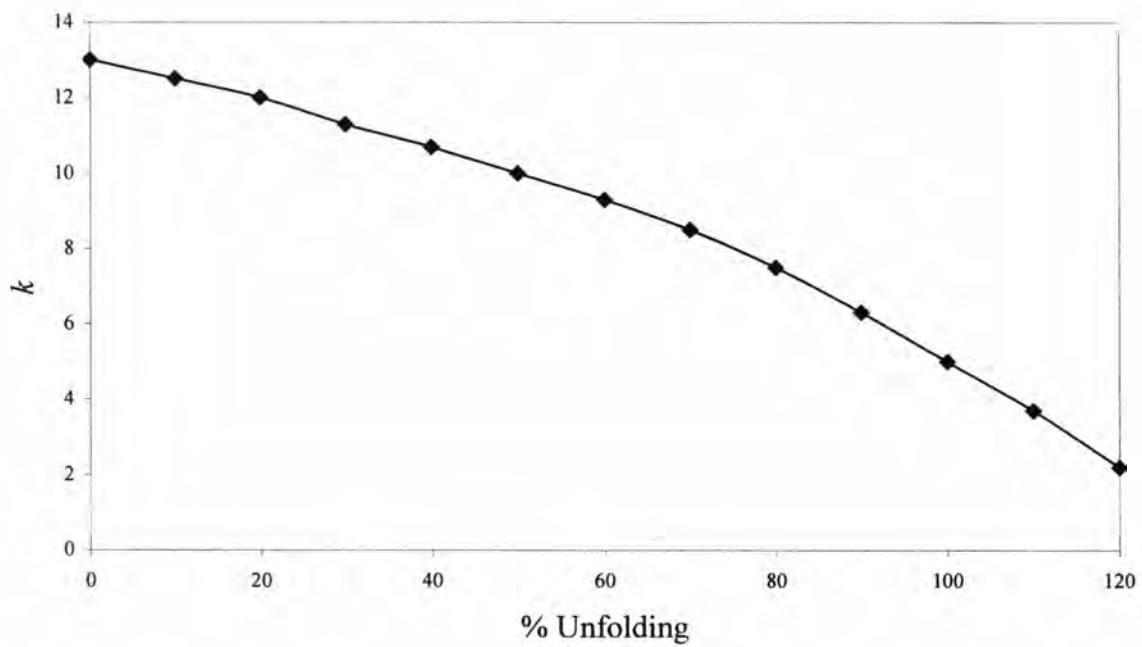


**Figure 32.** McFadden and McElhinny (1988) line-fit fold test for the low  $T_{ub}$  component linefits from the Lower Cretaceous One Tree Formation.

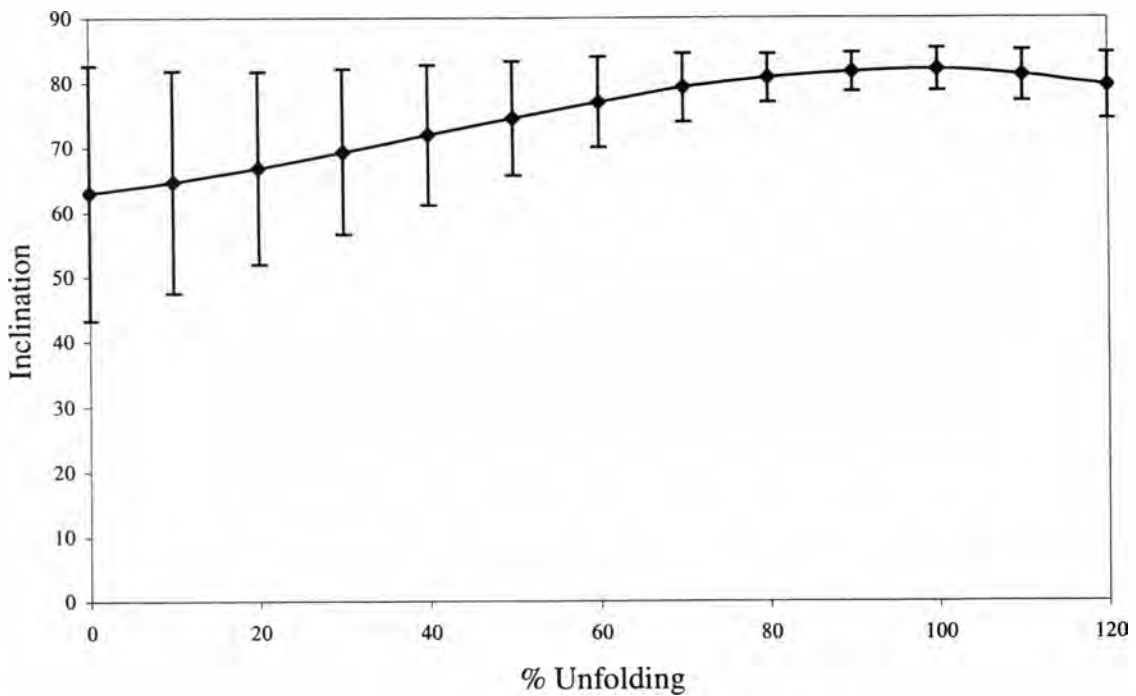
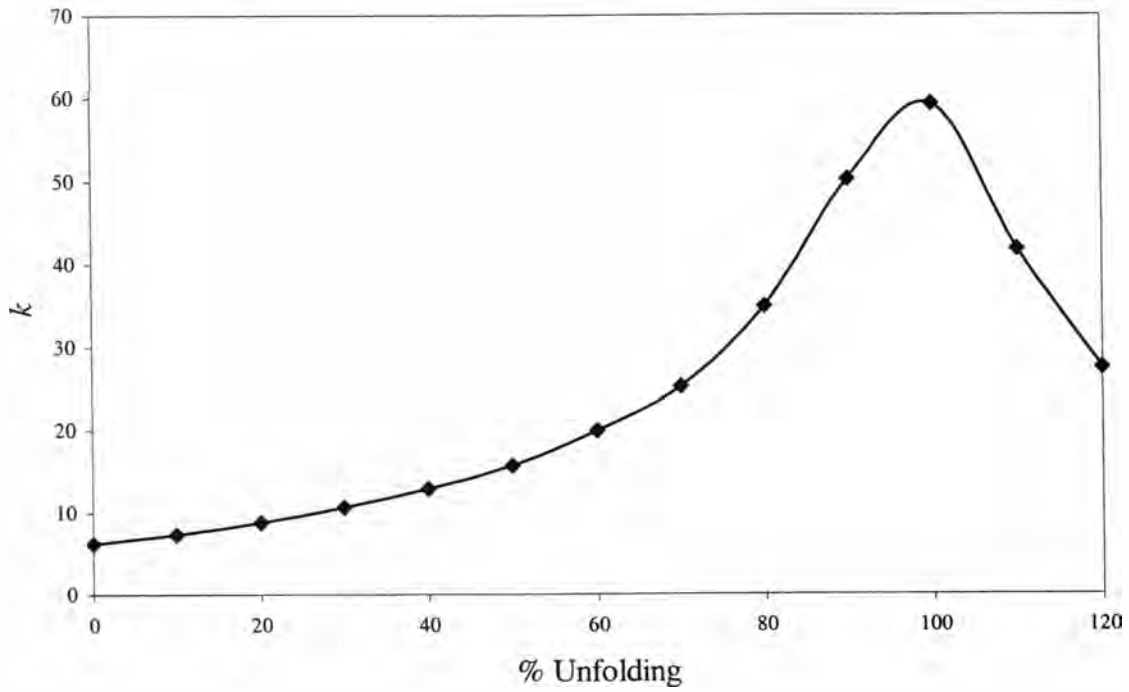


**Figure 33.** McFadden and Reid (1982) inclination only fold test for the high  $T_{ub}$  component line fits from the Lower Cretaceous One Tree Formation. Error bars on the inclination plot are  $\alpha_{95}$  limits.

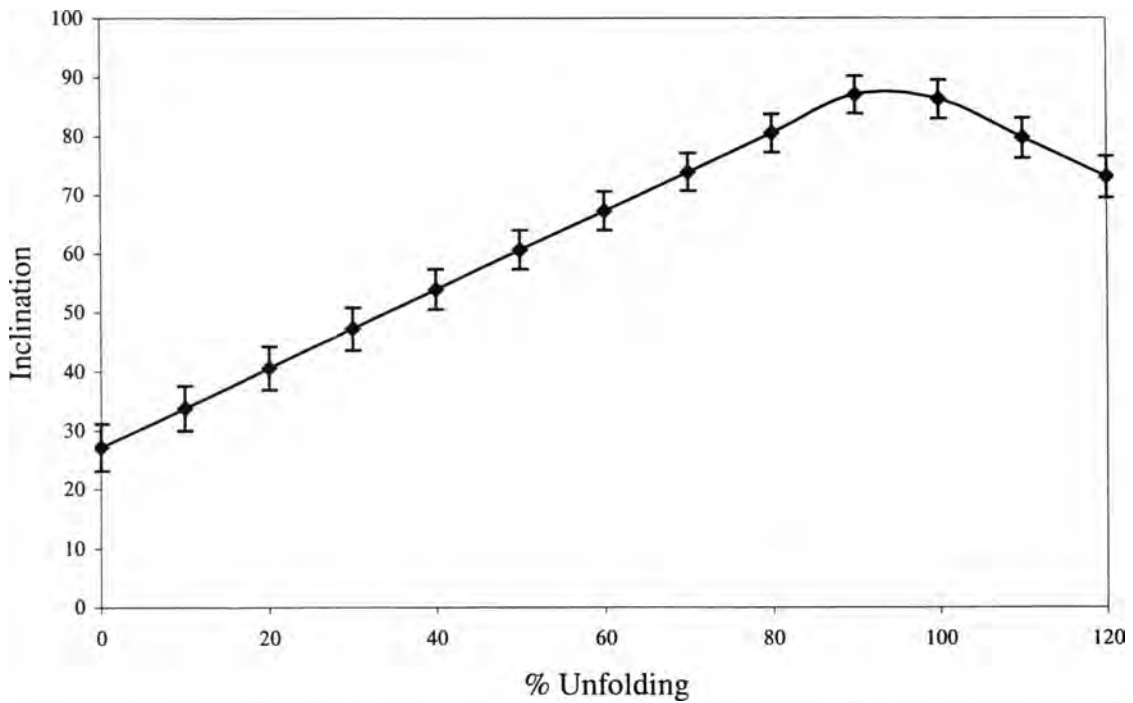
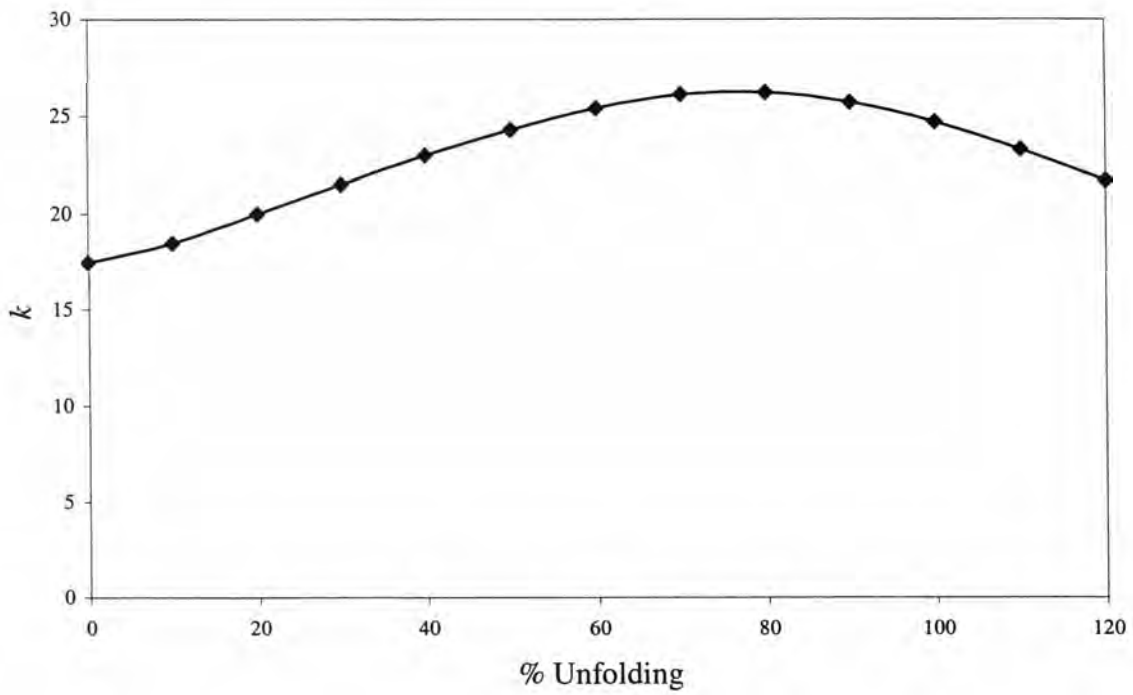


**Figure 34.** McFadden and McElhinny (1988) combined great circle and line-fit fold test for the high  $T_{ub}$  components from the Lower Cretaceous One Tree Formation.

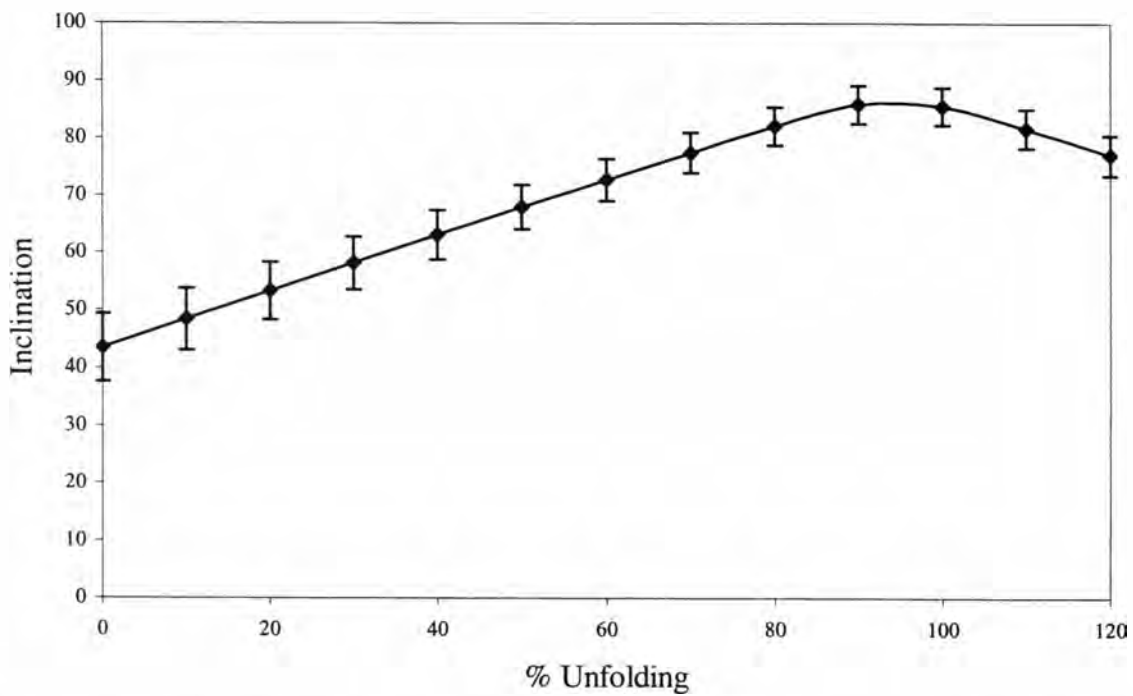
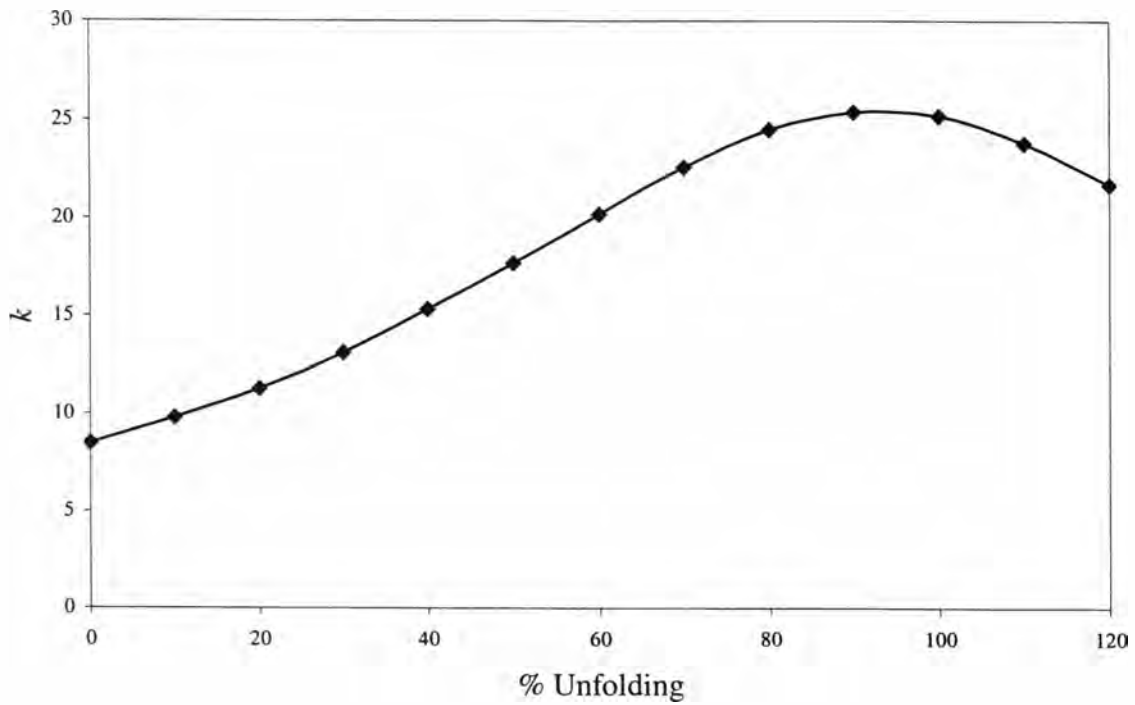
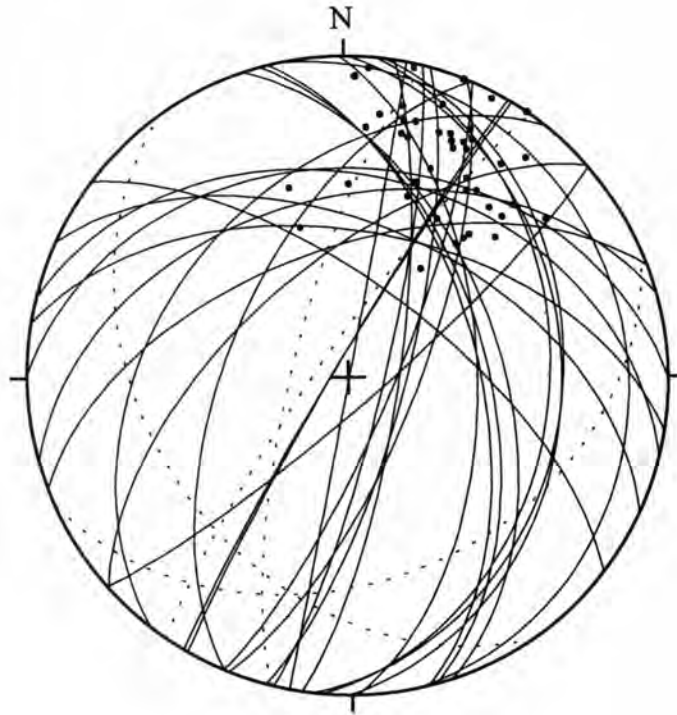


**Figure 35.** McFadden and McElhinny (1988) combined great circle and line-fit fold test for the high  $T_{ub}$  components from the Lower Cretaceous One Tree Formation after correction for fold plunge and small block rotation using the fold azimuths (see text).

A)



B)

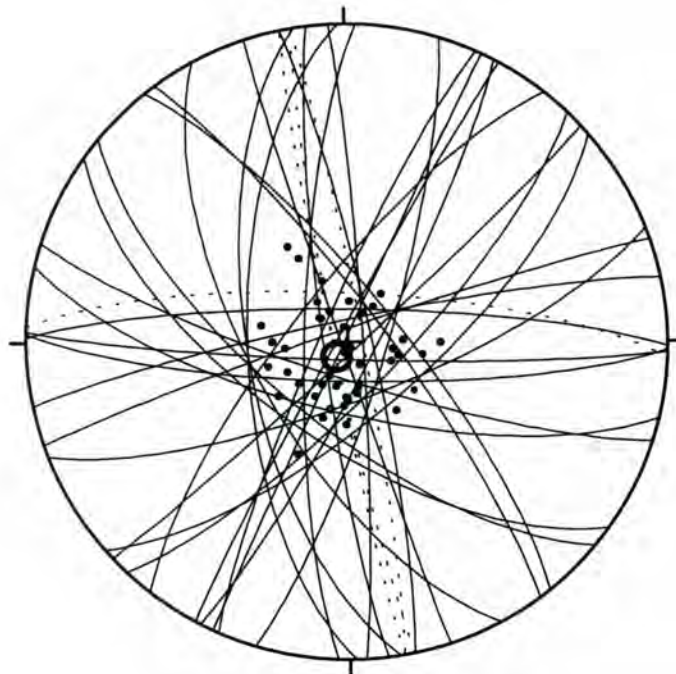


**Figure 36.** Equal area plots of the high  $T_{ub}$  component linefits and great circle fits from the Lower Cretaceous One Tree Formation. A) In situ data. B) Fold corrected and small block rotation corrected data shown with the 95% confidence circle. Closed circles and solid lines are projected on lower hemisphere, open circle and dashed lines are projected on upper hemisphere.

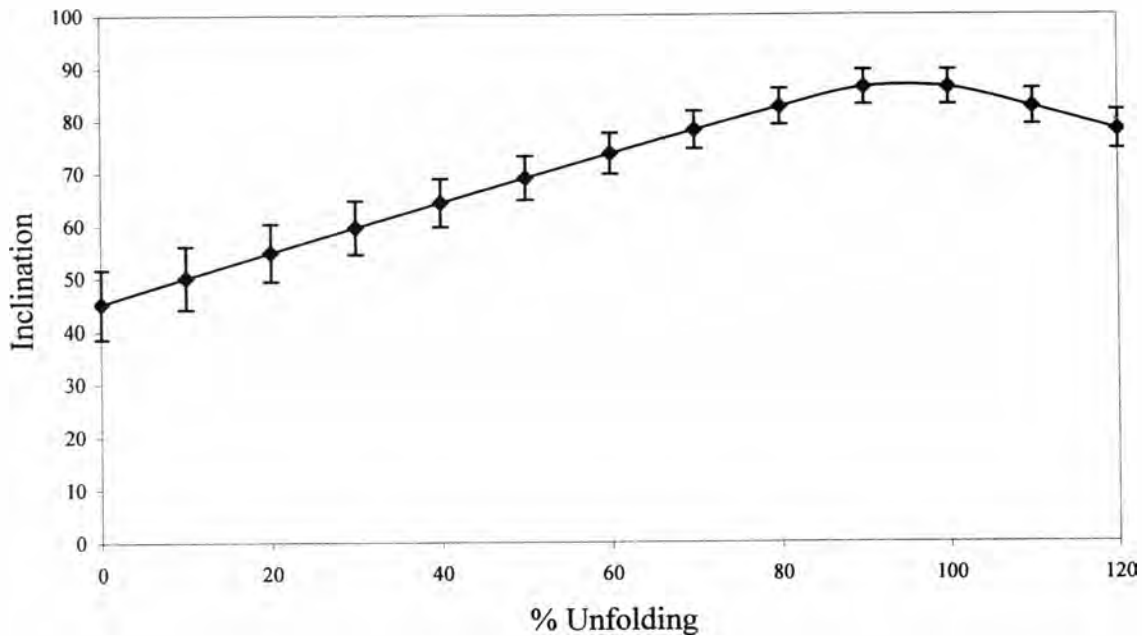
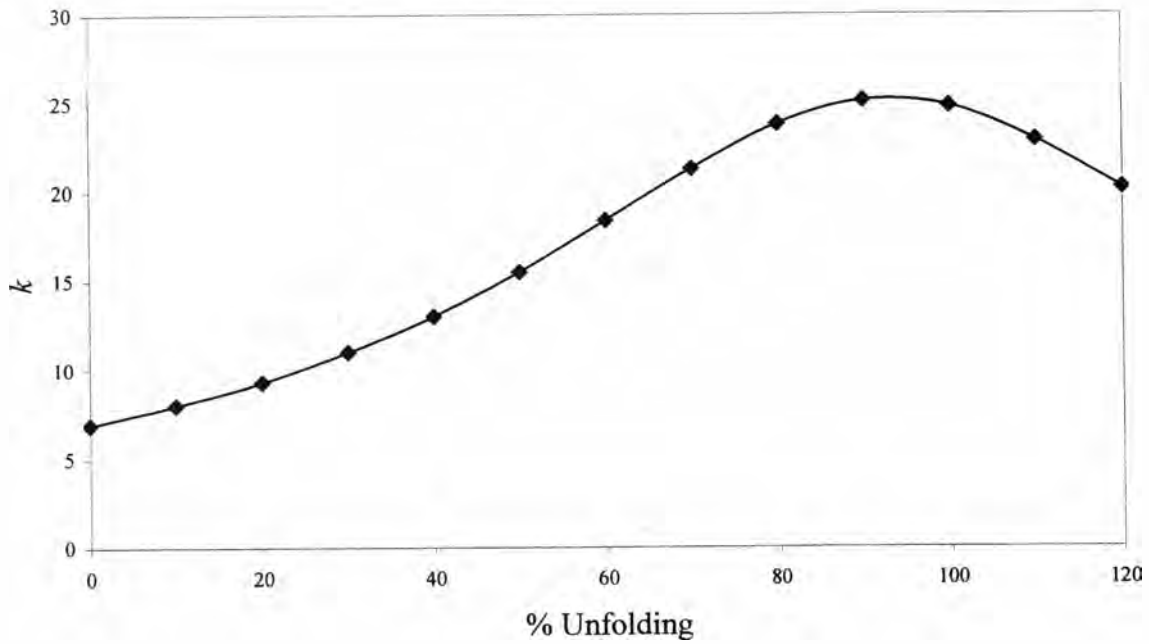


**Figure 37.** McFadden and McElhinny (1988) combined great circle and line-fit fold test for the high  $T_{ub}$  components from the Lower Cretaceous One Tree Formation after correction for fold plunge and small block rotation using the AMS mean maximum axis data (see Fig. 24, and text).

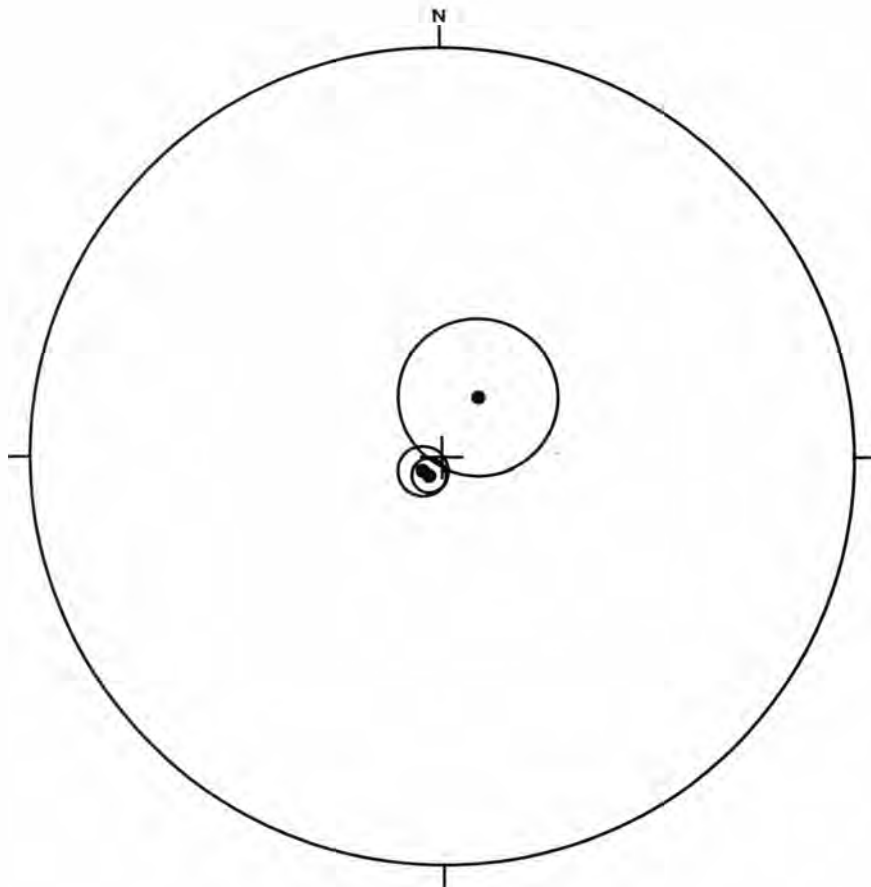


**Figure 38.** Lower hemisphere equal area plot of the 100% rotated and fold corrected mean of the 5 reversed directions from Clark Island, flipped to the antipode ( $D=28.5$ ,  $I=75.9$ ,  $\alpha_{95}=15.7$ ). Also shown is the 100% rotated and fold corrected mean of all acceptable high  $T_{ub}$  components from Clark Island ( $D=234.5$ ,  $I=85.4$ ,  $\alpha_{95}=4.7$ ), and the 100% rotated and fold corrected mean of all acceptable high  $T_{ub}$  components from both Clark Island and Grassy Island ( $D=214.4$ ,  $I=85.6$ ,  $\alpha_{95}=3.3$ ). The 95% confidence circle of the mean of the reversed directions does not envelop either of the overall mean directions. The reversed directions fail the reversal test at the 95% confidence level.



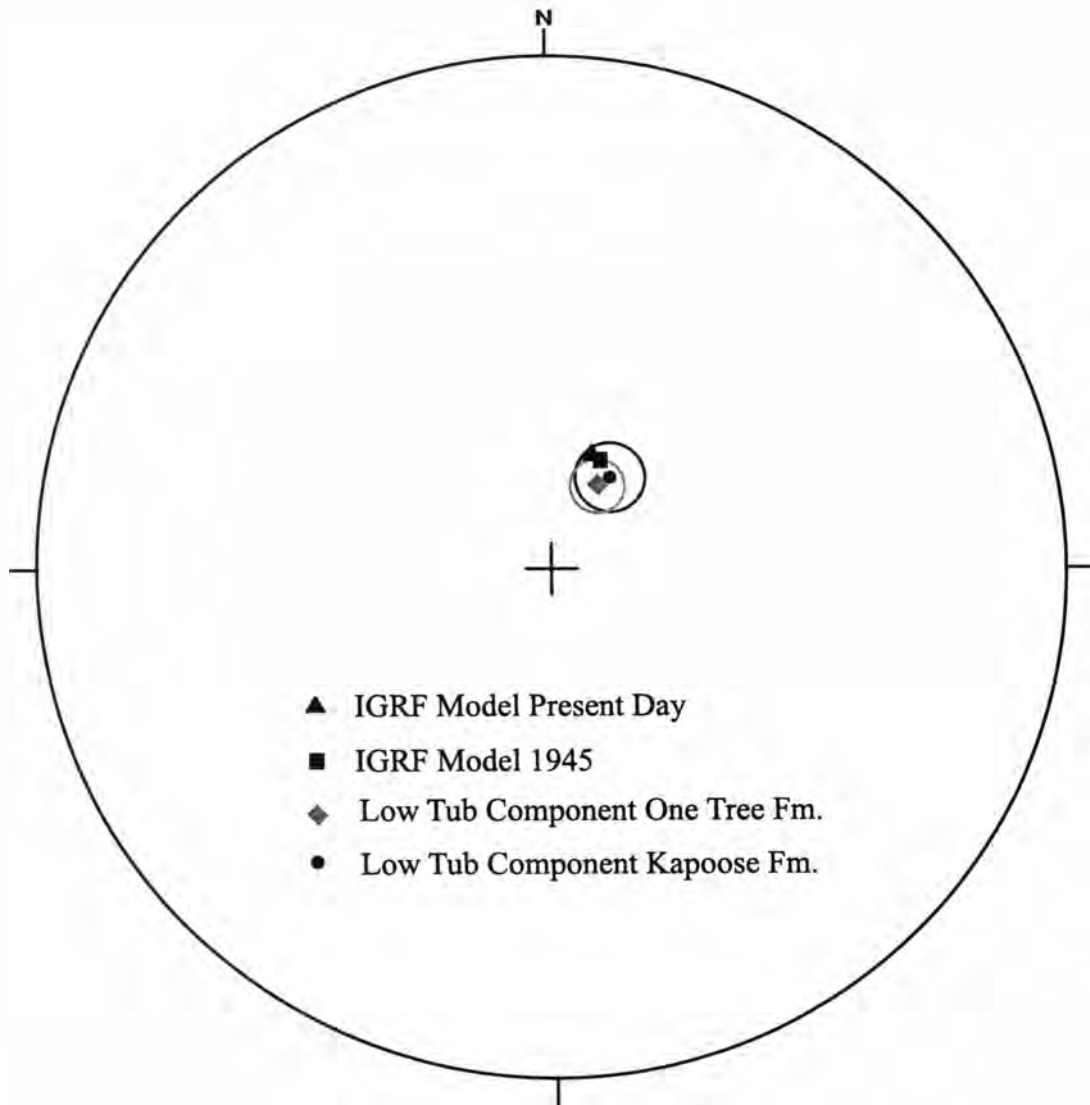


**Figure 39.** Lower hemisphere plot of the magnetic direction expected at the field area using the IGRF models for present day and 1945, compared to the in situ mean low  $T_{ub}$  component directions for the One Tree and Kapoose Formations.

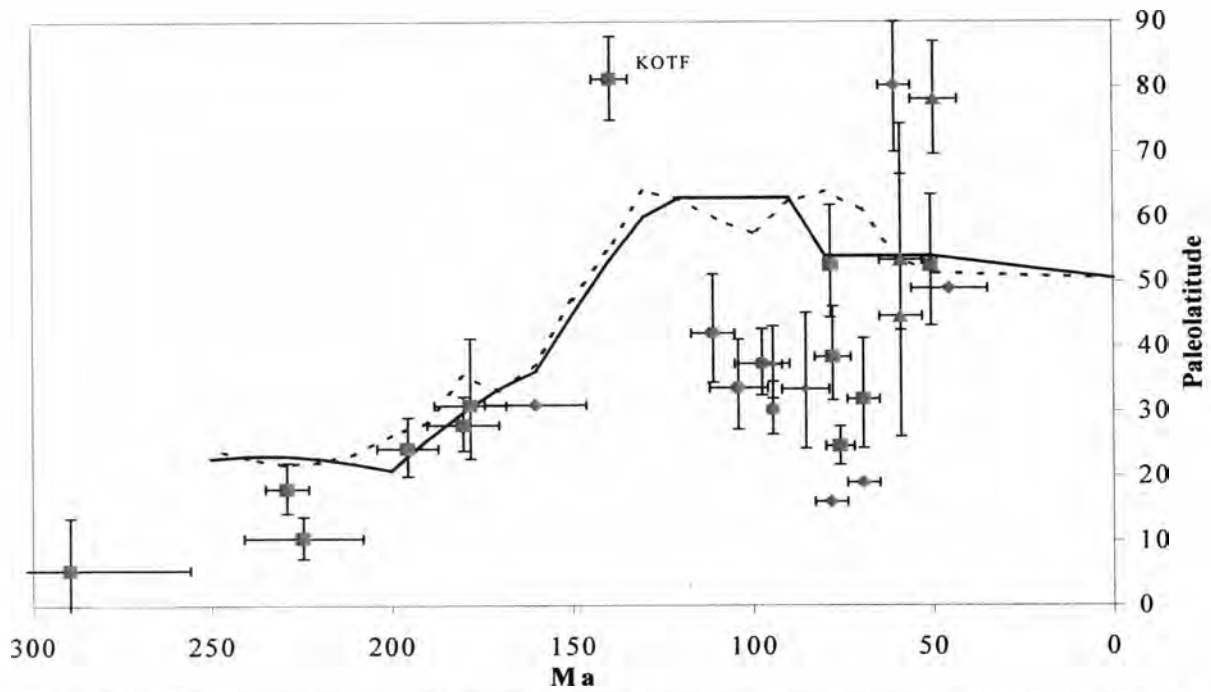


**Figure 40.** Paleomagnetic paleolatitudes from Wrangellia and connected terranes, calculated using the data shown in Table 1, shown with the paleolatitude determined from the Lower Cretaceous One Tree Formation (KOTF). ■- Wrangell Terrane (WR); ▲- Alexander Terrane (AX); ◆-Peninsular Terrane (PN); ●-Coast Plutonic Complex (CPC); • Coast Belt (CB).

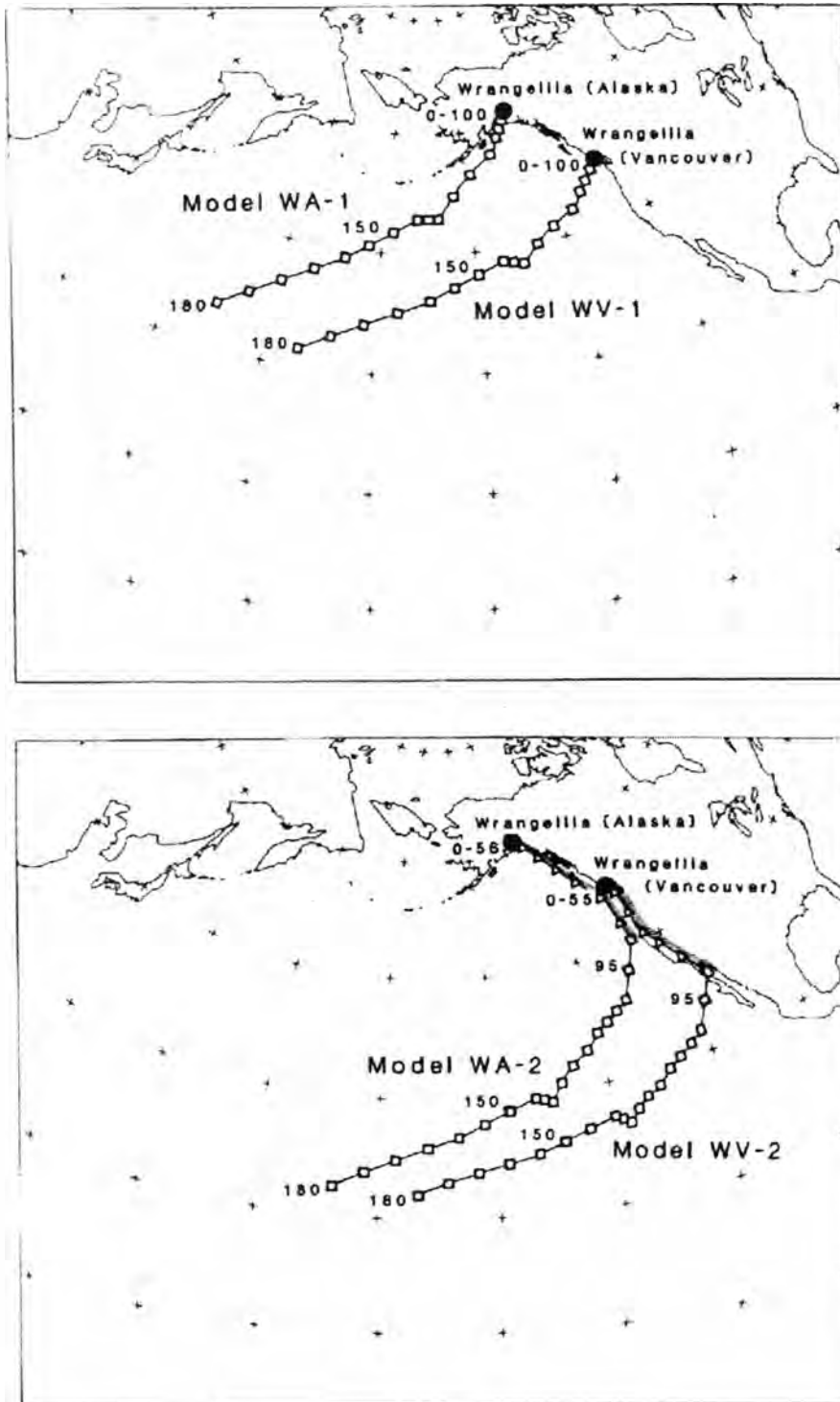


**Figure 41.** Vancouver Island terrane tracks developed by Debiche et al. (1987, Fig. 19, p. 37), based on the plate models by Engebretson et al. (1985). Top terrane tracks are for terranes traveling on the Farallon plate only. Bottom terrane tracks are for terranes traveling on the Farallon plate until ~90 Ma then semi-accreted onto North America, then shifted north by the Kula plate.

## Wrangellia—Vancouver Island

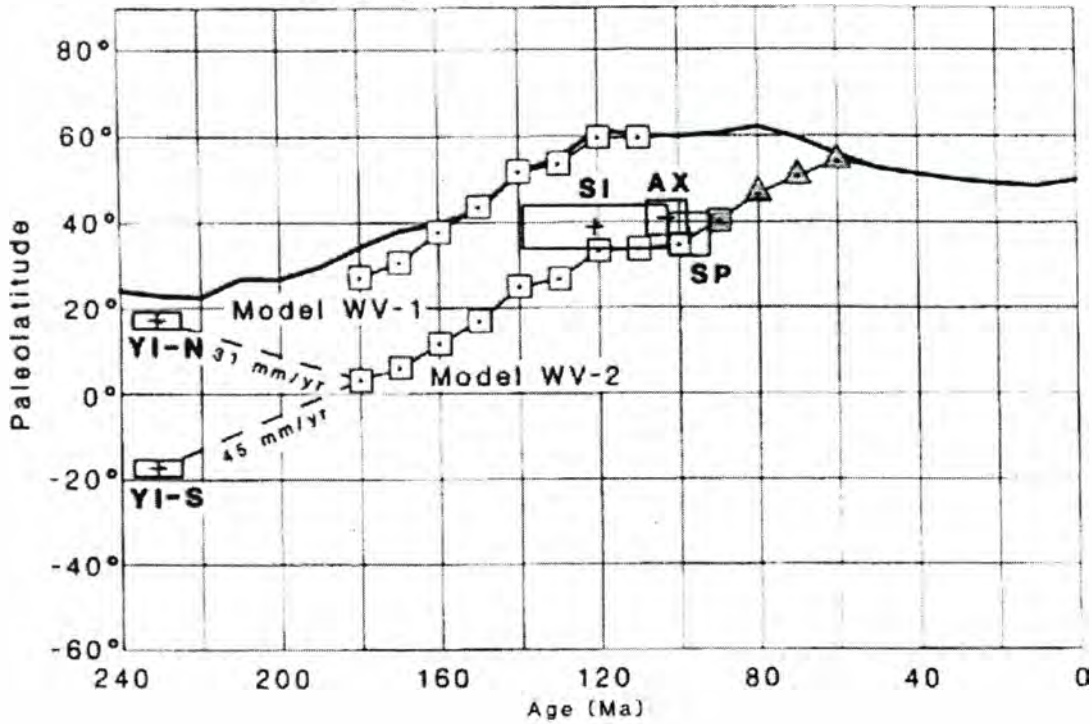


**Figure 42.** Paleolatitude models for Vancouver Island developed by Debiche et al. (1987, Fig. 19, p. 37), based on the plate models by Engebretson et al. (1985). Model WV-1 shows the paleolatitude of Vancouver Island as if it traveled only on the Farallon plate until it accreted onto North America by ~90 Ma. Model WV-2 shows the paleolatitude of Vancouver Island as if it traveled on the Farallon Plate until ~90 Ma, then oblique subduction of the Kula plate caused Vancouver Island to slide northward along the West Coast of North America until ~50 Ma. YI-S and YI-N, Karmutsen formation; SI, Stevens Island and Captain Cove intrusions; AX, Axelgold intrusions; SP, Spuzzum and Porteau plutons.

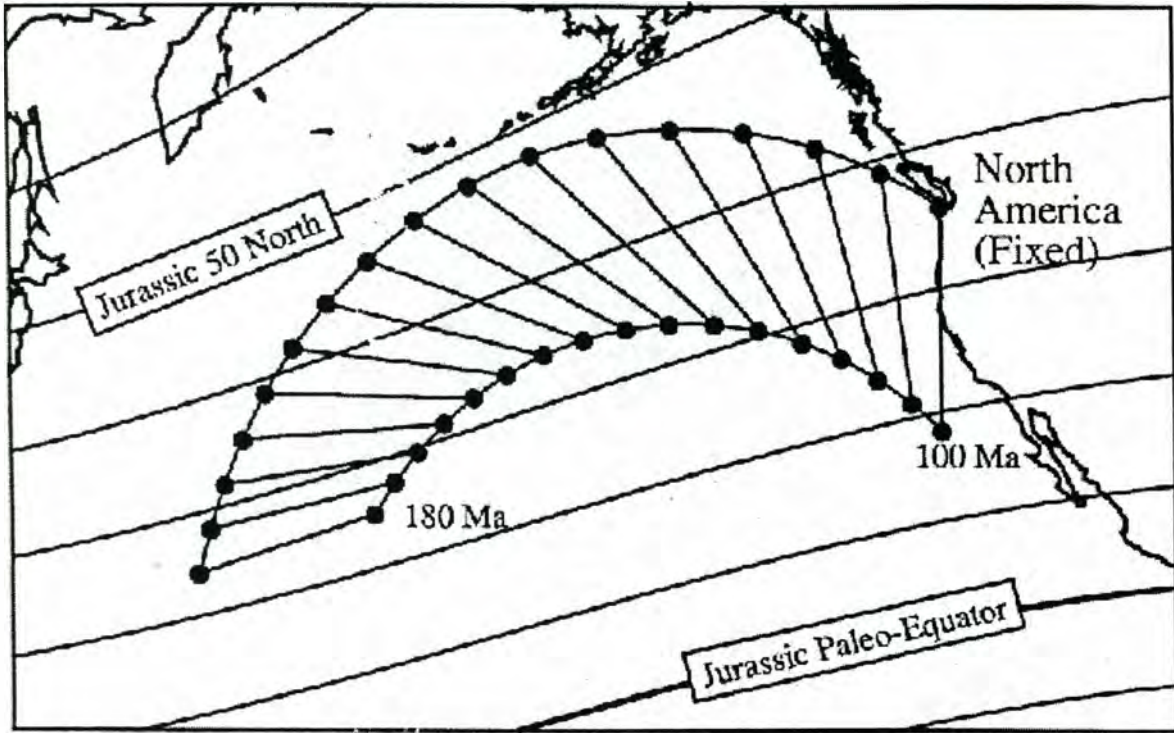


**Figure 43.** Terrane track model for a terrane traveling on the Kula plate, developed by Engebretson (personal communication), based on the postulated revised plate motions by Engebretson et al. (1995).

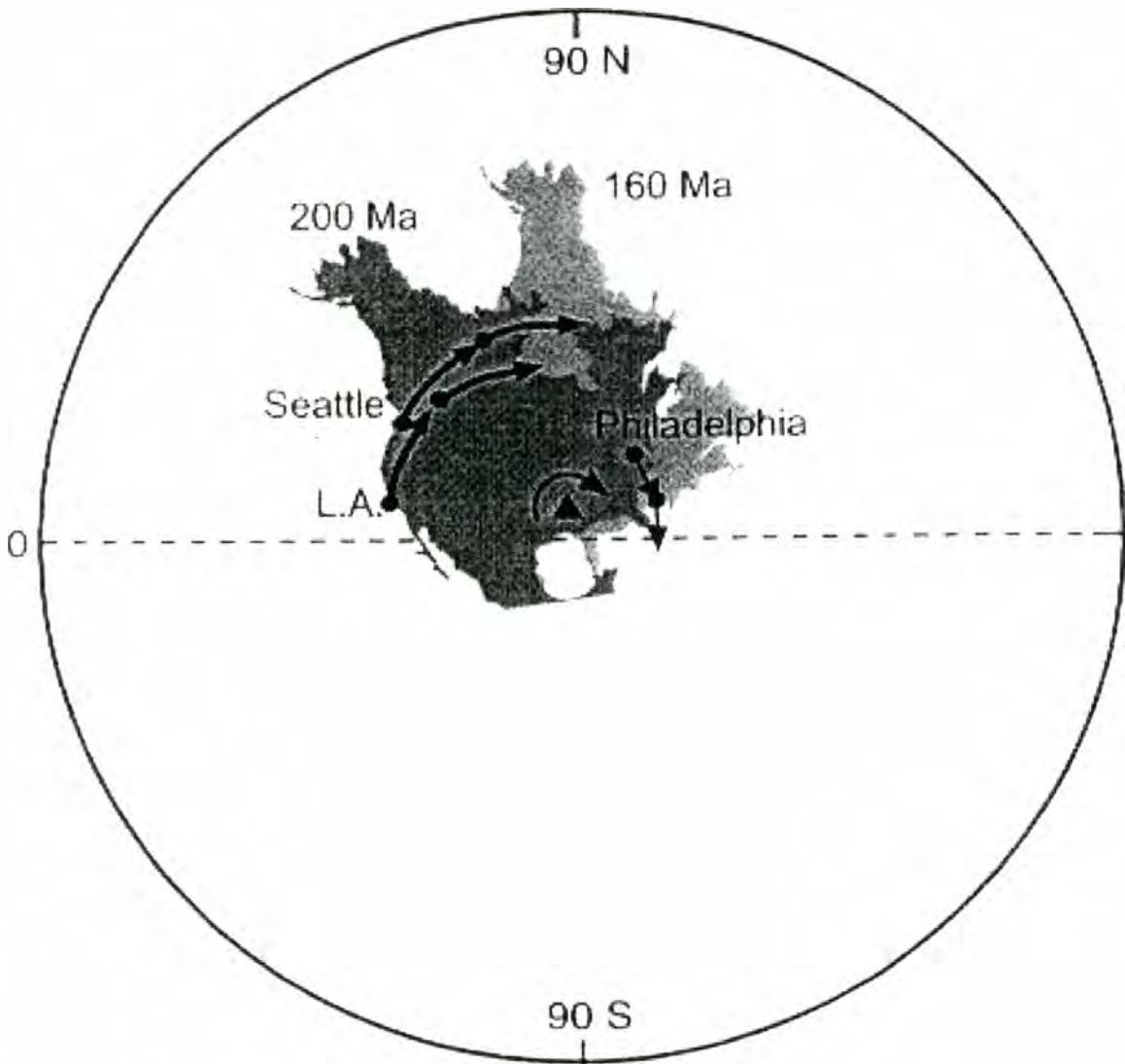


**Figure 44.** Absolute North American motions from Beck and Housen (2000). North America is rotated clockwise relative to its present orientation 160 Ma.

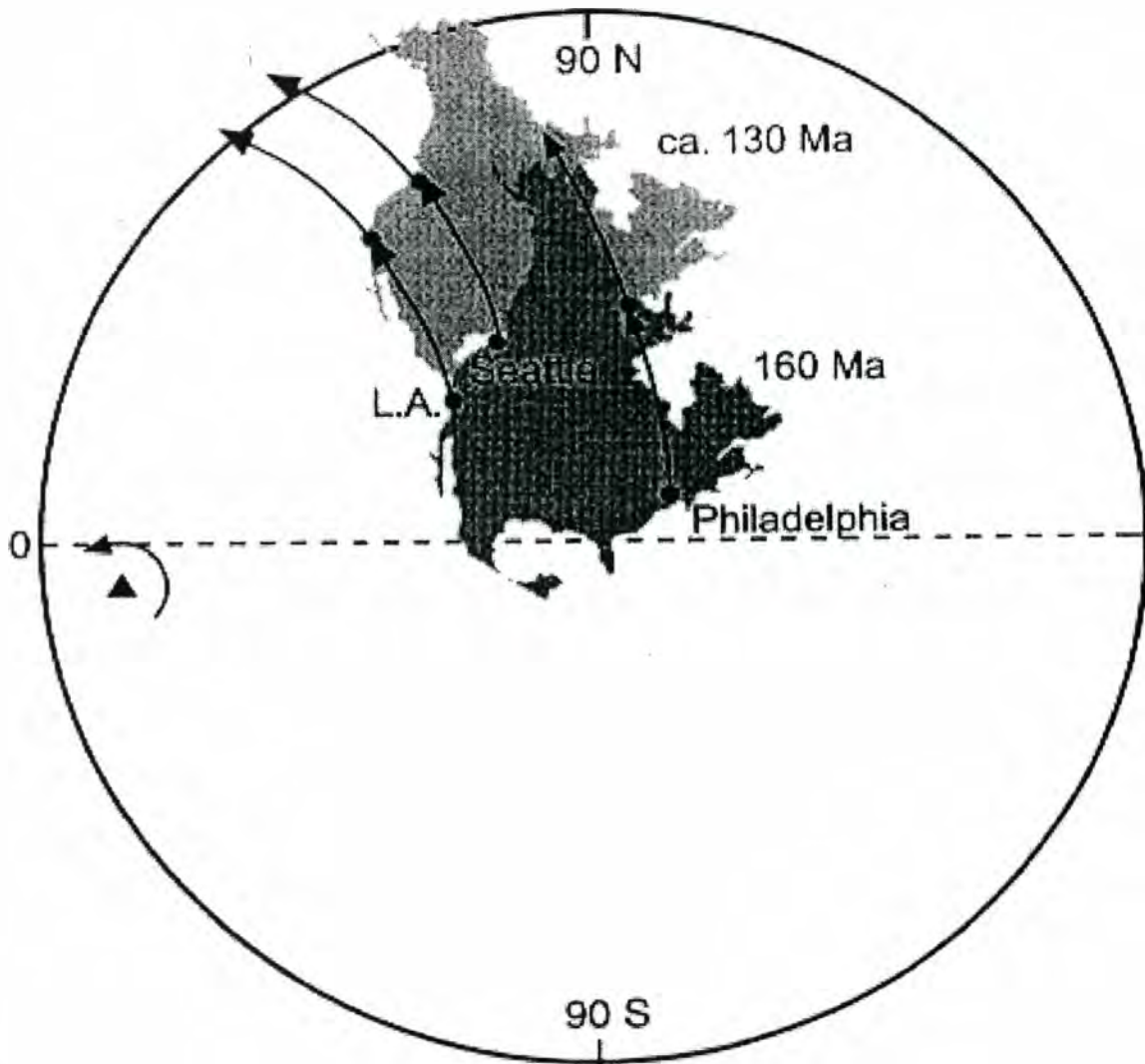


**Figure 45.** Absolute North American motions from Beck and Housen (2000). North America's west coast moved to its most northern position between 160 and 130 Ma (see Fig. 40).

## References

- Ague, J. J. and Brandon, M. T., 1996, Regional tilt of the Mount Stuart Batholith, Washington, determined using aluminum-in-hornblende barometry: Implication for northward translation of Baja British Columbia, *GSA Bulletin*, v. 108, no. 4, p. 471-488.
- Avé Lallemant, H. G., and Oldow, J. S., 1988, Early Mesozoic southward migration of cordilleran transpressional terranes, *Tectonics*, v. 7, p. 1057-1075.
- Beck, M. E., Jr., 1989, Paleomagnetism of continental North America; Implication for displacement of crustal blocks within the Western Cordillera, Baja California to British Columbia, in Pakiser, L. C., and Mooney, W. D., Geophysical framework of the continental United States, *Geological Society of America Memoir*, v. 172.
- Beck, M. E., Jr., Housen, B. A., 2000, A new paleomagnetic Euler pole model for the absolute motion of North America during the Mesozoic; implications for Cordilleran tectonics, *Abstracts with Programs, Geological Society of America*, v. 62, n. 3, p. 45.
- Berg, H. C., Jones, D. L., and Richer, D. H., 1972, Gravina-Nutzotin Belt-tectonic significance of an upper Mesozoic sedimentary and volcanic sequence in southern and Southeastern Alaska, *U.S. Geological Survey Professional Paper 800-D*, p. D1-D24.
- Brandon, M. T., Cowen, D. S., and Vance, J. A., 1988, The Late Cretaceous San Juan thrust system, San Juan Islands, Washington, *Geological Society of America, Special Paper 221*, 81 pp.
- Cowan, D. S., 1994, Alternative hypotheses for the mid-Cretaceous paleogeography of the western Cordillera, *GSA Today*, v. 4, p. 181-186.
- Day, R., Fuller, M. D., and Schmidt, V. A., 1977, Hysteresis properties of titanomagnetites: grain size and composition dependence, *Physics of Earth and Planets International*, v. 13, p. 260-266.
- Debiche, M. G., Cox, A., Engebretson, D. C., 1987, The motion of allochthonous terranes across the North Pacific Basin, *Special Paper - Geological Society of America*, v. 207, 49 pp.
- Ellwood, B. B., 1980, Application of the anisotropy of magnetic susceptibility method as an indicator of bottom-water flow direction, *Marine Geology*, v. 34, n. 3-4, p. M83-M90
- Engebretson, D. C., Kelley, K. P., Burmester, R. F., and Blake, M. C., 1995, North American plate interactions re-revisited, *Program with Abstracts, Geological Association of Canada, Mineralogical Association of Canada; Canadian Geophysical Union; Joint Meeting*, v. 20, p. 28.
- Engebretson, D. C.; Cox, A.; Gordon, R. G., 1985, Relative motions between oceanic and continental plates in the Pacific Basin, *Special Paper - Geological Society of America*, v. 206, 59 pp.
- Enkin, R. J., Baker, J., Mustard, P. S., 2001, Paleomagnetism of the Upper Cretaceous Nanaimo Group, southwestern Canadian Cordillera, *Canadian Journal of Earth Sciences*, v. 38, n. 10, p. 1403-1422.
- Flinn, D., 1962, On folding during three-dimensional progressive deformation, *Geological Society of London Quarterly Journal*, n. 118, p. 385-433.



- Gradstein, F. M., Agterberg, F. P., Ogg, J. G., Hardenbol, J., van Veen, P., Thierry, J., Huang, Z., 1994, A Mesozoic time scale, *Journal of Geophysical Research, B, Solid Earth and Planets*, v.99, n.12, p. 24,051-24,074
- Haggart, J. W., 1993, Latest Jurassic and Cretaceous paleogeography of the northern Insular belt, British Columbia, in: Dunn, G., and McDougall, K., eds., Mesozoic Paleogeography of the Western United States-II, *Pacific Section SEPM*, Book 71, p. 463-475.
- Hagstrum, J. T., 1993, North American Jurassic APW; the current dilemma, *Eos, Transactions, American Geophysical Union*, v.74, n.6, p.65, 68-69.
- Hammilton, N., Rees, A. I., 1970, Magnetic fabric in palaeocurrent estimation, *Palaeogeophysics*, p. 445-464.
- Hillhouse, J. W., 1977, Paleomagnetism of the Triassic Nikolai Greenstone, McCarthy Quadrangle, Alaska, *Canadian Journal of Earth Sciences*, v. 14, n. 11, p. 2578-2592.
- Hillhouse, J. W., Gromme, C. S., 1982, Limits to northward drift of Paleocene Cantwell Formation, Central Alaska, *Geology*, v. 10, p. 552-556
- Hodych, J. P., Bijaksana, S., and Patzold, R., 1999, Using magnetic anisotropy to correct for paleomagnetic inclination shallowing in some magnetite-bearing deep-sea turbidites and limestones, *Tectonophysics*, v. 307, n. 1-2, p. 191-205.
- Irving, E., Wynne, P. J., Thorkelson, D. J., Schiarizza, P., 1996, Large (1000 to 4000 km) northward movements of tectonic domains in the northern Cordillera, 83 to 45 Ma, *Journal of Geophysical Research*, v. 101, n. B8, p. 17,901-17,916.
- Irving, E., and Wynne, P. J., 1990, Paleomagnetic evidence bearing on the evolution of the Canadian Cordillera, *Philosophical Transactions, R. Society of London Series A*, v. 331, p. 487-509.
- Irving, E., and Yole, R. W., 1987, Tectonic rotations and translations in Western Canada; new evidence from Jurassic rocks of Vancouver Island, *Geophysical Journal of the Royal Astronomical Society*, v.91, n.3, p.1025-1048.
- Irving, E., Brandon, M. T., 1990, Paleomagnetism of the Flores Volcanics, Vancouver Island, in place by Eocene time, *Canadian Journal of Earth Sciences*, vol. 27, p. 811-817.
- Irving, E., Woodsworth, G. J., Wynne, P. J., and Morrison, A., 1985, Paleomagnetic evidence for displacement from the south of the Coast Plutonic Complex, British Columbia: *Canadian Journal of Earth Sciences*, v. 22, p. 584-598.
- Jackson, M., 1990, Diagenetic sources of stable remanence in remagnetized Paleozoic cratonic carbonates; a rock magnetism study, *Journal of Geophysical Research, B, Solid Earth and Planets*, v. 95, n. 3, p. 2753-2761.
- Jeletzky, J. A., 1950, Stratigraphy of the west coast of Vancouver Island between Kyuquot Sound and Esperanza Inlet, British Columbia (report and geologic map), *Paper - Geological Survey of Canada*, 52 pp.
- Jones, D. L., 1963, Upper Cretaceous (Campanian and Maestrichtian) ammonites from southern Alaska, *USGS, Professional Paper*, n. 432, 53 pp.
- Jones, D. L., Silberling, N. J., Hillhouse, J. 1977, Wrangellia - A displaced terrane in northwestern North America, *Canadian Journal of Earth Science*, v. 14, p. 2565-2577.
- Kirschvink, J. L., 1980, The least-squares line and plane and the analysis of palaeomagnetic data, *Geophysical Journal of the Royal Astronomical Society*, v. 62, n. 3, p. 699-718

- Lock, J., and McElhinny, M. W., 1991, The global paleomagnetic database: Design, installation and use with ORACLE, *Survey of Geophysics*, v. 12, p. 317-491.
- McClelland, W.C., Gehrels, G. E., and Saleeby, J. B., 1992, Upper Jurassic-Lower Cretaceous basinal strata along the Cordilleran margin: Implication for the accretionary history of the Alexander-Wrangellia-Peninsular terranes, *Tectonics*, v. 11, p. 823-835.
- McElhinny, M. W., and Lock, J., 1990a, IAGA global paleomagnetic database, *Geophysical Journal International*, v. 101, p. 763-766.
- McElhinny, M. W., and Lock, J., 1990b, Global paleomagnetic database project, *Physics of Earth and Planets International*, v. 63, p. 1-6.
- McElhinny, M. W., and Lock, J., 1993, Global paleomagnetic database supplement number one, update to 1992, *Survey of Geophysics*, v. 14, 303-329.
- McElhinny, M. W., and Lock, J., 1996, IAGA paleomagnetic databases with Access, *Survey of Geophysics*, v. 17, p. 575-591.
- McFadden, P. L., McElhinny, M. W., 1995, Combining groups of paleomagnetic directions or poles, *Geophysical Research Letters*, vol.22, no.16, Aug, 15, p.2191-2194.
- McFadden, P. L., McElhinny, M. W., 1988, The combined analysis of remagnetization circles and direct observations in paleomagnetism, *Earth and Planetary Science Letters*, v. 87, p. 161-172.
- McFadden, P. L., and Reid, A. B., 1982, Analysis of paleomagnetic inclination data, *Geophysical Journal of Research Astronomical Society*, v. 69, p. 307-319.
- Monger J. W. H., 1991, Correlation of Settler Schist with Darrington Phyllite and Shuksan Greenshist and its tectonic implications, Coast and Cascade Mountains, British Columbia and Washington. *Canadian Journal of Earth Sciences*, v. 28, p. 447-458.
- Monger J. W. H., Journeay, J. M., 1994, Guide to the geology and tectonic evolution of the southern Coast Mountains, *Geological Survey of Canada open file*, n. 2490, 77 pp.
- Monger J. W. H., Price, R. A., and Templeman-Kluit, D. J., 1982, Tectonic accretion and the origin of the two major metamorphic welts in the Canadian Cordillera, *Geology*, v. 20, p. 70-75.
- Monger, J. W. H., van der Heyden, P., Journeay, J. M., Evenchick, C. A., 1994, Jurassic-Cretaceous basins along the Canadian Coast Belt: Their bearing on pre-mid-Cretaceous sinistral displacements, *Geology*, v. 22, p. 175-178.
- Moore, E. M., 1998, Ophiolites, the Sierra Nevada, "Cordillera," and Orogeny along the Pacific and Caribbean margins of North and South America, *International Geology Review*, v. 40, n. 1, p. 40-54.
- Muller, J. E., Cameron, B. E. B., and Northcote, K. E., 1981, Geology and mineral deposits of Nootka Sound map-area (92E), Vancouver Island, British Columbia, *Canada Geological Survey*, Paper 80-16, 53 pp.
- Muller, J. E., Northcote, K. E., and Carlise, D., 1974, Geology and mineral deposits of Alert Bay – Cape Scott map-area, Vancouver Island, British Columbia, *Geological Survey of Canada*, Paper 74-8, 77pp.
- Mustard, P. S., Parrish, R. R., McNicholl, V. J., 1994, Paleolatitude of the western Canadian Cordillera in the Late Cretaceous; provenance evidence from the Upper Cretaceous Nanaimo Group, British Columbia, *Abstracts with Programs - Geological Society of America*, v.26, n.7, p.149.

- Oldow, J. S., Avé Lallemant, H. G., Schmidt, W. J., 1984, Kinematics of plate convergence deduced from Mesozoic structures in the western Cordillera, *Tectonics*, 3, 201-227, 1984.
- Panuska, B. C., 1985, Paleomagnetic evidence for a post-Cretaceous accretion of Wrangellia, *Geology*, v. 13, p. 880-883.
- Panuska, B. C., Stone, D. B., 1981, Late Paleozoic paleomagnetic data for Wrangellia: Resolution of the polarity ambiguity, *Nature*, v. 283, p. 561-563.
- Panuska, B. C., Stone, D. B., 1985, Latitudinal motion of the Wrangellia and Alexander Terranes and the Southern Alaska Superterrane, In: Circum-Pacific Tectonic Stratigraphic Terranes of Circum-Pacific Region, ed. D. Howell, *AAPG. Earth Science Seminars #1*, p. 109-120.
- Panuska, B. C., Stone, D. B., Turner, D. L., 1990, Paleomagnetism of Eocene volcanic rocks, Talkeetna Mountains, Alaska, *Journal of Geophysics Research*, v. 95, p. 6737-6750.
- Parry, L. G., 1982, Magnetization of immobilized particle dispersions with 2 distinct particle sizes, *Physics of the Earth and Planetary Interior*, v. 28, n. 3., p. 230-241.
- Potter, P. E., Pettijohn, F. J., 1963, Paleocurrents and Basin analysis, Academic Press, New York, 296 pp.
- Rubin, C. M., Saleeby, J. B., Cowan, D. S., Brandon, M. T., and McGroder, M. F., 1990, Regionally extensive west-vergent mid-Cretaceous thrust system in the northwestern Cordillera: Implications for continent-margin tectonism, *Geology*, v. 18, p. 276-280.
- Schwarz, E. J., Muller, J. E., and Clark, K. R., 1980, Paleomagnetism of the Karmutsen basalts from southeast Vancouver Island, *Canadian Journal of Earth Science*, v. 17, n. 3, p. 389-399.
- Stamatakos, J. A., Trop, J. T., Ridgeway, K.D., 2001, Late Cretaceous paleogeography of Wrangellia: Paleomagnetism of the MacColl Ridge Formation, southern Alaska, revisited, *Geology*, v. 29, p. 947-950.
- Stamatakos, J. A., Kodama, K. P., Vittorio, L. F., 1989, Paleomagnetism of Cretaceous and Paleocene sedimentary rocks across the Castle Mountain Fault, south central Alaska, in: Deep Structure and Past Kinematics of Accreted Terranes, *American Geophysical Union, Geophysics Monogram*, v. 50, ed. J. W. Hillhouse, p 151-177.
- Stone, D. B., and Packer, D. R., 1979, Paleomagnetic data from the Alaska Peninsula, *Geologic Society of America Bulletin*, Part I, v. 90, p. 545-560.
- Symons, D. T. A., 1977, Geotectonics of Cretaceous and Eocene pluton in British Columbia; A paleomagnetic fold test, *Canadian Journal of Earth Sciences*, v. 14, p. 1246-1262.
- Symons, D. T. A., 1984, Paleomagnetism of the Westcoast Complex and the geotectonics of the Vancouver Island segment of the Wrangellian subterrane, *Journal of Geodynamics*, vol. 2, p. 211-228.
- Tarling, D., and Hrouda, F., 1993, *The Magnetic Anisotropy of Rocks*, Chapman and Hall, London.
- Tauxe, L., 1998, *Paleomagnetic Principles and Practice, Modern Approaches in Geophysics*, v. 17, Kluwer Academic Publishers, 299 pp.
- Van der Heyden, P., 1992, A middle Jurassic to Early Tertiary Andean-Sierran arc model for the Coast Belt of British Columbia, *Tectonics*, v. 11, p. 82-97.

- Van der Voo, R., Torsvik, T. H., 2001, Evidence for late Paleozoic and Mesozoic non-dipole fields provides an explanation for the Pangea reconstruction problems, *Earth and Planetary Science Letters*, v. 187, n. 1-2, p. 71-81.
- Ward, P. D., Hurado, J. M., Kirshvink, J. L., Verosub, K., L., 1997, Measurements of the Cretaceous Paleolatitude of Vancouver Island: Consistent with the Baja-British Columbia Hypothesis, *Science*, v. 277, p. 1642-2645.
- Wynne, P. J., Irving, E., Maxon, J. A., and Kleinspehn, K. L., 1995, Paleomagnetism of the Upper Cretaceous strata of Mount Tatlow: Evidence for 300km of northward displacement of the eastern Coast Belt, British Columbia; *Journal of Geophysics Research*, v. 100, no. B4, p. 6073-6091.
- Yole, R. W., and Irving, E., 1980, Displacement of Vancouver Island: Paleomagnetic evidence from the Karmutsen Formation, *Canadian Journal of Earth Sciences*, v. 17, n. 9, p. 1210-1228.